UNIVERSITÀ
DEGLI STUDI
DI PADOVA

UNIVERSITA' DEGLI STUDI DI PADOVA

DIPARTIMENTO DI INGEGNERIA CIVILE, EDILE ED AMBIENTALE

LAUREA MAGISTRALE IN "ENVIRONMENTAL ENGINEERING"

Experimental observations of grain step length statistics:

Relatore: Prof. Andrea Marion

Correlatore: Prof. Simon Tait

Laureando: Luca Cotterle

ANNO ACCADEMICO 2014/2015

Desidero innanzitutto ringraziare l'Ingegner Martina Cecchetto: i suoi preziosi consigli sono stati indispensabili per la stesura della tesi. Un ringraziamento va anche al Professor Simon Tait che ha supervisionato al lavoro e al Professor Andrea Marion che mi ha dato l'opportunità di fare la tesi presso l'Università di Sheffield. Un ringraziamento va soprattuto ai miei genitori e la mia famiglia per il supporto morale ed economico senza i quali non avrei mai potuto laurearmi (si, con un anno di troppo, ma vabbè, è normale ad Ingegneria dicono...). Infine vorrei ringraziare i compagni di corso, la mia ragazza, gli amici e tutti quelli che mi hanno sopportato in questi anni e che spero continuino a farlo.

Contents

List of Figures

Chapter 1

Introduction

The direct access to the water resources has been a central issue for the development of the civilizations since the very early beginnings of human history. The first civilization which 'created' the writing (the Sumers) grew in the Mesopotamia region, between the well known rivers Tigris and Euphrates. The Egyptian civilization relied on the Nile flooding to fertilize the crops: the sediments carried by the river were rich of nutrients and their deposition on the cultivated lands helped the growth of plants. To manage the water resources properly the ancient civilizations built some hydraulic infrastructure around the river environment. Some notable examples are the hanging gardens of Babylon, the Sumerian irrigation channels network and even the Roman aqueducts. Sometimes those networks were used also for military purposes, for example in 2450 BC the king of Lagash diverted the surface waters to interrupt the water supply to the land of Umma (Kreamer 2012). In the last centuries the necessities of modern society led to an increase of civil constructions around the river environment: today it is common to see dams, levees, bridges and weirs along the rivers paths. All those kind of structures are exposed to considerable risks caused by the river, such as flooding and erosion.

The Erosion is a phenomenon particularly dangerous if not properly assessed. Erosion could compromise the stability of every artificial structure which is in direct contact with the flow like bridge pile foundations or levees. When the flow intensity is low the material of the bed is stable and no relevant erosion occurs. When the flow intensity grows the hydrodynamic forces grows too. If the hydrodynamic forces prevails on gravity forces and resistance forces present on the river bed the solid material is detached and carried by the flow: under this condition the sediment transport is triggered.

Sediment transport is constituted by three different "loads": The *Bed load*, the *Suspended load* and the *Wash load* (Graf 1984). The *Bed load* is constituted by the grains that are entrained by the flow, move through rolling or jumping on the bed and finally are deposited. The *Suspended load* is constituted by the grains that are in suspension

in the flow due to the drag force and are deposited when the flow conditions are milder. The *Wash load* is constituted by the finer material which is carried continuously by the river and does not tend to settle. The present study is mainly focused on the analysis of the features of the bed load transport.

The *Bed load* can be described as the composition of two processes. A particle is detached from the bed when the destabilizing forces prevails on the stabilizing forces. The minimum value of destabilizing forces for which this phenomenon occurs is called the *Incipient motion condition*. When the Hydrodynamic forces are smaller than the dynamic friction forces caused by the contact with the bed the particle stops and rests until it is entrained again. This process is called *Deposition*. A third relevant important measure for the bed load transport can be derived by combining the previous processes: the distance from the point in which a particle is entrained and the point in which a particle is deposited is called the "Step Length".

When studying the bed load transport primary importance must be given to the *Incipient Motion Condition*. The first studies on this issue used the Deterministic Approach. One famous study regarding the Incipient Motion Condition is the one proposed by Shields in 1939. In Shields study the Incipient motion condition is expressed as a function of two non dimensional numbers: the Shields shear stress parameter and the Reynolds grain number. Although the Shields study has been an object of many controversies (Buffington 1999) Shields criterion is one of the most widely used even today. The use of Shields criterion to determine the Incipient Motion Condition however led to unsatisfying results. For many authors the reason is that the Incipient Motion Condition is a quantity that is affected by many phenomena that are characterized by fluctuations of hydrodynamic forces. Therefore the Incipient Motion Condition must be considered as random in nature (Yang 1996). The fact that turbulence, bed arrangement and particle dimension are values that are hard (or even impossible) to represent deterministically led to to the development of stochastic approaches to study this phenomenon. One of the most successful stochastic approach was the one proposed by H. Einstein in 1942. In his approach the Incipient motion condition is neglected since it is difficult to define. He also supposed that the approach must include the effect of fluctuations of destabilizing forces due to the randomness of the turbulent fluctuations of velocity. Einstein proposed to evaluate the bed load transport with two basic concept. The Incipient motion condition is represented through a "pick up" probability of the particles lying on the bed. The deposition is represented with the assessment of the average step length that a particle travels before stopping.

On this optics the evaluation of the features of the step lengths is crucial since this quantity is of primary importance for the assessment of bed load transport. Idealistically, if two beds present the same probability of entrainment for a particle with size d but they are characterized by two different average step length the one with higher average step length will present a more intense bed load transport. The assessment of

this quantity has been studied in past studies (Niño et al. 1994), (Lee & Hsu 1994), (Lajeunesse et al. 2010). In those studies the analysis of statistical parameters like mean step length and standard deviation is performed. Lajeunesse in 2010 provided a description of the step lengths in probabilistic terms. Einstein in 1942 supposed that the average travel distance is on average 100 times the mean diameter.

The objective of the present study is to investigate the link between flow conditions (represented through the shear stress parameter) and the statistical features of the bed load transport. The result is achieved through the analysis of the experiments performed in 2009 at the laboratories of the University of Bradford (UK). The experiment were performed to investigate the link between flow field and grain entrainment and the result was published in two papers (Tregnaghi, Bottacin-Busolin, Marion & Tait 2012) and (Tregnaghi, Bottacin-Busolin, Tait & Marion 2012). The experimental apparatus consisted in a tilting flume with a mobile gravel bed. The video recording were obtained by the PIV system installed. The experiments analysed were part of a set of twelve experiments, each one with a different shear stress. The moving grains in the video recordings were manually tracked. Four databases were available: one fully tracked and three partially tracked. Two partially tracked databases on three were analysed a second time and two more tracked databases were added by the author. The analysis of grains rest times, step lengths, velocities and step lengths versus diameter was performed. Particularly, an accurate analysis of the grain step lengths was performed by the imposition of four different statistical models for two reasons. The first reason is to give a description of which is the statistical model which better approximates this phenomenon. The second is to overcome the technical issues caused by the limited amplitude of the examined window of the flume.

After the analysis of the stochastic features of grain motion an analysis of the diffusion was performed. If the recording of the grain trajectories is available it is possible to perform a study of the diffusion. In the case of bed load transport the particles alternates quick movement phases with long resting phases. This kind of process is an anomalous diffusion and can be described as a "random walk with traps" (Bouchaud & Georges 1990). A model for the diffusion for bed load grains was proposed and verified by Nikora in two papers (Nikora et al. 2002), (Nikora et al. 2001). The model assumed three different diffusion phases, depending on the trajectories followed by the grains. Three different diffusion regimes were assumed in the model: the ballistic range (super diffusive), the intermediate range (super diffusive) and the global range (sub diffusive). This kind of analysis was performed on the data obtained by manual tracking and the link between diffusion and the shields non dimensional shear stress parameter was studied.

1.1 Notation

γ_S: Specific weight of solid material

γ_W: Specific weight of water

ϕ: Friction angle

λ: Grain step length

λ_x: Stream-wise step length component

λ_y: Cross-stream step length component

$\overline{\lambda_x}$: Stream-wise mean step length

$\overline{\lambda_y}$: Cross-stream mean step length

ρ_S: Density of solid material

ρ_W: Density of water

τ: Shear stress

τ_0^*: Shields shear stress parameter

υ: Kinematic viscosity

σ: Standard deviation

ω: Terminal fall velocity

A: Area

C_D: Drag coefficient

C_L: Lift coefficient

d: Grain diameter

$d_5 0$: Mean grain diameter

f: Frequency

F_D: Drag force

F_L: Lift force

F_R: Resistance force

g: Gravity force

K_S: Gauckler-Strickler roughness coefficient

M: Moment

p: Probability

q: Specific flow-rate per unit of channel width

q_B: Bed load mass rate

q_C: Critical Water discharge

R: Scaling coefficient

R_e: Reynolds number

R_H: Hydraulic radius

S: Slope

u_*: Shear velocity

u_{g_X}: Grain stream-wise velocity

u_{g_Y}: Grain cross stream velocity

V: Velocity of water

v: Time and depth averaged stream-wise water velocity (flow mean velocity)

v_X: Time averaged stream-wise water velocity

V_d: Water velocity at a distance d above the bed

V_X: Time and depth averaged stream-wise water velocity (flow mean velocity)

W_S: Submerged weight

X: Stream-wise position

$X'(t)$: Fluctuation over the mean

Chapter 2

Literature Review

2.1 Introduction

In this chapter a literature review on the sediment transport is provided. Most of the informations given in this chapter are taken from academic books such as (Yang 1996) and (Graf 1984). The complementary and most recent papers are reported in the Bibliography section.

2.2 Water-Sediment Interface:

To trigger the sediment transport a particle lying on the bed must be entrained by the flow and displaced from its original position. If the flow velocity increases, then an increase of hydrodynamic forces occurs as well. Then, when hydrodynamic forces prevail over stabilizing forces the particles start detaching from the bed and they begin to move: this condition is called incipient motion condition (critical condition).

However, over the years scientists argued that it is hard to define this condition accurately. The reason why it is difficult to determine is that there is not a threshold yet determined above which all the particles in the flow move, and below which the particles remain still. Researchers found that the threshold is highly dependend on the investigator's definition of movement (Beheshti & Ataie-Ashtiani 2008), therefore laboratory analysis are biased from human error. In addition the problem is affected by a wide range of random charachtersitcs such as turbulence, or grain shape and size (Buffington & Montgomery 1997),(Yang 1996). Most of approaches used in the past are based on the balance of forces that are acting on a particle located on the bed. The

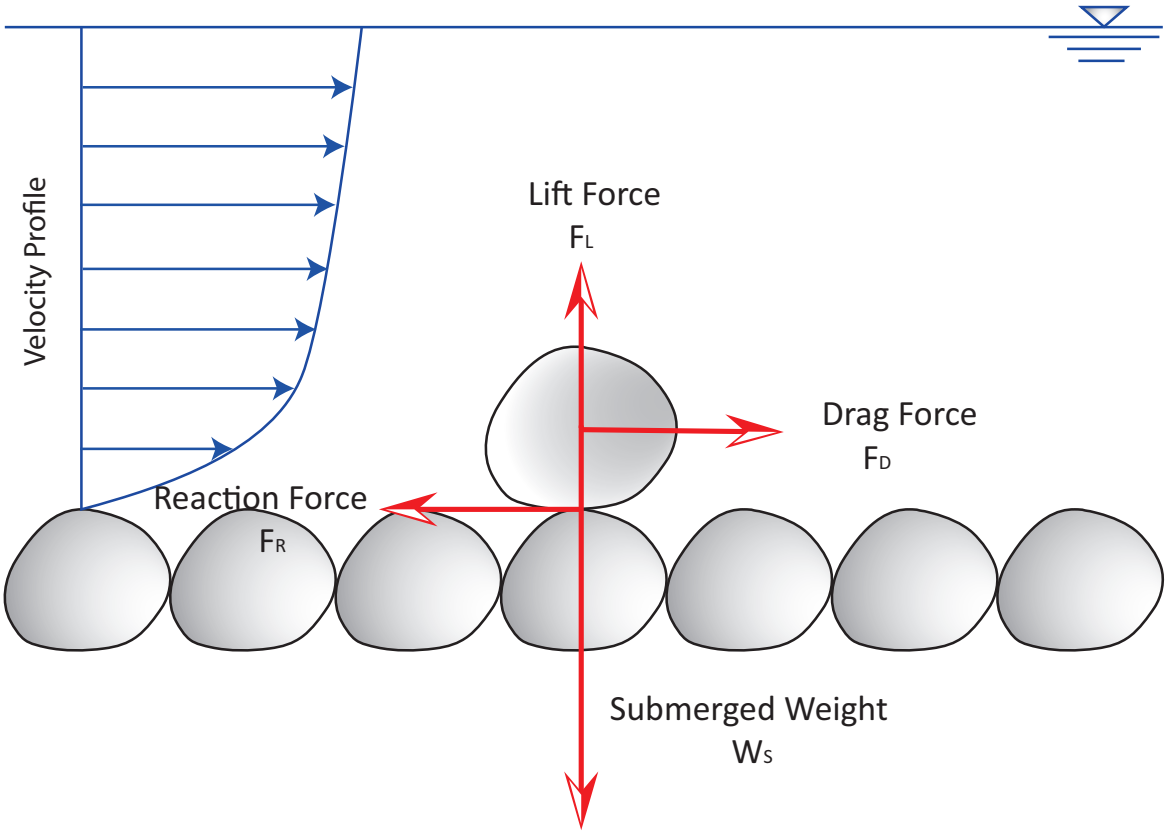

Figure 2.1: Forces acting on a particle invested by water flow

force system considered is reported in Figure 2.1.

In this case four forces acting on the particle are considered: F_L is the lift force, F_D is the drag force, W_S is the submerged weight and F_R is the resistance force. An accurate description of these forces is reported in the next paragraphs. The sediment transport is composed by three different processes as reported in Figure 2.2.

- Bed load: This category involves all the particles that moves along the bed through rolling, sliding and jumping. Usually it is composed by the coarser fraction of the river bed material. This is the transport modality analysed in the present study.
- Suspended load: This category is composed by the particles that once entrained are kept in suspension for a relevant time. The suspended load is deposited where the current decelerates and the magnitude of hydrodynamic forces decreases.
- Wash load: The wash load is composed by material that is usually finer than the one found in the river bed. The magnitude of the wash load is dependent on the properties of the watershed and not on the characteristics of the river.

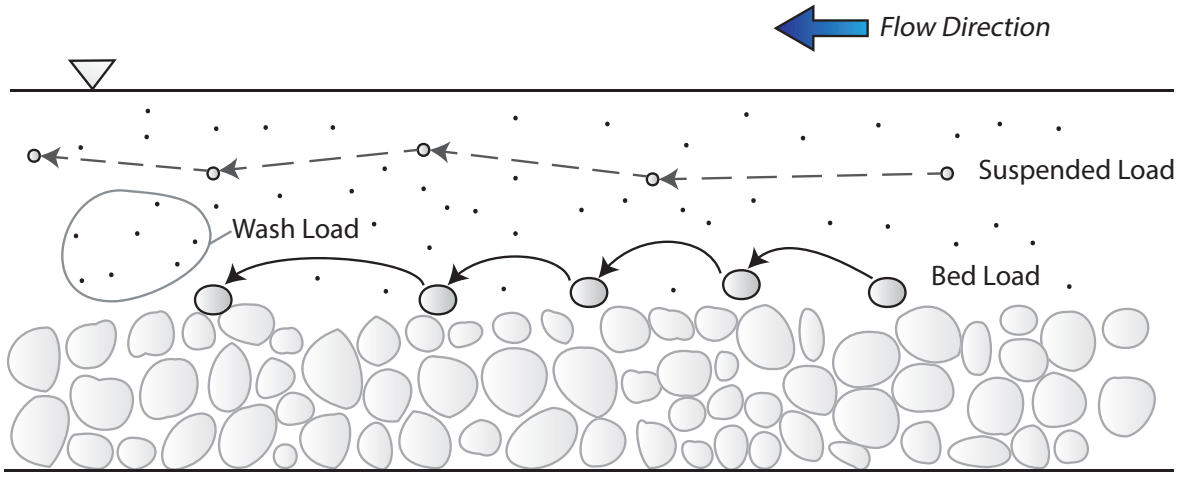

Figure 2.2: Different transport processes

2.2.1 Hydrodynamic Forces

The first force to define is the Drag force. This force is present in a wide range of phenomena, for example when a plane is moving in the air, a boat is sailing in the sea, or a soil particle is surrounded by moving water. This force is caused by turbulent wakes that are generated by the flow due to the presence of an obstacle. The case of a particle invested by a fluid is reported in Figure 2.3.

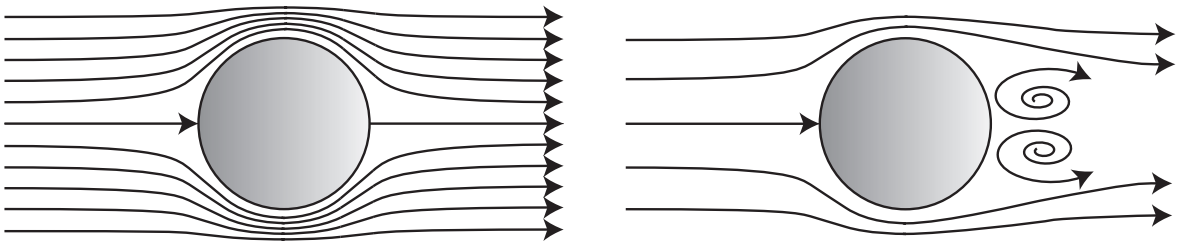

Figure 2.3: Streamlines for ideal flow (left) and real flow (right)

The ideal flow is reported in Figure 2.2 (left). Streamlines goes around the obstacle and are symmetric to vertical axis. In this case the drag force is zero, since there is not a pressure variation between the upstream and downstream side of the obstacle. However, in Figure 2.2 (right) it is reported what happens in a real flow. The streamlines are not symmetric, a turbulent wake is generated in the downstream side and the pressure decreases. The pressure gradient generates a force that was found proportional to

the relative velocity of the particle in the fluid. This force can be computed through the following formula:

$$F_D = C_D \cdot A \cdot \rho_w \cdot \frac{v^2}{2} \tag{2.1}$$

Where C_D is the drag coefficient, A is the area of the particle invested by the flow (usually the projection of the particle surface in the direction of the relative velocity), ρ_W is the density of the fluid and v is the relative velocity. The drag coefficient depends on two variables: The Reynolds number and the particle shape and smoothness. The C_D coefficient in the case of a smooth spherical particle in water is reported in Figure 2.4.

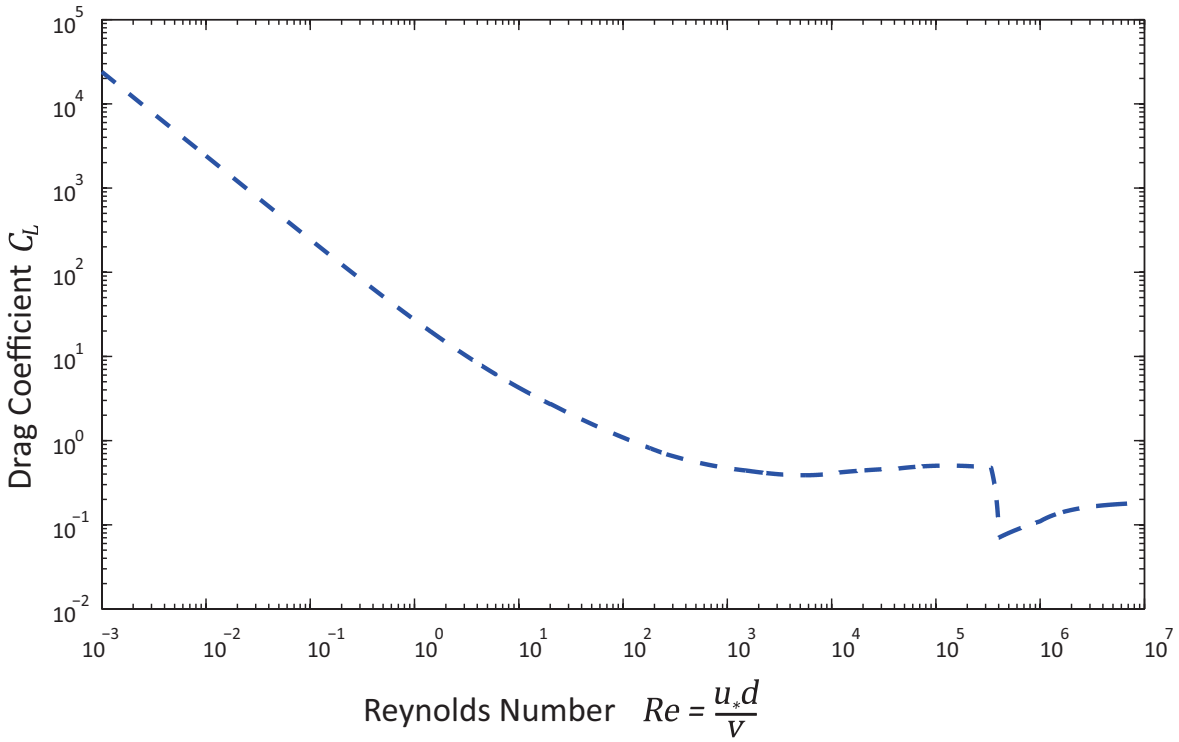

Figure 2.4: Drag coefficient versus Reynolds Number for a spherical particle

The drag coefficient is a linear function for low values Reynolds number:in this condition the viscous forces play a major role. For higher values (when turbulent forces prevail) the drag coefficient is less dependent by the Reynolds number. This diagram however is valid for a spherical shape only. Unfortunately, the relationship between Drag coefficient and Reynolds number is strongly affected by the particle shape and surface characteristics.

The second force to define is the Lift force. This force is of fundamental importance for a wide range of applications. Lift force is studied in lots of fields, and it is one of the principal forces studied in aerodynamics: this force is the main mechanism that allows the aeroplanes to take off. The origin of this effect is very similar to the drag force. This force is caused by a vertical pressure gradient generated by a velocity gradient along the vertical direction. The example reported in Figure 2.5 represents a particle in the river bed invested by the flow.

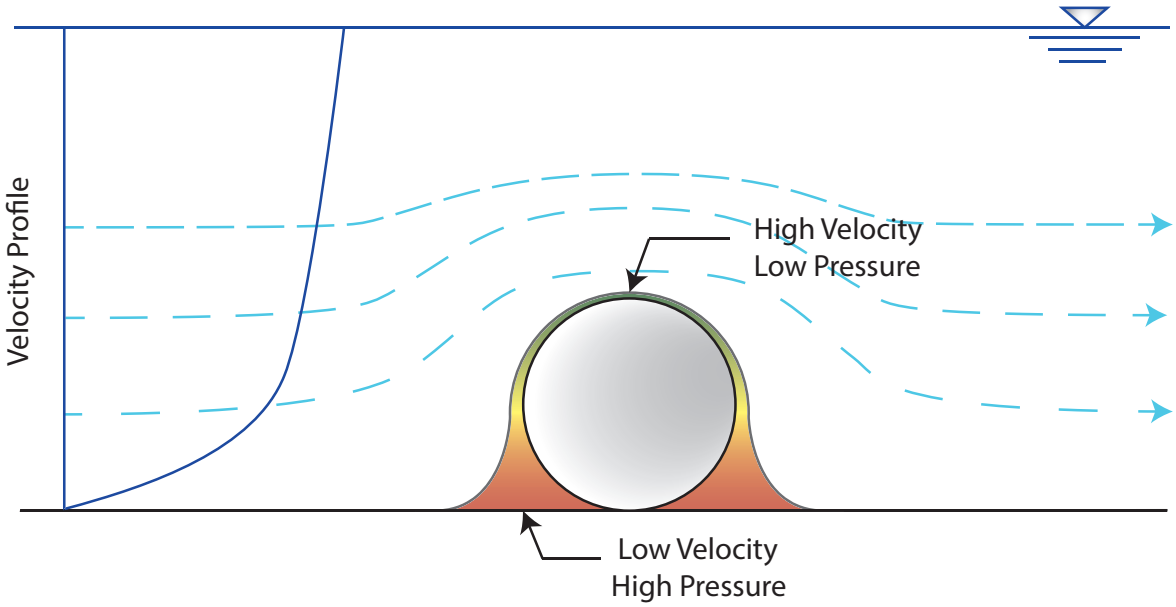

Figure 2.5: Lift force acting on a bed particle

Lift effect in water was modelled by researchers exactly like the drag force with just a substitution in the formula. The drag coefficient C_D was replaced with the lift coefficient C_L. Therefore the formula used in this case will be:

$$F_L = C_L \cdot A \cdot \rho_w \cdot \frac{v^2}{2} \tag{2.2}$$

The value of C_L was determined in function of the Reynolds number and the particle characteristics, just like the drag force. However, previous considerations regarding the use of different values of lift coefficient for different particle shapes are valid also in this case.

2.2.2 Gravity Forces

The third force to define is the submerged weight. The submerged weight is the only force that can be computed exactly if the particle volume is known. It is just the weight of a particle in water: the net gravitational weight subtracted with the Archimedean's uplift. For a spherical particle of diameter d the submerged weight is:

$$W_S = (\gamma_S - \gamma_W) \cdot \frac{4}{3} \cdot \pi \cdot \frac{d^3}{3} \tag{2.3}$$

The Resistance force is the force that determines if a particle is in equilibrium or not. Usually, it is a function of the weight acting on the supporting plane multiplied by a friction factor. For the simple geometry described in the figure above (if the soil is modelled as surface with friction) the resistance force can be expressed as:

$$F_R = (W_S - F_L) \cdot \tan(\phi) \tag{2.4}$$

Where ϕ is the friction angle of the soil, therefore $\tan(\phi)$ will be the friction factor in this case. However, this force is highly dependent upon the geometry of the system. A particle which is located the bottom of a pocket in the river bed will be harder to remove respect to a particle which protrudes significantly. Those effects are hard to describe deterministically. Usually an accurate description of the resistance force is a very complicated task.

2.3 Incipient motion condition:

The incipient motion condition can be idealistically defined when the equilibrium between destabilizing and stabilizing forces along one direction is reached or when the overturning moment is equal to the resisting moment: a little increase of the destabilizing forces will start the particle motion. By studying the equilibrium condition of the forces three different entrainment mechanism can be identified:

- $F_D > F_R$: The particle is entrained by the flow through an horizontal displacement (sliding).
- $F_L > W_S$: The particle is entrained by the flow through a vertical displacement (lifting)
- $M_{Destamilizing} > M_{Stabilizing}$: The particle is entrained through a rotation (rolling)

In most of the cases the condition that fails earlier is the one defined for the horizontal displacement. Unfortunately, the exact expression of these stabilizing or destabilizing forces is possible for very simplified systems only. Some notable criteria are provided here, based on the different approaches used to study the problem.

2.3.1 Shear Stress Approach: Shields (1936)

The aim of shear stress approaches is to define the incipient motion condition as a critical shear stress. Therefore if the shear stress acting on the bed is higher than the "critical shear stress" the sediment transport is triggered. One of the most famous and widely used approaches to study the incipient motion condition is the Shields approach (Shields 1936). This approach is based on dimensional analysis. The first step to perform a dimensional analysis is to define which factors drive the phenomenon. The parameters considered in Shields analysis are:

- τ : Average shear stress at the bottom $[N/m^2]$
- $\rho_S - \rho_W$: Submerged density of the particle $[g/m^3]$
- d : Particle's diameter $[m]$
- v : Kinematic viscosity $[m^2/s]$
- g : Gravitational Acceleration $[m/s^2]$

By applying Buckingham's theorem there is a function of these quantities that has value zero, as stated below:

$$f(\tau, \rho_S - \rho_W, d, v, g) = 0 \tag{2.5}$$

Since there are 5 parameters and 3 dimensions, the problem can be expressed as a function of two non-dimensional numbers. The numbers (chosen by Shields) are:

$$f\left(\frac{\tau}{(\gamma_S - \gamma_W)d}, \frac{u_* d}{v}\right) = 0 \Rightarrow \frac{\tau}{(\gamma_S - \gamma_W)d} = f'\left(\frac{u_* d}{v}\right) \tag{2.6}$$

Where the first number is called Shields number or Shields parameter, and the second is called the shear Reynolds number (or grain Reynolds number). The points obtained through experimental observations of the incipient motion condition were plotted in a plane with Shear stress parameter against Reynolds number. The result was the well-known Shields diagram. The digram is reported in Figure 2.6.

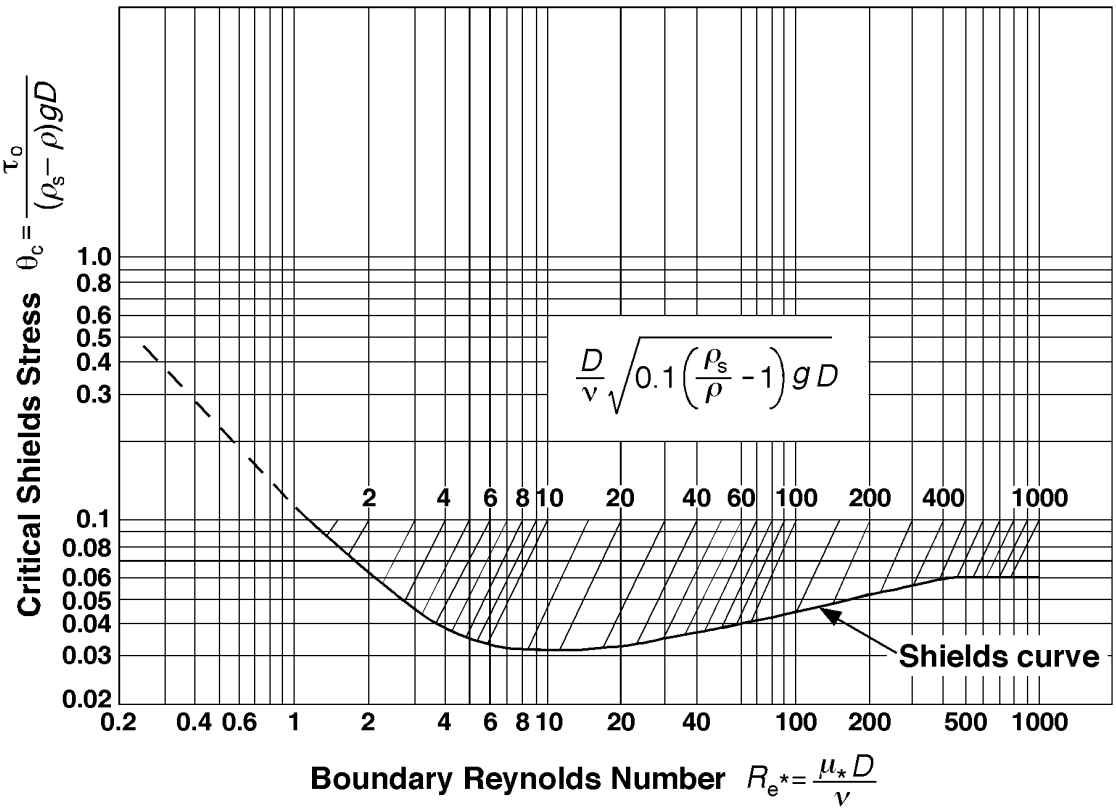

Figure 2.6: Shields Critical Stress Diagram

The "no-motion" condition is a critical definition since it depends on the investigator's sensibility. The criterion followed by Shields was composed by two steps. The first was the construction of shear stress against transport rate curves. The second was the calculation of the shear stress value corresponding to zero transport rate through the extrapolation of those curves. For low values of the Reynolds grain number, the dependency of these two quantities is very strong. For high values of shear Reynolds number the Shields parameter assumes a constant value. This approach is generally well accepted and widely used.

2.3.2 Velocity Approach: Yang (1973)

The purpose of the velocity approach is to define an incipient motion condition based on the average velocity of the flow. If the mean flow velocity is greater than the critical velocity the sediment transport is triggered. Yang's approach (Yang & Sayre 1971) starts by considering the force balance on a particle under these assumptions:

- Negligible channel slope (stream wise gravitational force component is neglected)
- Spherical bed material
- Logarithmic velocity distribution
- Incipient motion condition happens when drag force prevails over resistance force

The purpose of the approach followed by Yang is to obtain a dimensionless critical velocity which is a ratio between the average flow velocity V_X and the terminal fall velocity ω. The drag force acting on a spherical particle can be expressed as:

$$F_D = C_D \cdot \pi \cdot \frac{d^2}{4} \cdot \rho_w \cdot \frac{v^2}{2} \tag{2.7}$$

Where C_D is the Drag coefficient (function of Reynolds number and particle's shape), V_d speed at a distance d above the bed, d particle diameter and ρ_w water density. When the terminal fall velocity is reached:

$$F_D = W_S \Rightarrow C'_D \cdot \pi \cdot \frac{d^2}{4} \cdot \rho_w \cdot \frac{\omega^2}{2} = \pi \cdot \frac{d^3}{6} \cdot g \cdot (\rho_S - \rho_w) \tag{2.8}$$

Where ω is the terminal fall velocity. By imposing $C'_D = \psi_1 \cdot C_D$ and substituting 2.8 in 2.7 the resulting expression for the drag force in function of the terminal fall velocity is:

$$F_D = \pi \cdot \frac{d^3}{6 \cdot \psi_1} \cdot g \cdot (\rho_S - \rho_w) \cdot \left(\frac{V_d}{\omega}\right)^2 \tag{2.9}$$

The next step is to express the drag force in function of the mean velocity instead than the velocity just in top of the grain (d height). If the velocity profile is logarithmic the mean velocity can be written as:

$$\frac{v_X(z)}{u_*} = 5.75 \cdot \log \frac{z}{d} + B \tag{2.10}$$

Where v_X is the mean stream wise velocity in function of the height z, u_* is the shear velocity and B a function of the roughness. At $z = d$ the argument of the logarithm is 1, therefore:

$$v_X(z=d) = V_d = B \cdot u_* \tag{2.11}$$

The average velocity of the logarithmic profile can be obtained through integration and can be expressed as:

$$\frac{V_X}{u_*} = 5.75 \cdot \left[\log\left(\frac{D}{d} - 1\right) + B\right] \tag{2.12}$$

By substituting u_* from 2.12 in 2.11 and substituting the expression found for V_d from 2.11 in 2.9 the result is:

$$F_D = \pi \cdot \frac{d^3}{6 \cdot \psi_1} \cdot g \cdot (\rho_S - \rho_w) \cdot \left[\frac{B}{5.75 \cdot \log\left(\frac{D}{d} - 1\right) + B}\right]^2 \cdot \left(\frac{V_X}{\omega}\right)^2 \tag{2.13}$$

Since that it is possible to determine the relation between drag coefficient and the lift coefficient experimentally, we can consider $C_D = \psi_2 \cdot C_L$. Therefore lift fore can be expressed as:

$$F_L = \pi \cdot \frac{d^3}{6 \cdot \psi_1 \cdot \psi_2} \cdot g \cdot (\rho_S - \rho_w) \cdot \left[\frac{B}{5.75 \cdot \log\left(\frac{D}{d} - 1\right) + B}\right]^2 \cdot \left(\frac{V_X}{\omega}\right)^2 \tag{2.14}$$

The resistance force can be obtained as the friction factor ψ_3 multiplied by the difference between the submerged weight and the lift force. Therefore:

$$F_R = \psi_3 \cdot (W_S - F_L) = \psi_3 \cdot \pi \cdot \frac{d^3}{6} \cdot g \cdot (\rho_S - \rho_w) \cdot \left\{1 - \frac{1}{\psi_1 \cdot \psi_2} \cdot \left[\frac{B}{5.75 \cdot \log\left(\frac{D}{d} - 1\right) + B}\right]\right\}^2 \cdot \left(\frac{V_X}{\omega}\right)^2 \tag{2.15}$$

Now all forces have been expressed as function of the dimensionless average velocity. If the incipient motion condition is assumed through the equilibrium along horizontal direction therefore: $F_D = F_R$ and $V_X = V_{cr}$. After few algebraic operations the following result can be obtained:

$$\frac{V_C}{\omega} = \left[\frac{5.75 \cdot \log(D/d - 1)}{B} + 1\right] \cdot \left(\frac{\psi_1 \cdot \psi_2 \cdot \psi_3}{\psi_2 + \psi_3}\right)^{\frac{1}{2}} \tag{2.16}$$

The model for the roughness function is the one reported in (Schlichting et al. 2000). In that study it is assumed that there are three conditions:

- Hydraulically Smooth Regime:

$$\frac{u_* \cdot d}{\nu} < 5 \Rightarrow B = 5.5 + 5.75 \cdot \log\left(\frac{u_* \cdot d}{\nu}\right)$$

- Transition Regime:

$$5 < \frac{u_* \cdot d}{\nu} < 70 \Rightarrow \texttt{B is weakly dependent on } \frac{u_* \cdot d}{\nu}$$

- Completely Rough Regime:

$$\frac{u_* \cdot d}{\nu} > 70 \Rightarrow B = 8.5$$

The coefficients ψ_1, ψ_2, ψ_3 can be obtained from experimental investigations. The result proposed by Yang is reported in Figure 2.7.

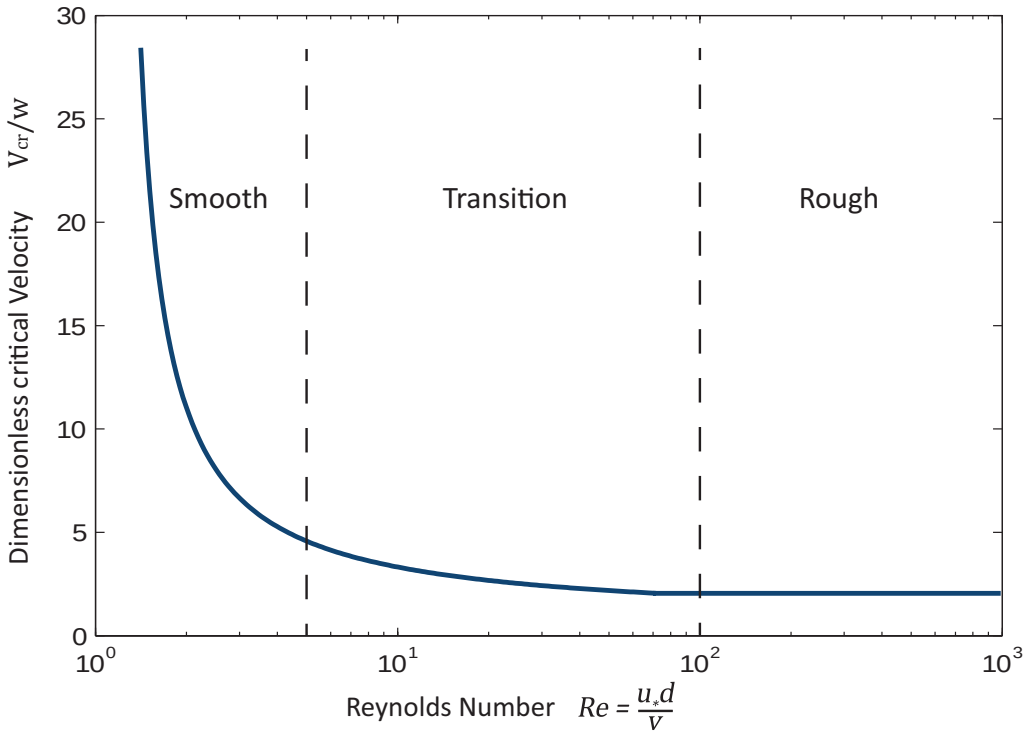

Figure 2.7: Yang's Critical Velocity Diagram

2.3.3 Review on Probabilistic Approach

The introduction of a probabilistic approach to study the incipient motion condition was necessary due to difficulties in defining all the phenomena that occurs in the

water-soil interface. Many of these phenomena (like turbulence) have a random nature. Many others, like particle diameters, particle elevation respect to the mean bed level or particle shape are also hard to describe deterministically. However, a stochastic approach can be successfully used to describe those quantities.

One notable approach is the one followed by Gessler in (Gessler et al. 1968). He studied the probability that a given grain will stay still and will not be entrained by the flow. He found that the probability that a particle will stay is mainly correlated with the Shields shear stress parameter. The result is shown in Figure 2.8.

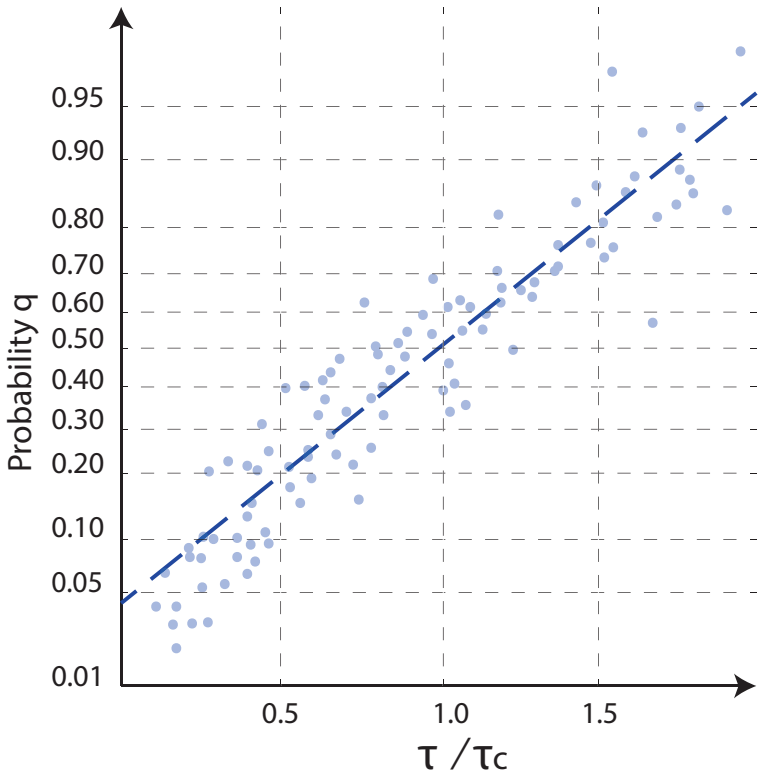

Figure 2.8: Gessler Probability of Removal

Scattering is quite high, but it is important to notice that for shear stress values equal to the critical shear stress obtained by Shields diagram ($\tau/\tau_c = 1$), there's a probability of 50% that a particle will stay. Therefore sediment transport is happening also at shear stresses lower than the critical one. This approach allows to calculate the eroded bed grain composition given the original grain size distribution and the flow conditions. Given $p_0(d)$ the probability distribution of the bed grains, the armour layer frequency function p_a (or the probability distribution of the grains that are not moving) is defined as:

$$p_a(d) = k_1 \cdot q(d) \cdot p_0(d) \tag{2.17}$$

Where $q(d)$ is the probability that a grain of size d will stay and k_1 a constant factor to keep the area of the pdf equal to the unit. Therefore the grain size distribution will be:

$$P(d) = \int_{d_{min}}^{d} p_a(x)dx = \int_{d_{min}}^{d} k_1 \cdot q(x) \cdot p_0(x)dx \tag{2.18}$$

One of the most important stochastic approaches to study incipient motion condition in sediment transport was the one developed by Grass in 1970 . He proposed to compute the stress acting on the particle through the study two different statistical distributions (Grass 1970):

- $p(\tau_w)$: Probability density function of the shear stress that is induced by the flow on the bed particles
- $p(\tau_{wc})$: Shear stress threshold, in other words the probability density function of the shear stress required to entrain a particle

When the two probability distribution overlaps the grains with lower shear stress threshold begin to move. He proposed to evaluate the overlapping as follows:

$$\overline{\tau_w} - n \cdot \sigma_w = \overline{\tau_{wc}} - n \cdot \sigma_{wc} \tag{2.19}$$

Where n is a factor that quantifies the overlapping of the two distributions. This value can be used as proxy for the intensity of particle entrainment. When $n = 0.625$ he found that the curves merges with the ones found by Shields.

After Grass formulation, several studies were focused on understanding which phenomena should be considered to study the entrainment probability.

In recent studies (Cheng & Chiew 1998),(Wu & Lin 2002) the formulation of entrainment probability was related to the instantaneous velocity probability distribution. They looked at the definition of a particle entrainment probability in relation to flow conditions. In a recent study (Wu & Chou 2003) the work was extended with the inclusion of turbulent fluctuations in the instantaneous velocity and the randomness of the bed for the calculation of lifting and rolling probabilities.

Other researchers used the probabilistic approach to study which is the main physical phenomenon that starts particle entrainment. In recent years many scientists argued that the definition of a critical shear stress to define particle entrainment is not suitable for bed forms, since under those conditions the turbulence cannot be successfully described by the local shear stress. In a recent paper it was found that the entrainment depends on the kind of turbulence interaction with the bed (Nelson et al. 1995), increasing the interest in quadrant analysis of the turbulence velocity fluctuations.

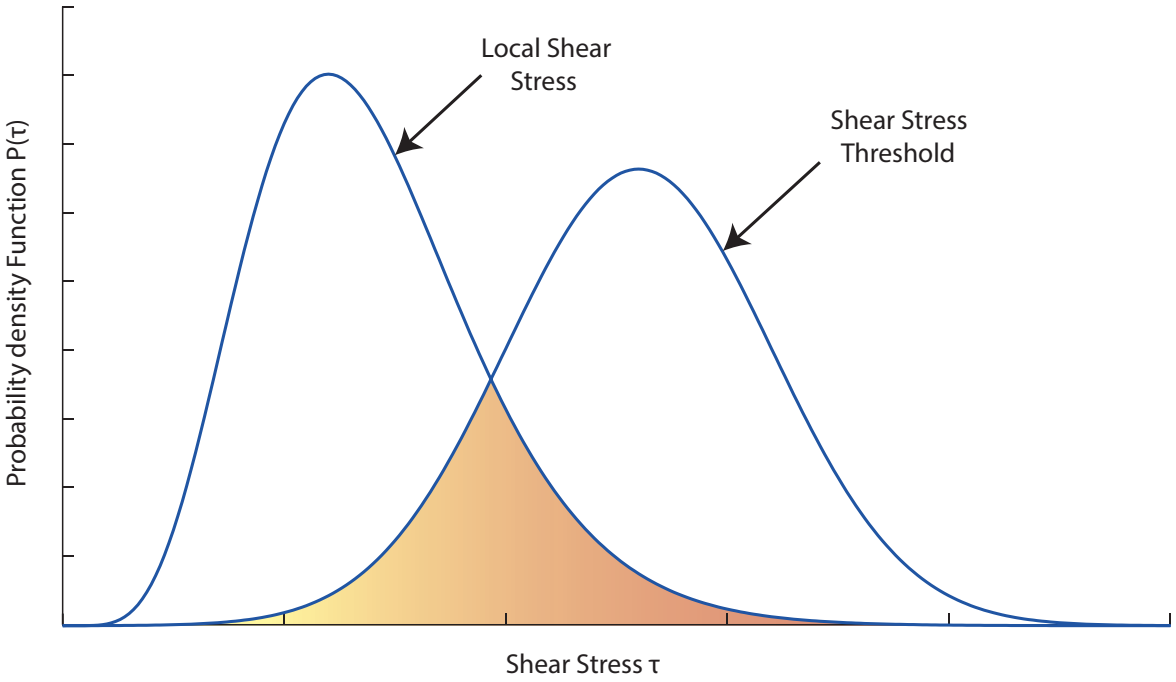

Figure 2.9: Grass Approach: PDFs of local and critical shear stress

In a recent paper by Tregnaghi (2012) a statistical framework following the approach supposed by Grass was provided. The entrainment risk was evaluated through the following relation:

$$\int_0^{\tau_f} \int_{-\infty}^{+\infty} \int_{-\infty}^{+-\infty} f_{T_f}(\tau_f|z_g) \cdot f_{T_g}(\tau_g|z_g) \cdot f_{z_g}(z_g) \cdot dz_g d\tau_g d\tau_f \tag{2.20}$$

Where the different components of this equation can be described as follows:

- f_{z_g} is the probability density function of the grain elevations. Laboratory experiments showed that grain elevations in water worked gravel deposits follow a normal distribution.
- $f_{T_f}(\tau_f|z_g)$ is the probability density function of fluid shear stress. The author proposed a model for shear stress accounting the following effect:
  - The effect due to the hiding or exposure of a particle.
  - The effect of the vertical distributions of mean fluid velocity.
- $f_{T_g}(\tau_g|z_g)$ is the probability density function of the critical shear stress. When evaluating this quantity the following dependencies should be considered.

- The turbulence of the near bed field
- The stochastic nature of the resisting forces due to the relative position of bed grains.
- The variation in local velocity due to the presence of protruding grains.

2.3.4 Empiric Approach: Meyer-Peter and Müller (1948)

A famous equation to estimate the incipient motion condition was the one proposed by Meyer-Peter and Müller in 1948 (Yang 1996),(Meyer-Peter & Müller 1948). This formula was obtained by the experimental relations of well-known hydraulic parameters.

$$d = \frac{S \cdot D}{0.058 \cdot \left(n/d_{90}^{1/6}\right)^{2/3}} \tag{2.21}$$

Where S is the channel slope, D the mean flow depth, d_{90} the diameter corresponding to the bigger 10% grains and n is Manning's roughness coefficient (or $n = 1/K_s$ where K_s is Gauckler-Strickler's coefficient). This formula implies that incipient motion condition is always reached for very low diameters.

2.4 Bed Load Transport:

2.4.1 Introduction

If the flow intensity exceeds the threshold imposed from the incipient motion condition then sediment transport is triggered. Bed material is entrained and carried by the stream for a while, then deposited. Sometimes in natural rivers it is quite easy to spot if this process is happening, due to the drastic change in water color as shown in Figure 2.10.

The intensity of sediment transport is the quantity that is of primary matter to assess phenomena such as erosion. It is important to understand if some areas will be eroded in one, ten, fifty or more years. One of the most relevant part of sediment

Figure 2.10: River Sheaf during 2007 flooding, Sheffield, U.K.

transport is the bed load transport: the material transported through rolling, jumping and sliding along the bed. In the following section some relevant criteria about the quantification of sediment transport will be provided.

2.4.2 Shear Stress Approach: DuBoy's (1879)

DuBoy approached the problem by conceptually dividing the bed in moving layers. Each layer moves due to the action of the tractive force of the moving fluid. Every layer must not accelerate or decelerate, therefore the tractive force should be balanced by the sum of the resistance forces between all layers. Therefore:

$$\tau = \gamma_w \cdot D \cdot S = C_f \cdot m \cdot \varepsilon \cdot (\gamma_s - \gamma_w) \tag{2.22}$$

Where C_f is the friction coefficient, m is the total number of layers, ε is the thickness of a layer, D is the water depth, γ_S and γ_W the specific weight of the grain and water respetively and S is the slope. A graphic representation is reported below in Figure 2.11.

The velocity profile is supposed to be linear dependent with the number of layers. The total discharge per unit of width will be:

$$q_B = \varepsilon \cdot V_S \cdot \frac{m(m-1)}{2} \tag{2.23}$$

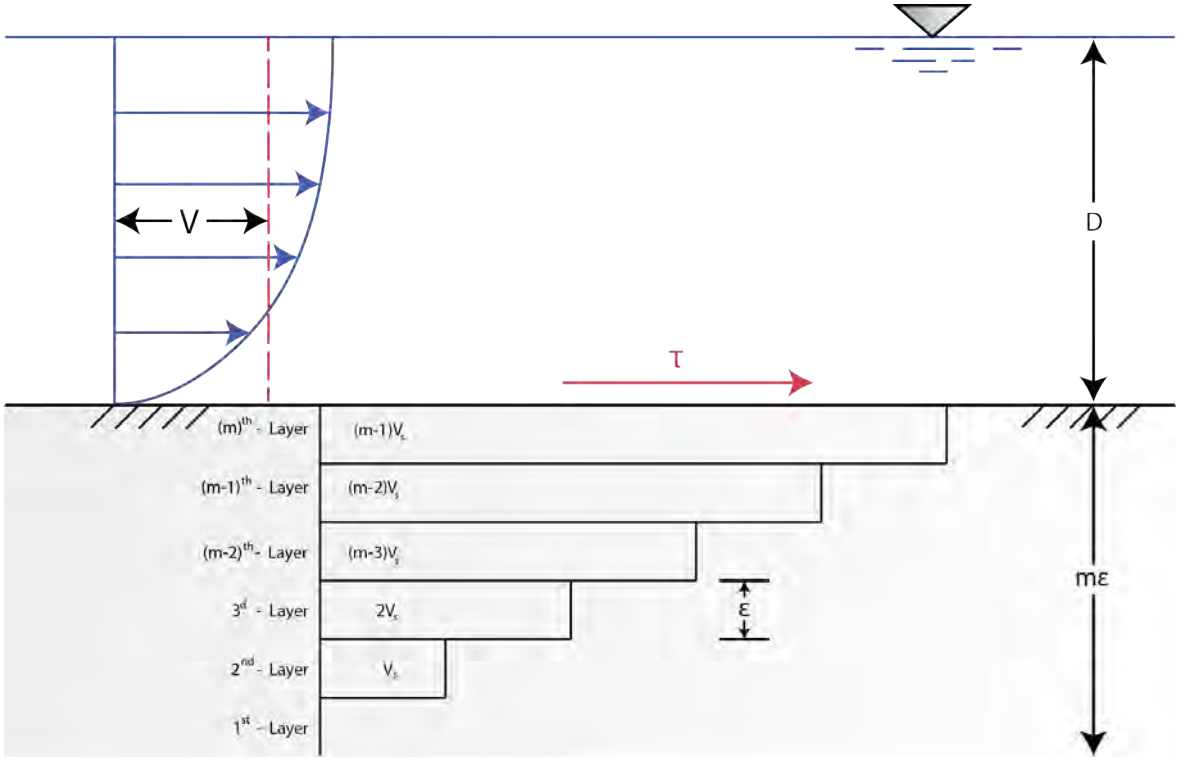

Figure 2.11: System under DuBoy's Approach

Where V_S is the velocity corresponding to the second layer as shown by the figure. The critical condition to start the motion is defined when $m = 1$: idealistically no motion is occurring, but any further increase in shear stress will trigger bed load transport. Under those conditions, from equation 2.23:

$$\tau_c = C_f \cdot \varepsilon \cdot (\gamma_s - \gamma_w) \Rightarrow m = \frac{\tau}{\tau_c} \tag{2.24}$$

Therefore where τ_c is defined as the "critical" tractive force acting on the bed. If m is substituted in equation 2.23, the result will be:

$$q_B = \frac{(\varepsilon \cdot V_s)}{2 \cdot \tau_c^2} \cdot \tau \cdot (\tau - \tau_c) = K \cdot \tau \cdot (\tau - \tau_c) \tag{2.25}$$

In this case the coefficient K is a proxy for the bed material. Therefore, DuBoys formula states that bed load grows as a squared function of the shear stress at the bottom when flow conditions exceeds the critical threshold. Strobe in 1935 found that the K coefficient is inversely proportional to the bed particle diameter d through the following relation:

$$K = \frac{0.173}{d^{3/4}} \tag{2.26}$$

However, the fundamental hypothesis of this approach (the sliding layer bed load) does not represent what happens in reality. However, at the time this formula was widely used for its simplicity. Many channels were designed according to this criterion. Further investigations were conducted on this approach.

One approach carried on by Shields (1936) was through dimensional analysis. His formula is still a DuBoys kind of formula with a more specified coefficient. Shields formula for bed load is reported below:

$$\frac{q_B}{q} \cdot \frac{\gamma_S}{\gamma_W \cdot S} = 10 \cdot \frac{\tau - \tau_C}{(\gamma_S - \gamma_W) \cdot d} \tag{2.27}$$

With q water discharge per unit of width. The other parameters have the same meaning used in previous equations. The parameters list and their meaning can be found in the summary.

2.4.3 Discharge Approach: Schoklitsh (1934)

The approach followed by Schoklitsh in 1934 was to determine the bed load transport as a function of water discharge. In this kind of approach the "critical" condition can be defined in terms of water discharge at incipient motion condition. The Schoklitsh formula is reported below:

$$q_B = 7000 \cdot \frac{S^{3/2}}{d^{1/2}} \cdot (q - q_c) \tag{2.28}$$

Where q_B is the bed load per unit of width $[kg/(s{\cdot}m)]$, d is the particle size expressed in $[mm]$, q_C is the specific flux per unit of width at critical conditions $[m^3/(s \cdot m)]$ and q is the specific flux per unit of width $[m^3/(s \cdot m)]$.

Therefore following Schoklitsh approach, bed load transport is linearly related with the excess of discharge. Where q and q_c are water discharge and water "critical" discharge respectively. The entrainment condition in terms of water discharge was expressed through the following formula:

$$q_C = \frac{1.944 \cdot 10^{-5}}{S^{4/3} \cdot d} \tag{2.29}$$

2.4.4 Energy Slope Approach: Meyer-Peter and Müller (1948)

A famous approach proposed by Meyer-Peter and Müller relates the bed load transport as a function of the energy slope. Their formula is reported in Equation 2.30.

$$\gamma_W \cdot \left(\frac{K_S}{K_R}\right)^{2/3} \cdot R_H \cdot S = 0.047 \cdot (\gamma_s - \gamma_W) \cdot d + 0.25 \cdot \rho_W^{1/3} \cdot q_B^{2/3} \tag{2.30}$$

Where ρ_W is the density of water, R_H is the hydraulic radius, K_S is the Gauckler-Strickler's coefficient and K_R represents that only a portion of energy is lost through grain resistance. The energy slope S can be determined through Strickler's formula, instead K_S and K_R are both expressed as a function of the diameter d. Particularly, K_R is expressed as follows:

$$K_R = \frac{26}{d_{90}^{1/6}} \tag{2.31}$$

Where d_{90} is the size for which the 90% of the bed material is finer.

2.4.5 Probabilistic Approach: Einstein (1942)

The probabilistic approach followed by Hans Einstein in 1942 is totally different from the approaches used to study bed load proposed in the previous years. All previous approaches were based on the definition of a critical threshold that can be defined in terms of shear stress, discharge, velocity ecc. Those conditions are hard to define deterministically for the reasons reported in section 2.2.2. Furthermore, Einstein supposed that the bed load transport in primarily related to the magnitude of fluctuations around mean quantities, instead previous approaches are based on average quantities.

For these reasons the model proposed by Einstein separates the problem in three different processes that can be studied through a probabilistic approach. The bed load is the effect of three processes:

- Starting condition: A particle lying on the bed has a probability to be entrained that can be related to flow conditions. A threshold can't be defined in terms of a value, but it can be defined as a probability distribution of entrainment risk. This leads to a continuous exchange between the grains lying on the bed and moving grains. This continuous exchange is what determines the entrainment rate.

- Moving condition: Once that a particle is entrained by the flow, its path is a sequence of steps. A particle is supposed to move downward by alternating quick moving phases and long resting periods. Einstein supposed that the average step is about 100 times the particle diameter, therefore it is not related to flow intensity.

- Deposition condition: A particle entrained will deposit if the hydrodynamic forces will allow it. Therefore the deposition condition can be defined in terms of probability. The rate of deposition can be defined as a function of the transport rate and the deposition probability.

As reported in the introduction the transport is made of these three different processes. A channel is under stable condition if the rate of entrainment is equal to the rate of deposition. If the entrainment rate exceeds the deposition rate, erosion is occurring (Einstein 1950).

1. The number of particles that are deposited per unit of area and time can be expressed as reported in equation 2.32

$$N_d = \frac{q_{bw} \cdot i_d}{(A_L \cdot d) \cdot (\gamma_S \cdot A_2 \cdot d^3)} \tag{2.32}$$

   Where q_{bw} is the bed load discharge in terms of weight per unit of channel width $[N/(m \cdot s)]$, i_{bw} is the percentage in weight of bed load made by a given size d (if the material is uniform $i_d = 1$) ,$A_L \cdot d$ is the average step length ($100d$) and $\gamma_S \cdot A_2 \cdot d^3$ is the weight of a particle with size (therefore A_2 represents a volume coefficient i.e. $\frac{4 \cdot \pi}{3 \cdot 8}$ for a sphere).

2. The number of entrained particles (or eroded) per unit of area and time is reported in equation 2.33

$$N_e = \frac{i_b}{A_1 \cdot d^2} \cdot \frac{p}{t_1} \tag{2.33}$$

   Where: i_b is the number of particles available in the bed, p the probability of entrainment of a particle (or removal), t_1 is the time of exchange between the bed and the flux (bed-load) and $A_1 \cdot d^2$ is the bed particle area (therefore A_2 represents a surface coefficient i.e. $\pi/4$ for a circular section). The scale time can be expressed as:

$$t_1 = A_3 \cdot \left[\frac{\gamma_W \cdot d}{g \cdot (\gamma_S - \gamma_W)} \right]^{1/2} \tag{2.34}$$

At equilibrium condition, as stated above, the number of particles that are "eroded" and the number of particles that are deposited must be equal. By imposing $N_d = N_e$ the function reported in equation 2.35 can be obtained:

$$\frac{q_{bw} \cdot i_d}{(A_L \cdot d) \cdot (\gamma_S \cdot A_2 \cdot d^3)} \cdot A_3 \cdot \left[\frac{\gamma_W \cdot d}{g \cdot (\gamma_S - \gamma_W)}\right]^{1/2} = \frac{i_b}{A_1 \cdot d^2} \cdot \frac{p}{t_1} \tag{2.35}$$

After some basic operations and by substituting t_1 in equation 2.35 from 2.34 the following formula can be obtained:

$$\frac{q_b w}{\gamma_s \cdot d)} \cdot \left[\frac{\gamma_W \cdot d}{g \cdot (\gamma_S - \gamma_W)}\right]^{1/2} = \frac{i_b}{i_d} \cdot \frac{A_L \cdot A_2 \cdot d}{A_1 \cdot A_3} \cdot p \tag{2.36}$$

The exchange probability p is defined by as the amount of time in which the lift force is greater than the weight of the particle. However, it is possible to express the travel distance (the distance between two rest positions, also referred to as "step") as a function of the probability of entrainment. If p is small enough the travel distance is constant, and it is assumed that $\lambda = 100 \cdot d \Rightarrow A_1 = 100$. If p is high the deposition is less likely to occur.

Let us imagine that after a travel distance λ, $(1-p)$ particles deposit and p particles keep moving. After a distance 2λ, $p(1-p)$ particles will deposit and p^2 particles will keep moving. Therefore the average travel distance can be expressed as:

$$\overline{\lambda} = \sum_{n=0}^{\infty}(1-p) \cdot p^n \cdot (n+1) \cdot \lambda = \frac{\lambda \cdot d}{1-p} = A_L \cdot d \Rightarrow A_L = \frac{\lambda}{1-p} \tag{2.37}$$

By substituting A_L in formula 2.37, after some algebraic operations the following result can be obtained:

$$\overbrace{\frac{q_{bw}}{\gamma_s \cdot d)} \cdot \left[\frac{\gamma_W \cdot d}{g \cdot (\gamma_S - \gamma_W)}\right]^{1/2}}^{\phi_*} \cdot \overbrace{\frac{i_d}{i_b} \cdot \frac{A_1 \cdot A_3}{A_2 \cdot \lambda}}^{A_*} = A_* \cdot \Phi_* = \frac{p}{1-p} \tag{2.38}$$

Where A_* is a constant value that has to be determined through experimental investigations and Φ_* is a dimensionless number that represents the bed load transport (also called as intensity of bed load transport).

Einstein in 1942 proposed an analytical method to determine the probability p and the relationship A_* versus Φ_*. The probability p of the intervalsin which hydrodynamic lift is greater than the particle submerged weight can be expressed as a ratio between those forces as follows:

$$\frac{W_S}{F_L} = \frac{(\gamma_S - \gamma_W) \cdot A_2 \cdot d^3}{\rho_W \cdot C_L \cdot A_1 \cdot d^2 \cdot u_b^2 \cdot (1+\eta)} < 1 \tag{2.39}$$

Where u_b is the fluid velocity in proximity of the bed, and $(1+\eta)$ represents a random fluctuation of the velocity. Some investigations carried later by Einstein showed that

the lift coefficient assumes a constant value of $C_L = 0.178$, η is a normal error law with variance $\sigma_\eta = 0.5$ and u_b is the velocity at a distance of $y = 0.35 \cdot X$ where X is the characteristic grain size of the mixture. The velocity u_b can be calculated by using the logarithmic velocity profile:

$$\frac{u_b}{u_*} = 5.75 \cdot \log\left(30.2 \cdot \frac{y}{\Delta}\right) \tag{2.40}$$

Where the shear velocity can be calculated as usual ($u_* = \sqrt[2]{\cdot g \cdot S \cdot R_H}$), $\Delta = k_s/x$ where $k_s = d_{65}$ and $x = f(d_{65}/(\delta))$ with δ boundary layer thickness. By substituting all these values in formula 2.39 the result is:

$$\frac{W_S}{F_L} = \frac{1}{1+\eta} \cdot \overbrace{\frac{\rho_S - \rho_W}{\rho_W} \cdot \frac{d}{R_H \cdot S}}^{\psi} \cdot \overbrace{\left[\frac{2 \cdot A_2}{0.178 \cdot A_1 \cdot 5.75^2}\right]}^{B} \cdot \overbrace{\left[\frac{1}{\log\left(19.6 \cdot X/\Delta\right)}\right]^2}^{1/\beta_X^2} = \frac{1}{1+\eta} \cdot \frac{\psi \cdot B}{\beta_X^2} < 1 \tag{2.41}$$

Therefore the following equation can be obtained assuming that lift force is always positive:

$$|1+\eta| > \frac{\psi \cdot B}{\beta_X^2} \tag{2.42}$$

This equation was rewritten later by Einstein in 1950 with the addition of two correction coefficients to consider effects such as hiding and non-constant lift coefficient.

$$|1+\eta| > \xi \cdot Y \cdot \frac{\psi \cdot B}{\beta_X^2} \tag{2.43}$$

The correction factors for hiding and lifting (ξ and Y respectively) can be obtained from Figures 2.12 and 2.13.

2.4.6 Stochastic Approach: Yang and Sayre (1971)

The concept of the bed load transport, constituted by a sequence of quick steps followed by long resting times was re-developed by Yang and Sayre (Yang & Sayre 1971). They proposed to describe the step length of a particle in terms of independent and identically distributed random variables. Therefore a set of step length $X_i = \{X_1, X_2, X_3 \dots\}$ following a probability density function $f_X(X)$ can be defined. A similar description can be assumed for rest times too.

Therefore a set of resting times $T_i = \{T_1, T_2, T_3 \dots\}$ following a probability density function $f_T(t)$ can be defined. The total travel distance followed by a particle after n steps can be described (under independence and identically distribution assumption) as the sum of all step length, therefore:

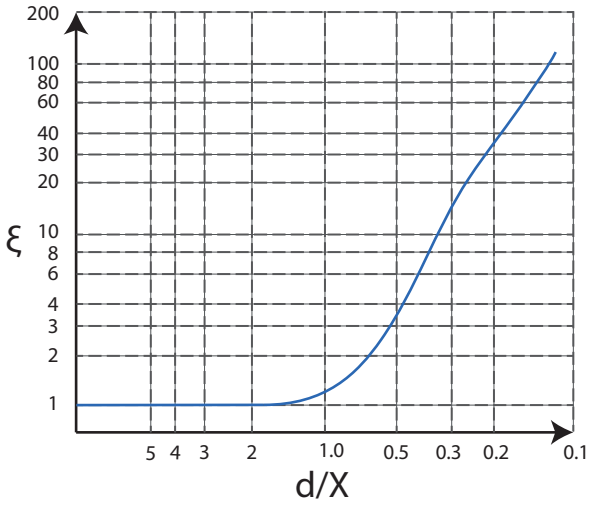

Figure 2.12: Hiding factor ξ

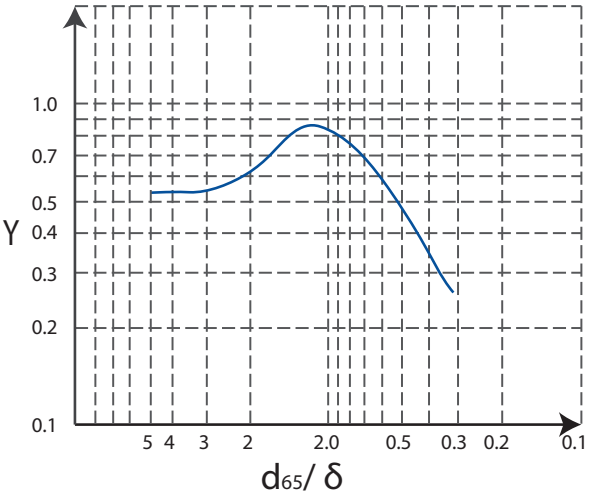

Figure 2.13: Lifting factor Y

$$X(n) = \sum_{i=1}^{n} X_i \tag{2.44}$$

The probability that a particle has followed a travel distance lower than x at time t can be defined as reported below:

$$F_t(x) = \sum_{n=0}^{\infty} P\left(\sum_{i=1}^{N(t)} X_i < x | N(t) = n\right) \tag{2.45}$$

Where P is the probability that a particle has travelled for a distance lower or equal than x after n steps in time t. By applying the conditional probability definition equation 2.45 can be rewritten as below:

$$F_t(x) = \sum_{n=0}^{\infty} P\left[\sum_{i=1}^{N(t)} Xi \leq X\right] \cdot P[N(t) = n] + P[X_0 < x] \cdot P[N(t) = 0]; \tag{2.46}$$

By applying the probability theory, it was shown by Yang and Sayre (1971) that the pdf of step length in a time t can be written as below:

$$f_t(x) = \sum_{n=1}^{\infty} \underbrace{f_x(x)^n *}_{1st} P[N(t) = n] \tag{2.47}$$

Where the 1^{st} term represents the n-times convolution of the step length probability density function. The physical meaning of that formula is the probability density

function of the travel distance after n steps. If probability density function for the step length is a gamma distribution then:

$$f_x(x) = \frac{\beta^\alpha}{\Gamma(\alpha)} \cdot x^{\alpha-1} \cdot e^{-\beta \cdot x} \tag{2.48}$$

Where α is a shape parameter and β is a scale parameter. Mean and variance of gamma distribution are related to shape and scale parameter through: $\mu = \alpha/\beta$ and $\sigma^2 = \alpha/\beta^2$. If rest periods are exponentially distributed then:

$$f_T(t) = \lambda \cdot e^{-\lambda \cdot t} \tag{2.49}$$

With mean $\mu = 1/\lambda$. Under those assumptions the equation 2.49 can be written as:

$$f_t(x) = \beta \cdot e^{-\lambda \cdot t + \beta \cdot x} \cdot \sum_{n=1}^{\infty} \frac{(\beta \cdot x)^{n \cdot \alpha - 1}}{\Gamma(n \cdot \alpha)} \cdot \frac{(\lambda \cdot t)^n}{n!} \tag{2.50}$$

Once the stochastic model is assumed the parameters that define the distributions can be obtained directly through laboratory experiments.

Chapter 3

Experimental Set-up

3.1 Introduction

In this chapter a detailed description will be given of the experimental apparatus used in the experiment. A description of the software used to track the databases, the structure of the databases and the modified structure used to perform the analysis is also provided.

3.2 Experiment Objectives

The experimental data used as a starting point in this study are obtained from a series of experiment carried in 2009 in the laboratories of the University of Bradford (UK). The aim was to investigate the entrainment through an analysis of the near bed flow conditions corresponding to an event of grain detachment from the bed.

The investigation of the near bed flow field was carried on through the use of a Particle Image Velocimetry (PIV) system. The outputs of the PIV system were the velocity components in three directions for every instant of time in some selected points defined by a grid. The investigation of the entrainment condition of the individual grains that detach from the the bed were performed with the use of video recording and through the manual tracking of the grains.

By associating the results of those two investigations it was possible to investigate the link between flow conditions, turbulence and grain entrainment. The experimental apparatus used in those experiments is reported in Figure 3.1.

Figure 3.1: Experimental apparatus used in 2009 experiments (Gruarin, 2010)

3.3 Experimental Apparatus

The series of experiments were carried out in the Laboratory of Hydraulics at the University of Bradford (UK) in the Summer and Autumn of 2009. In this period a total of 12 experiments were executed at different flow conditions. The flow conditions for the experiments analysed in the present study are reported in Table 3.1.

Where Q is the flow rate, V is the mean flow velocity, S is the slope of the flume,

Test	S(%)	Q(l/s)	V(m/s)	$R_e(\cdot 10^5)$	$u_s(m/s)$	τ_0^*	Date
T3	0.59	32.2	0.94	2.98	0.070	0.061	24^{th} Aug
T5	0.65	44.8	0.97	3.19	0.074	0.068	2^{nd} Sept
T9	0.77	48.1	1.05	3.34	0.080	0.080	22^{nd} Sept
T10	0.80	49.0	1.07	3.40	0.081	0.083	23^{d} Sept
T11	0.83	49.8	1.08	3.45	0.083	0.086	29^{th} Sept
T12	0.86	50.9.1	1.11	3.53	0.085	0.090	1^{st} Oct

Table 3.1: Flow conditions for each experiment

$R_e = 4 \cdot R_H \cdot V/\nu$ is the Reynolds number, $u_s = \sqrt[2]{g \cdot R_H S}$ is the shear velocity and $\tau_0^* = \tau_0/g(\rho_S - \rho_W)d_{50}$ is the Shields parameter. The criterion to decide the steepness of the flume was to keep the flow depth always constant. The fixed flow depth is $h_u = 100mm$. In the experiments analysed have values for Shields shear stress parameters ratio θ/θ_{cr} ranges from 1.1 to about 1.7. The choice was justified because at low shear stress parameter it is easier to recognize the grain entrainment.

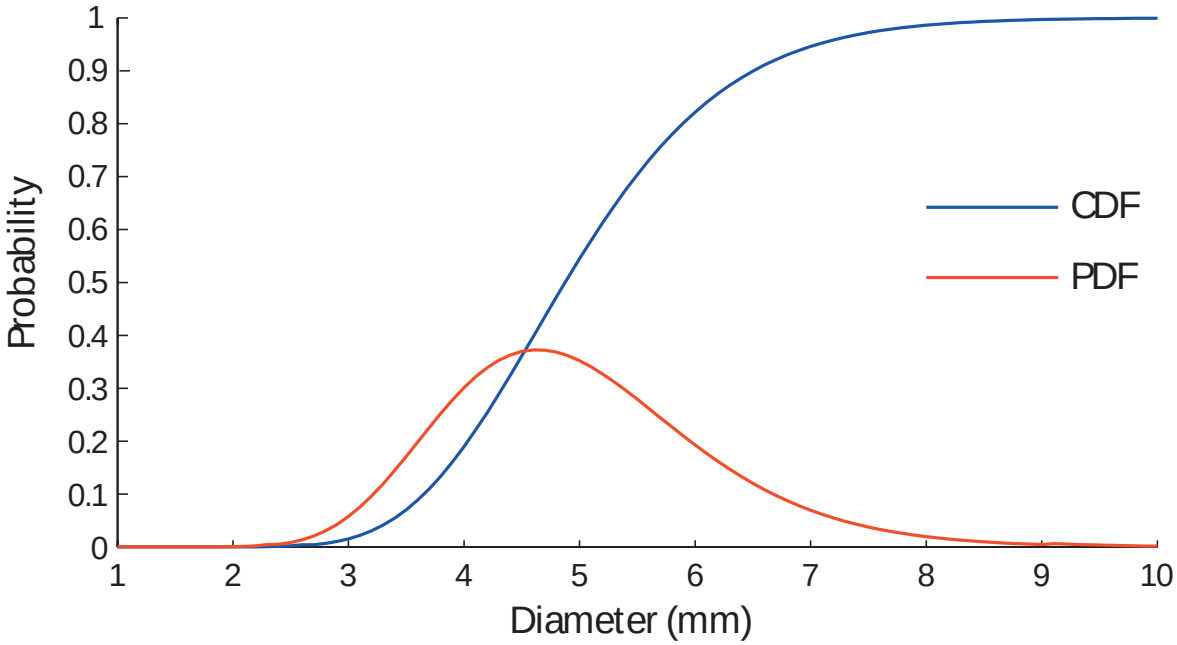

Figure 3.2: Log-normal distribution of grain size

3.3.1 Flume and measurement equipment description

The experimental apparatus consisted in a tilting flume with a length of $12m$ and a width of $0.5m$. The first 1.5 meters of the flume is constituted by a fixed gravel bed. The necessity of a fixed bed was to grant the development of a stable boundary layer for the experiment. In the remaining part of the flume the bed was mobile. The bed was realized with a constant thickness, without any bed form.

The bed was constituted by natural gravel, with mean grain diameter of $d_{50} = 50mm$. The distribution of grain diameters chosen was a log-normal distribution with standard deviation $\sigma_g = 1.3mm$. The original grain size distribution of the bed material is reported in Figure 3.2.

The density of bed material was $\rho_s = 2650 kg/m^3$. The area examined by the PIV system was located about in the middle of the flume (6.70m from the inlet). The flume is represented in Figure 3.3

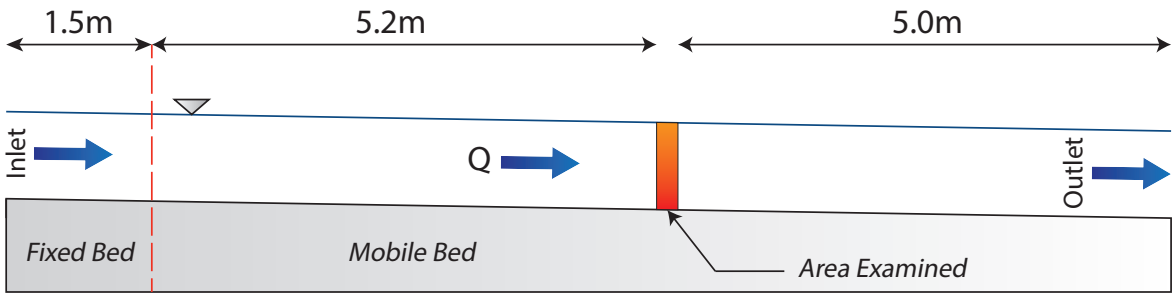

Figure 3.3: Flume scheme

The window monitored had a length of 220 mm and a width 40mm. The area examined was equipped with three cameras that took pictures with a frame rate of 45 FPS (a frequency of 45Hz). Therefore the minimum unit in which the displacements of a grain can be observed is $1/45 \cdot s \simeq 0.022 \cdot s$. The recording time was of about ten minutes for each experiment, but in the present study only a maximum of 6000 frames (about 2min and a half) were analysed.

3.3.2 Particle Image Velocimetry

A Particle Image Velocimetry (PIV) system is an optical technology used to measure the velocity of a fluid in a section of the flow field. A schematic representation of the components of a PIV system is reported in Figure 3.4. The system is made of three apparatus:

- Seeding Particles: The seeding particles are small particles that are mixed with the fluid and carried by the flow due to drag force. The choice of the suitable particles is of fundamental importance for the PIV. The ideal particle should have the same density as the fluid and be spherical. Seeding particles should be small enough to react instantaneously to the variations of the flow field. On the other hand, they should be also big enough to scatter lights in order to be visible. Typical tracing particle size is around $10\mu m$ to $100\mu m$. In the experiment the density of seeding particles used was of $\rho_P = 995 kg/m^3$ and the size was of $200\mu m$.
- Camera: The camera has the task of taking pictures of the area illuminated by the laser layer. If the pictures are taken with an adequate frame-rate then it

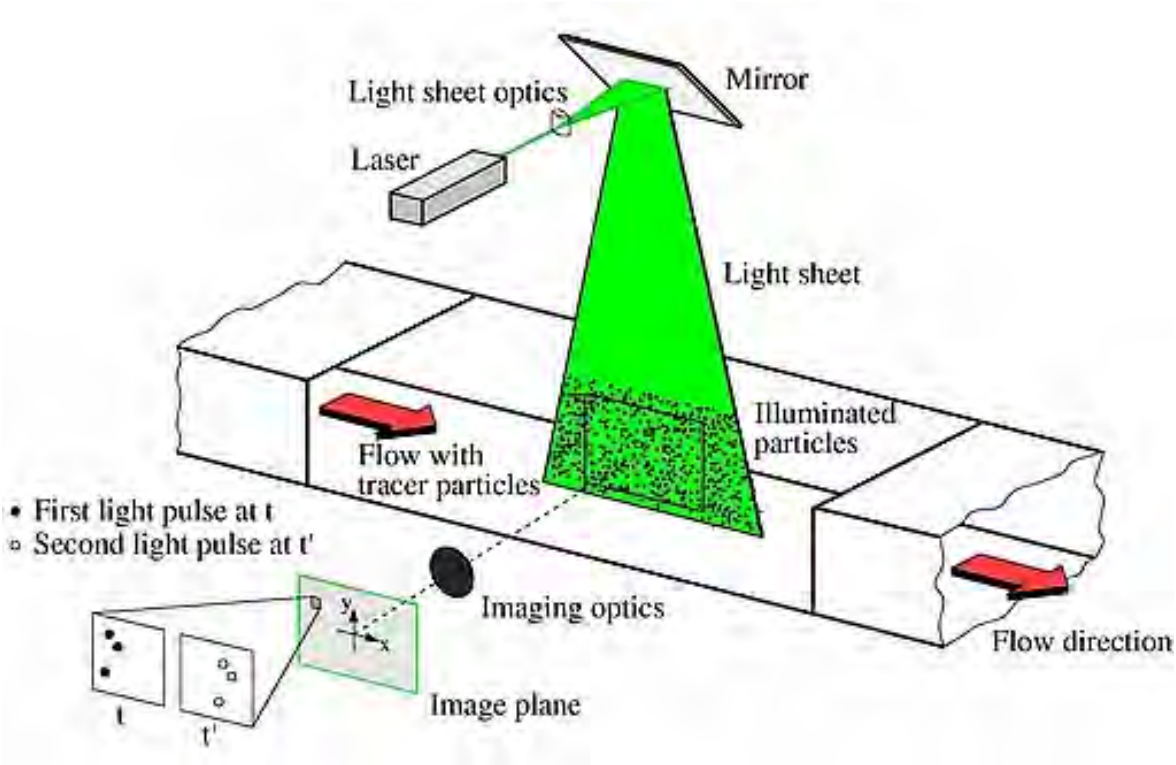

Figure 3.4: Schematic representation of a PIV system (from aim2 website)

is possible to carry on an accurate image analysis. The objective of the image analysis is to estimate the velocity by measuring the position of a seeding particle in two different frames. The frame rate used in the experiment was set to 45Hz. The system used in the experiments was composed by three cameras above the bed.

- Laser: The laser must light the section in which the estimation of 3D velocity component is desired. In the experiment the laser sheet was located at 8-10mm height from the bed. Velocity components were measured in a grid with a resolution of 1.07mm. The grid points are $35 \cdot 185 = 6475$.

The system used in the experimental investigations elaborated in the present study is reported in Figure 3.5.

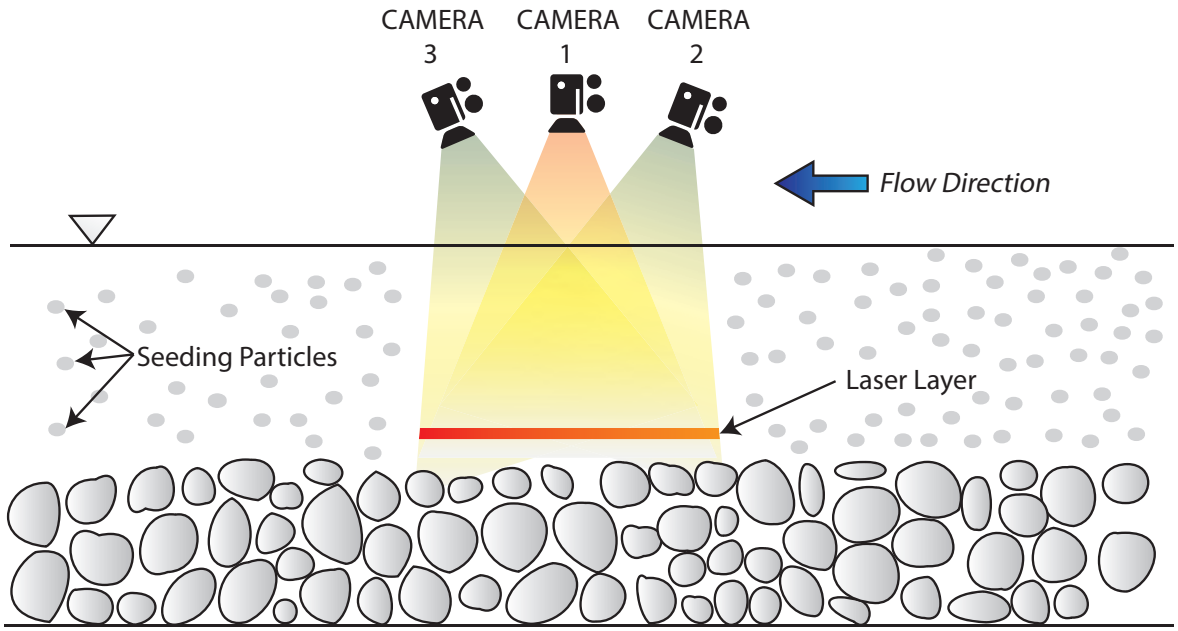

Figure 3.5: PIV system used during the experiments

3.4 Grain Tracking Software

In the present study it is of fundamental importance the knowledge of the trajectories followed by grains meanwhile they are in motion. To spot if a grain is starting, moving or stopping it would be necessary to perform an automated image analysis. For the 2009 experiments it wasn't possible to perform an automated image analysis due mainly to the presence of seeding particles from the PIV system. The high concentration of seeding particles caused a relevant decrease on the visibility of the bed. For this reason the quality of the images is quite poor and a manual tracking of moving particles was necessary. An example of a frame is reported in Figure 3.6.

3.4.1 Gslab: Software Inputs

The software used to perform the manual tracking of the particles is called Gslab. Gslab is a code created in 2005 by *Bottacin Andrea* that helps the user to track manually the grains that are moving in the flume. This result is achieved by providing a Graphical User Interface (GUI) in which the user can quickly draw the boundary of a grain frame by frame. The software inputs are reported in the list below:

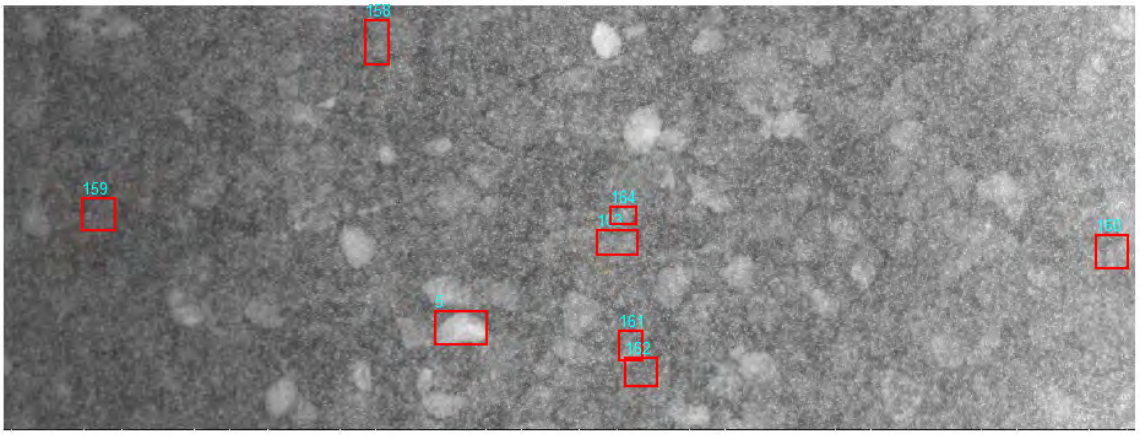

Figure 3.6: Example of frame (frame 63 of September 29^{th})

- image#n.image: The sequence of frames recorded in the experiments. The letter n represents a progressive number: The first frame of the experiment will have $n = 0$ and the last will be $t \cdot f$, where t is the time in seconds in which a frame is taken and f is the frame rate (or frequency). In the present study the frequency is 45Hz and there is a maximum of 6000 frames analysed.
- GRAINdata: The GRAINdata file contains two fundamental informations for the code:
  - Path: The path corresponding to the location of the images for all the three cameras used for the experiment
  - Frame: The frame structure: a structure that contains the grains information for each frame. A better description will be provided in the next section.

3.4.2 Gslab: Software Outputs (GRAINdata)

The output of the Gslab software is the GRAINdata file that contains the database of the spotted grains. The grains are organized in a database structured as reported in Figure 3.7.

The main structure is a vector that contains all the frames in which there's at least 1 grain spotted. In each element of frames (*frame(i)*) there are 4 parameters saved:

- frame(i).rectime: The number in the sequence corresponding to the i^{th} frame. It is the time in seconds, multiplied by 45 in which a frame in the video has been taken (i.e. $rectime = 45 \Rightarrow t = 1s$)
- frame(i).prev: The index of the previous frame in the frame list $(i - 1)$
- frame(i).next: The index of the following frame of the list $(i + 1)$
- frame(i).grain(): The vector that contains the grains registered at the i^{th} frame. For each grain the following properties are registered:
  - frame(i).grain(j).number: The code associated to the grain that is registered at the i^{th} frame. The number is a property that univocally identifies a grain.
  - frame(i).grain(j).position: The (x;y) position of the barycentre of a grains in millimetres.
  - frame(i).grain(j).border: A vector that contains the position of the relevant points chosen by the user to draw the border of a grain.
  - frame(i).grain(j).area: A vector that contains the value of the area of a tracked grain.
  - frame(i).grain(j).bbox: A vector that contains the position of the south-west corner of the rectangle in which a grain is inscribed and the dimension of the x side of the rectangle and the y side of the rectangle.
  - frame(i).grain(j).state: A value that represents the state that the j^{th} grain assumes in the i^{th} element of the frame structure. The "state" can have three values:
    - If a grain is STARTING then the value of state must be set to 1.
    - If a grain is MOVING then the value of state must be set to 2.
    - If a grain is STOPPING then the value of state must be set to 3.
  - frame(i).grain(j).movedby: If a grain undergoes a collision, then movedby assumes the number of the grain that impacts the j^{th} grain.

In Figure 3.8 it is reported a scheme of the parameters saved in the GRAINdata database described previously. The overall scheme of the tracking process is represented in 3.9.

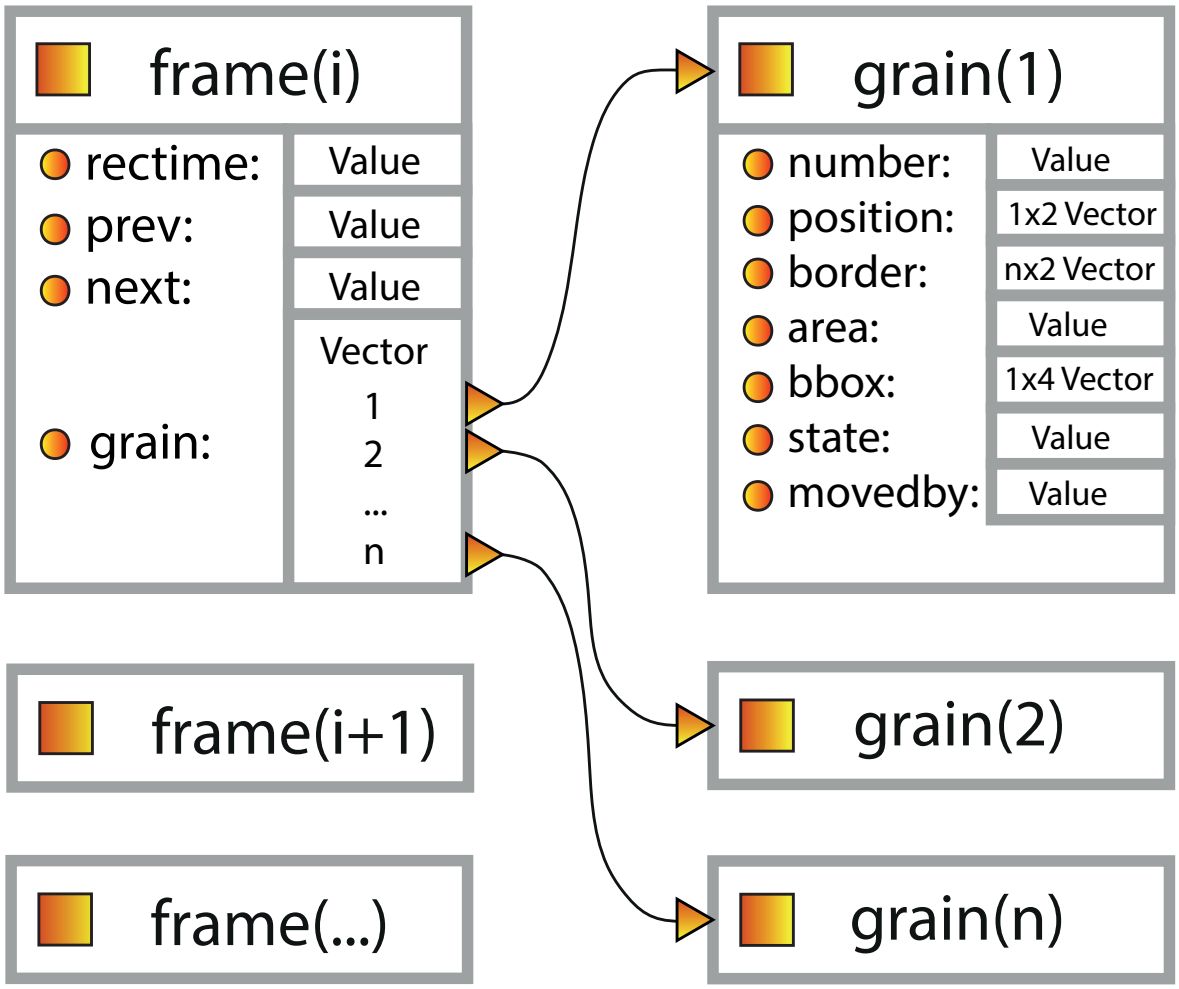

Figure 3.7: Structure of the GRAINdata

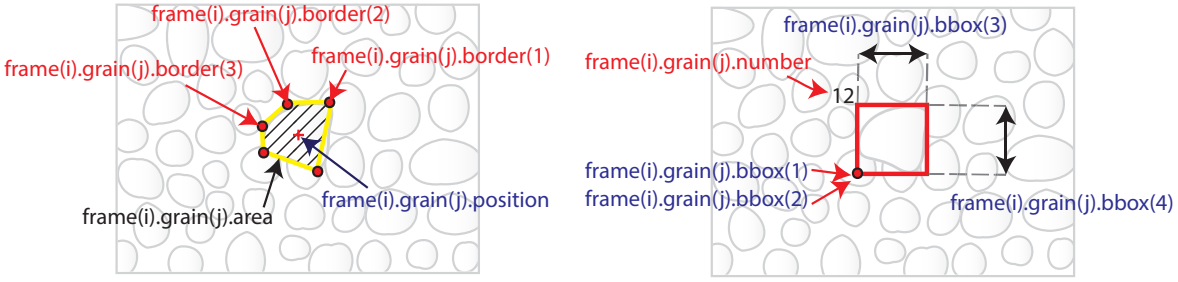

Figure 3.8: Parameters saved in the GRAINdata database during manual tracking

3.4.3 Gslab: Tracking procedures and Critera

In order to track a grain and find all the parameters that are described above, the following operations must be followed. When a grain moves from it the position in the previous frame the user must manually trace the borders of the grain. After that the code will automatically calculate the position of the barycentre from the borders. A boundary box will be displayed after those operations. The last action to do is to assign the state value, as described in the previous section.

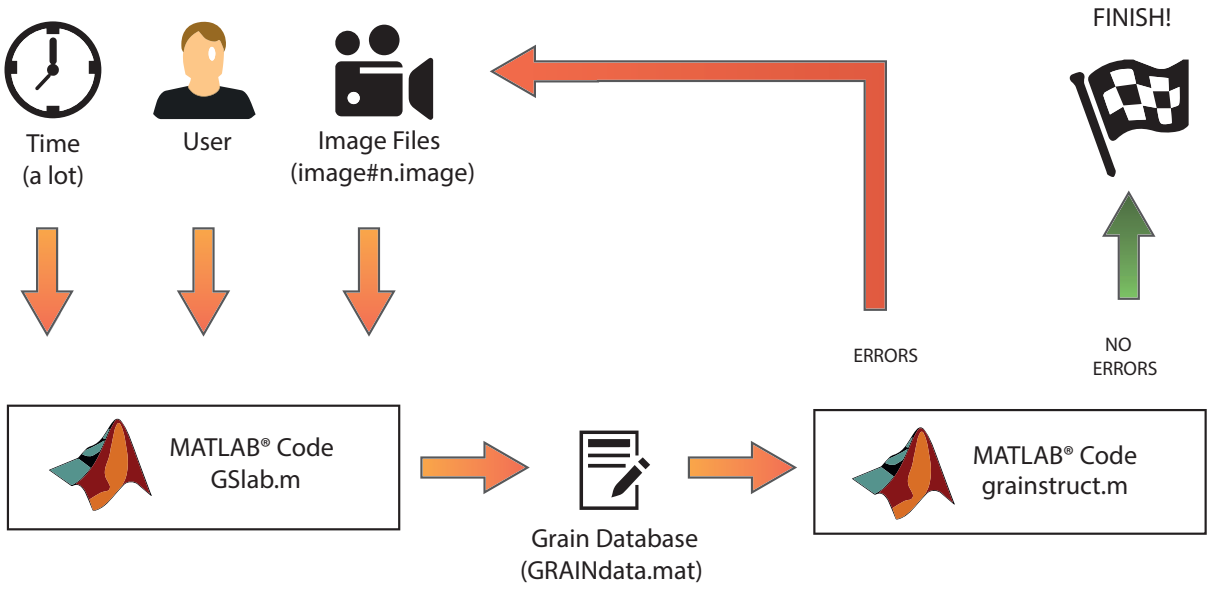

Figure 3.9: Drawing of the tracking procedure with gslab

The manual tracking procedure however is not a strong and reliable procedure, since systematic errors can be made by the user. The sensibility of the user in the tracking procedure and the poor quality of images can significantly bias the results. However, a code was provided to look for errors made in the tracking of an experiment. The code is called "grainstruct.m" and uses the "GRAINdata" database as an input. If there are mistakes it is necessary to go back again to the tracking. If everything is ok the tracked database can be analysed.

Furthermore, there are also technical issues that can have an important effect on data. Those problems and the necessary arbitrary suppositions to overcome the issues are reported below:

- Stop condition: The Stop condition of a grain depends on how much time a grain stays still. This problem can be solved by an arbitrary choice only. During the tracking procedure many grains apparently stopped for a couple of frames, then

started again. The only possibility to define a stop condition is to fix a minimum time interval for which a particle doesn't move significantly. If a particle stays still for a time (or number of frames) lower than the threshold the stop condition will not be assigned. If the particle's rest time exceeds the threshold the stop will be assumed. Since the time elapsed between two consecutive frames is (as stated before) $t = 0.022s$ the threshold for the minimum rest time will be assumed as $t = 0.22s$ (10 frames).

- Start condition: When a grain starts (especially in the last frames analysed) the user sometimes may not be sure if the grain which is about to start was registered previously for other movements. To know this without any doubt the user should scroll the previous frames and examine if there were previous movements. This can be a heavy, time demanding and hard task due to the poor image quality. Therefore, if the user is not sure if a grain has started in the previous frame a general rule was fixed. The user must check only the 500 frames before the one in which the grain is starting. If it hasn't moved in those 500 frames ($\simeq 11s$) then a new code to the grain can be assigned.

3.4.4 Database Manipulation - (Grain History)

The database as an output from Gslab software presents a structure which is sorted by frame. In each frame grain statistics are available. In order to create easier codes to perform the analysis reported in the following sections the GRAINdata structure was reworked as reported in Figure 3.10.

The database in the present structure is organized as a vector of grains. Each element of the vector represents the same grain. The parameters of each grains are the characteristics that a grain assumes in the different frames it was spotted. Therefore in this database the complete history of every particle movement is directly accessible. The parameters inside each grains are the following:

- X.grain(i).number(): A vector that contains the number (or code) of the i^{th} grain.
- X.grain(i).x(): A vector that contains the x position of the i^{th} grain in every frame in which it was spotted.
- X.grain(i).y(): A vector that contains the y position of the i^{th} grain in every frame in which it was spotted.
- X.grain(i).state(): A vector that contains the state of the i^{th} grain in every frame in which it was spotted.

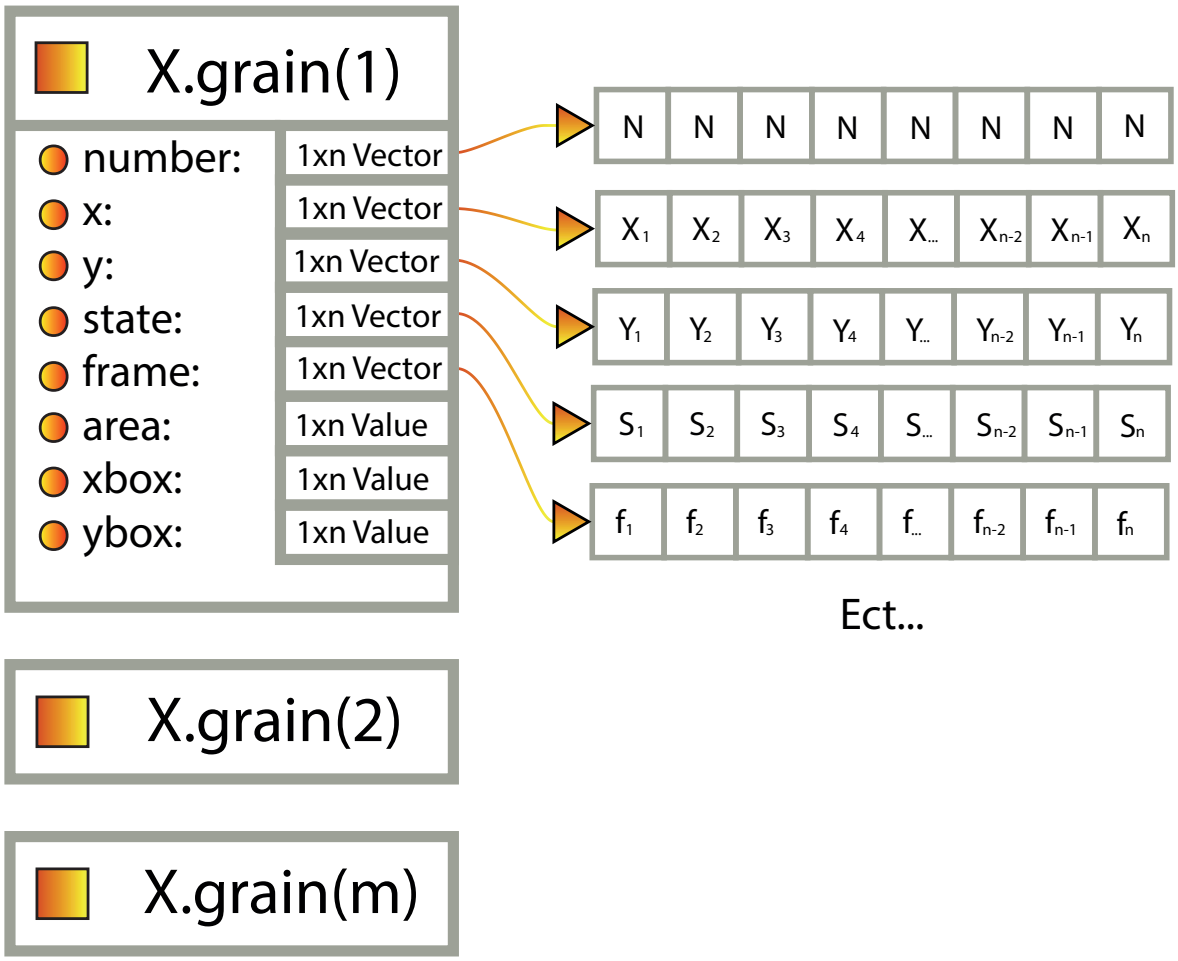

Figure 3.10: New database structure

- X.grain(i).frame(): A vector that contains the number of every frame in which the i^{th} grain was spotted.
- X.grain(i).area(): A vector that contains the value of the area that the i^{th} grain in every frame it was spotted.
- X.grain(i).xbox(): A vector that contains the value of the x dimension of the boundary box that contains the i^{th} grain in every frame it was spotted.
- X.grain(i).ybox(): A vector that contains the value of the y dimension of the boundary box that contains the i^{th} grain in every frame it was spotted.

Chapter 4

Grain Statistics Analysis

4.1 Introduction

For the development of stochastic models about the bed load transport it is important to study the interactions between flow conditions and the properties of the path followed by a grain. In this chapter the description of the analysis performed on the databases will be provided. In this section 5 quantities will be investigated:

1. Step length distributions $p(\lambda)$
2. Grains velocity distributions $p(u_g)$
3. Grains rest time distributions $p(\tau)$
4. The link between the step length λ and the grain diameter d
5. Entrainment rate

4.2 Step Lengths Analysis

As stated by scientists in the past, the movement of particles along the river bed is constituted by long periods of resting time alternated with quick movement of the grain. The purpose of this section is to study the link between the shear stress and step lengths and to find the probabilistic model that better represents the step lengths. In the study here presented the "step" is defined as follows:

Step Length λ: The length covered by a grain between two rest positions.

Therefore the step length can be simply defined as the difference between the starting position and the stopping position $X_1 - X_0$.

4.2.1 Step Lengths Population

The images available are taken from the top of the flume, therefore the present study is performed in a 2D reference system. In a planar system the position of a grain can be written as (X_i, Y_i). Therefore the step length can be written as:

$$\begin{pmatrix} \lambda_x \\ \lambda_y \end{pmatrix} = \begin{pmatrix} X_1 \\ Y_1 \end{pmatrix} - \begin{pmatrix} X_0 \\ Y_0 \end{pmatrix} \tag{4.1}$$

In this study about the step length only the stream-wise component (X) will be considered since for transport purposes only this component is relevant. Under this assumption the step length can be calculated simply as reported in Equation 4.2.

$$\lambda_x = X_1 - X_0 \tag{4.2}$$

To obtain the step length population the manual tracking is a fundamental operation. When the grains of an experiment are tracked (through gslab) it is possible to obtain the step lengths after some simple operations. The first one is to pass from the "GRAINdata" database (as defined in Section 3.4.2) to the "Grain History" database (as defined in Section 3.4.4). The second structure for the database is preferred, because it allows to study the behaviour of a single grain frame by frame, instead of studying the group of grains that are moving in a certain frame. To obtain the step lengths population some preliminary considerations must be done.

The grain movements are registered by applying different codes to grain movements. As explained in Section 3.4.2 the "start" condition is represented with the value 1, the "move" with 2 and the stop "with" 3. Therefore there are four possible movements:

- START-MOVE: This kind of steps includes all movements that start inside the window and stop outside. This is registered in the databases with the absence of a stop condition (State=3). The last registered state is a move (State=2) preceded by a start (State=1). In this case no value can be assigned to the step length.

- MOVE-STOP: This action is the exact opposite of the previous one. This kind of steps includes all movements that start outside the window and stop inside. This is registered in the databases with the absence of a start condition (State=1). The last registered state is a stop (State=3) preceded by a move (State=2). In this case no value can be assigned to the step length.

- MOVE-MOVE: This action means that a grain does not start or stop inside the window. In this case only move conditions are present (State=2). There is a total absence of any start or stop. This kind of steps is made by grains that just go through the window without stopping.
- START-STOP: This condition means that the grain starts (State=1), move (State=2) and stops (State=3) inside the window. When this happens the step length can be calculated as the difference between the X coordinate of the starting position subtracted with the X coordinate of the stopping condition.

The four different step modalities are reported in Figure 4.1

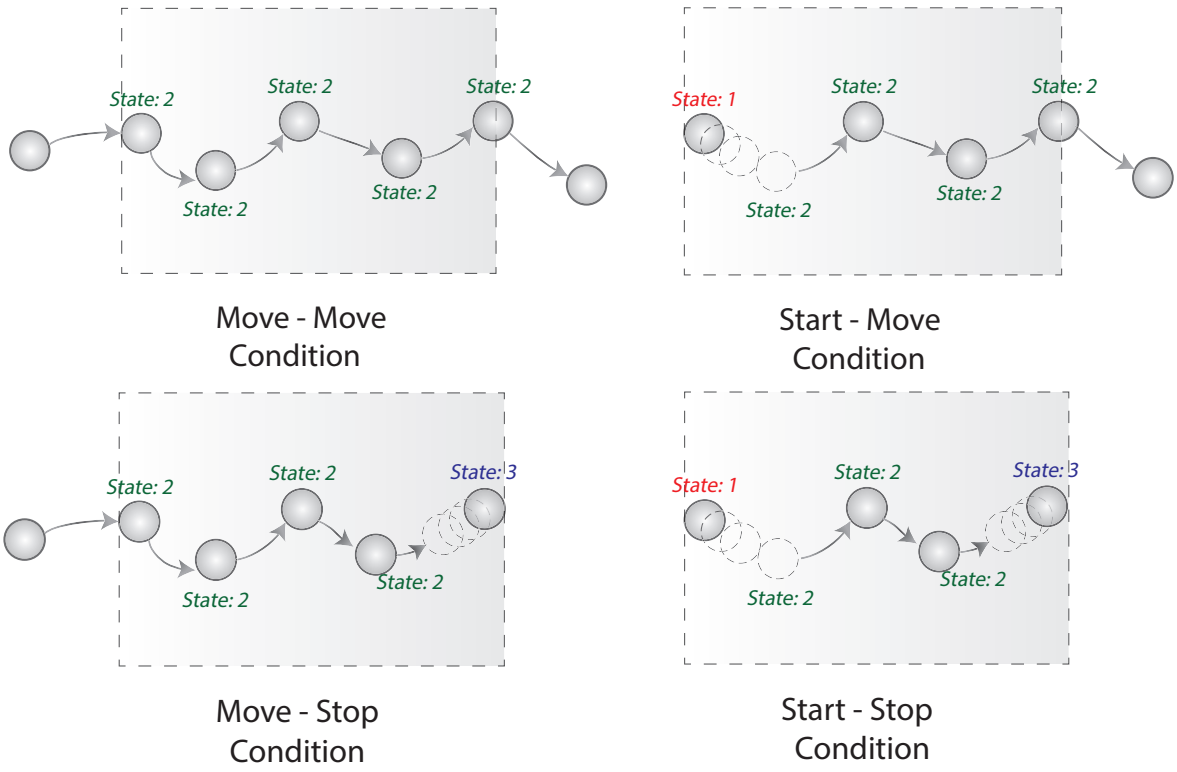

Figure 4.1: Different grain steps recorded

After those considerations the Step Length population for each experiment was obtained through the use of an algorithm written in Matlab. In the population constituted by the grains that have a registered start and stop inside the window also very little steps are considered: If a grain shakes and moves of just few millimetres this is considered as a step. The threshold to define a 'shake' is reported below:

- $\lambda_x < d_{50}$: If the step length λ is lower than the mean diameter d_{50} then then the step is considered as a "Shake".

- $\lambda_x > d_{50}$: If the step length λ is higher than the mean diameter d_{50} then then the action can be considered as a "Step".

In the present study both populations (shakes included and excluded) will be considered and analysed.

4.2.2 Statistics Stability and Preliminary Results

Before carrying on any step length analysis it is necessary to check if the step lengths population is enough numerous. To assess if there are enough data to get reliable statistics from the population the mean and variance were calculated versus the number of data used. The result for the case of August 24th (Shakes Included) is reported in Figure 4.2.

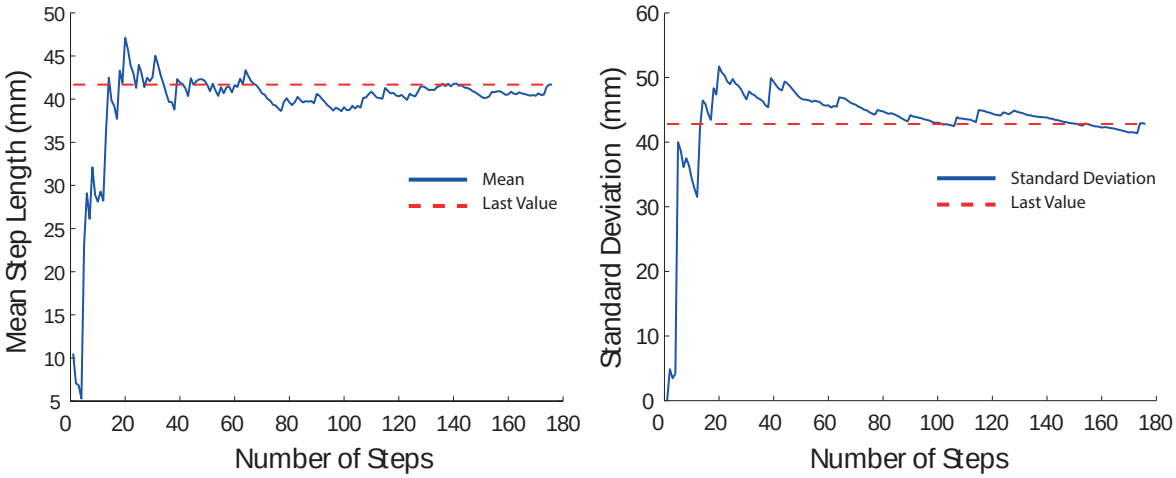

Figure 4.2: Mean (left) and Standard Deviation (Right) vs Number of steps (24th Aug. Shakes Included)

The blue line represents the values for mean and standard deviation by varying the number of steps considered. The red line is the value for mean and standard deviation calculated on the whole population. The same procedure is applied for all experiments, for the cases of both shakes included and excluded: the result is reported in Appendix 1 (Chapter 7, Figure 7.1, Figure 7.2 Figure 7.3, Figure 7.4).

As can be noticed by the plots it is impossible to define a proper threshold to state if the statistics are stable or not that is valid for all experiments. The stability of the statistics is strongly dependent on the experiment considered. No relevant differences are found between the cases of "shakes" included or excluded: the effect is an horizontal

translation. The non-dimensional stream-wise mean step length (normalized over the mean diameter d_50) versus the shear stress acting on the bed is reported in Figure 4.3.

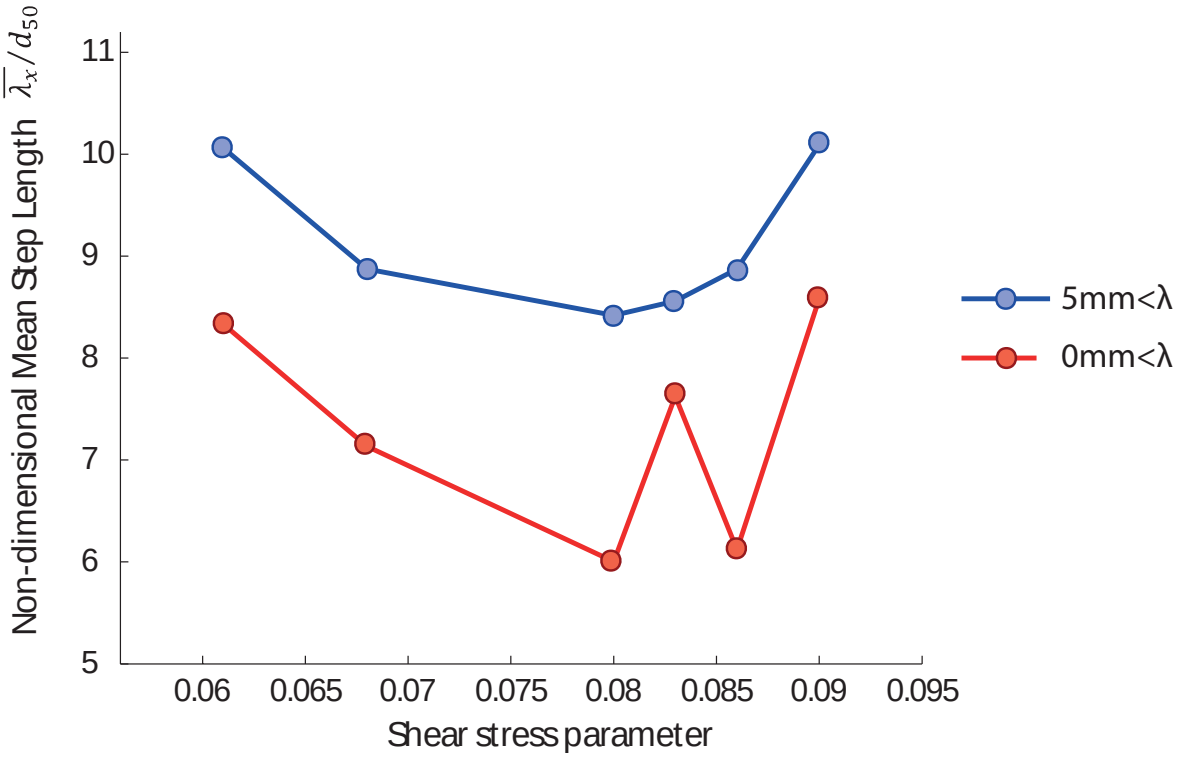

Figure 4.3: Non dimensional shear stress vs Mean Step Length

The plot shows that the step length seems to be weakly dependent on the shear stress paramater, especially in the case of step lengths λ_x greater than 5mm. The data obtained, however, does not take into account the other step possibilities (STOP-MOVE, MOVE-STOP, MOVE-MOVE). In the next sections a more accurate analysis of the step lengths will be performed.

4.2.3 Grain Movement-Types Analysis

During the tracking procedure two different modalities of transport can easily be spotted. The first is made of grains that are entrained by the flow and move slowly (usually by rolling). In this case many steps can usually be registered, since those kind of grains tends to be entrained and to stop very frequently. The second modality instead is composed by grains that pass through the window very quickly, usually without stopping at all. The analysis in the previous sections were made by considering the former

Test:	$24^{th}Aug$	$2^{nd}Sept$	$22^{nd}Sept$	$23^{d}Sept$	$29^{th}Sept$	$1^{st}Oct$
τ_0^*	0.061	0.068	0.080	0.083	0.086	0.090
Start-Stop ($\lambda_x > 5mm$)	144	318	174	179	205	105
Start-Stop ($\lambda_x < 5mm$)	32	84	76	24	100	20
Move-Stop	80	235	133	106	236	154
Start-Move	88	177	122	96	202	126
Move-Move ($\lambda_x > 200mm$)	23	42	35	41	57	32
Move-Move ($\lambda_x < 200mm$)	13	59	61	31	165	71

Table 4.1: Step type by experiment

modality only. However, to correctly assess the step lengths also the latter should be considered. The steps registered by type are reported in Table 4.1.

As Table 4.1 shows, the grain movements are divided into four types: Start-Stop, Start-Move, Move-Stop, Move-Move. Start-Stop movements are subsequently divided in two subcategories: Step lengths lower than 5mm ($\lambda_x < 5mm$) and higher than 5mm. Splitting the "Steps" from the "Shakes" is useful to carry on the analysis. The Move-Move category was split as well with a threshold set to $\lambda_x = 200mm$. This is shown in Figure 4.4

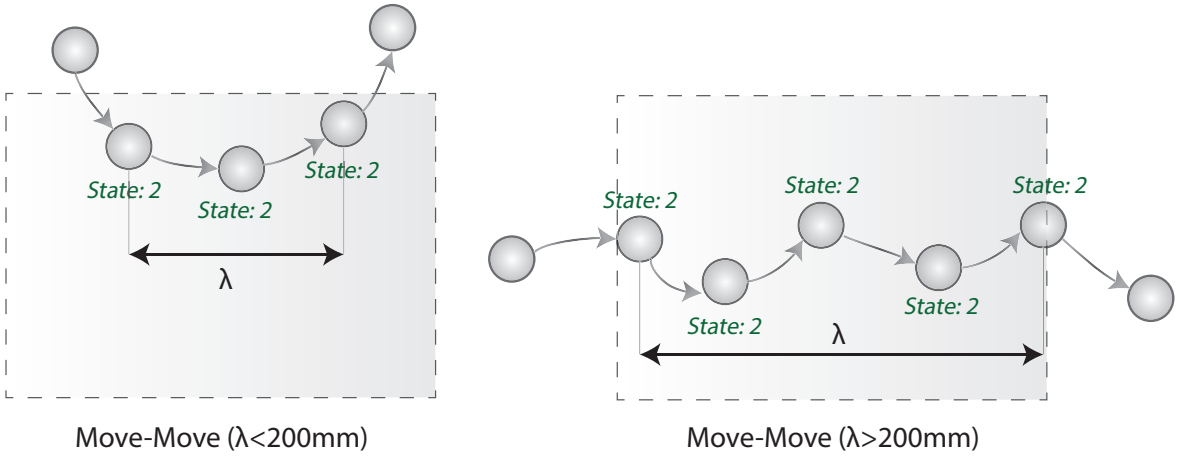

Figure 4.4: MOVE-MOVE Steps with threshold lower than 200mm (% values)

This operation was necessary to find the amount of grains that actually travel through the whole window from one side of it to the other. For these grains it can be stated that their step length is higher than 200mm.

In Figure 4.5 it is reported the types of movements per experiment. Each box represents the number of steps of a particular type over the total number of movements registered for each experiment. For the purpose of the step length analysis the following

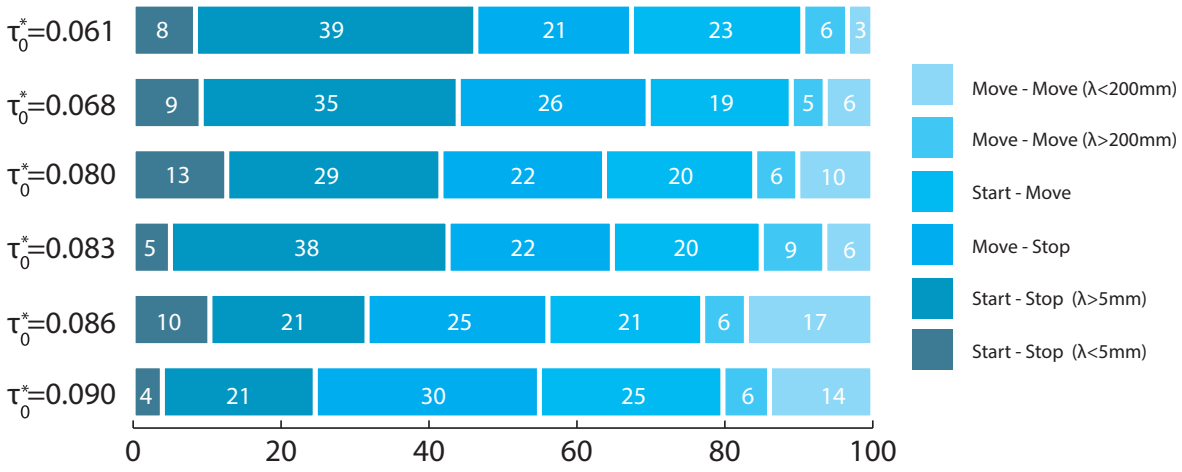

Figure 4.5: Step types for each experiment (% values)

assumptions are made:

1. : START-STOP movements are the ones that defines the Step Length Probability distribution function. However, this probability distribution function is considered as *truncated* over the value (arbitrarily chosen) of 200mm since the window amplitude is 220mm.

2. : MOVE-MOVE movements are considered only if the difference between the last recorded position and the first one is greater than a threshold of 200mm. The following ratio is then calculated:

$$R = \frac{n^{\circ}_{START-STOP}}{n^{\circ}_{MOVE-MOVE(\lambda>200mm)} + n^{\circ}_{START-STOP}} \tag{4.3}$$

   In the next sections this ratio will be named as 'Reduction Index'. The remaining MOVE-MOVE movements are not considered in the calculation of the Probability Density Function.

3. : MOVE-STOP and STOP-MOVE steps are supposed to belong to the same category. Therefore for the purpose of the PDF calculation the sum between the number of MOVE-STOP and STOP-MOVE will be considered. The following assumption is made:

   (a) $R \cdot (n^{\circ}_{START-MOVE} + n^{\circ}_{MOVE-STOP})$ will act as a START-STOP by following the same probability distribution. Therefore they will contribute to the known area of the PDF.

(b) $(1-R)\cdot(n^{\circ}_{START-MOVE}+n^{\circ}_{MOVE-STOP})$ will act as a MOVE-MOVE with a step length greater than 200mm. Therefore they will contribute to the area of the truncated part of the PDF.

Under those assumptions this two categories can be neglected, since they contribute equally to both the truncated part of the PDF and the known part of the PDF.

By following those hypothesis the truncated area of the pdf will have value $(1-R)$, while the area defined by the START-STOP step lengths will have value R. The effect of those assumptions on the Probability Density Function is reported in Figure 4.6

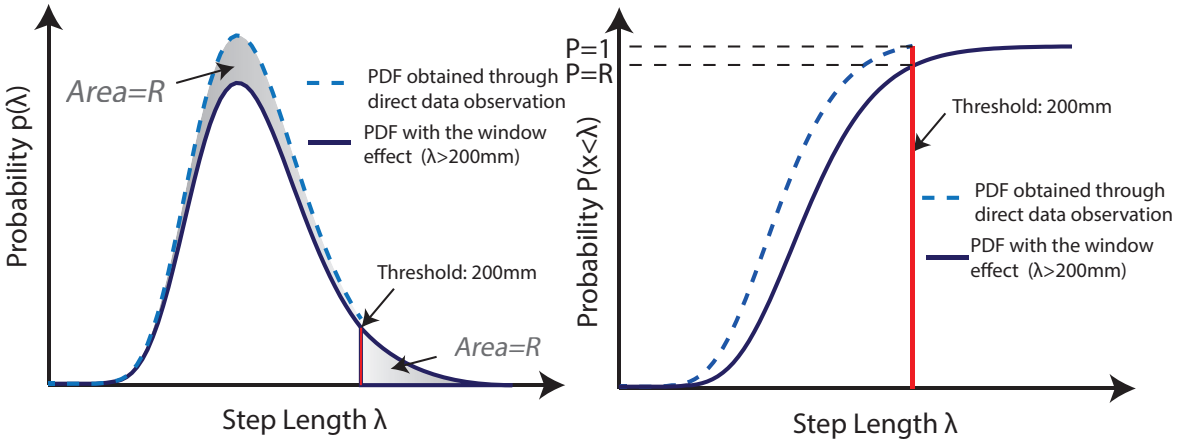

Figure 4.6: PDF (left) and CDF (right) under the hypothesis of truncated PDF

The grain population obtained through the assumptions previously made is reported in Table 4.2. Values for the ratio between Start-Stop and Move-Move is also reported. R is calculated by including the 'shakes' (Start-Stop with step length lower than the mean diameter), while R' is calculated by excluding them.

In Figure 4.7 the Reduction index is plotted against the Shear Stress parameter. As can be observed in the Figure by increasing the shear stress the Reduction index R seems to decrease. The trend is more clear when the 'shakes' are not considered. This means that when the shear stress parameter is higher (stronger flow conditions) more grains tend to pass through the window without stopping.

Test:	$24^{th}Aug$	$2^{nd}Sept$	$22^{nd}Sept$	$23^{d}Sept$	$29^{th}Sept$	$1^{st}Oct$
τ_0^*	0.061	0.068	0.080	0.083	0.086	0.090
Start-Stop ($\lambda_x > 5mm$)	144	318	174	179	205	105
Start-Stop ($\lambda_x < 5mm$)	32	84	76	24	100	20
Move-Move ($\lambda_x > 200mm$)	23	42	35	41	57	32
R (Shakes included)	0.88	0.91	0.88	0.83	0.84	0.80
R' (Shakes excluded)	0.86	0.88	0.83	0.81	0.78	0.77

Table 4.2: Step type used for the calculation of the PDF

4.2.4 Step Lengths PDF and CDF

After the considerations about the grains movements the Step Length Probability density function can be calculated. The first step to calculate the PDF is to define the number of classes in which the step lengths can be divided. Two analysis were carried out: one with 7 classes and one with 10. The number of classes is kept constant and independent from the amount of data available in each experiment. The interval considered for the step lengths are:

- : $X \in [X_{min} = 5mm, X_{MAX} = 200mm]$ for the case of 'Shakes' excluded
- : $X \in [X_{min} = 0mm, X_{MAX} = 200mm]$ for the case of 'Shakes' included

The interval is divided in classes with an equal amplitude. The amplitude of the intervals can be calculated as:

$$dX = \frac{X_{MAX} - X_{min}}{N^{\circ}_{classes}} \tag{4.4}$$

The point of the PDF are calculated by counting how many data fall inside each class. The probability that a step length is inside a class can be calculated as follows:

$$p(x \in [X_i, Xi + 1]) = \frac{n^{\circ}}{dX \cdot N^{\circ}_{steps}} \tag{4.5}$$

Where X_i and $Xi + 1$ are the extreme values of a class, n° is the number of data inside the class, dX the width of the interval and N°_{steps} the total number of steps. The pdf obtained in this manner has an area with unitary value. For the considerations reported in Section 4.2.3 the area must be scaled. The result is achieved by scaling the result obtained through Formula 4.5 with the values of R in Table 4.2. The values of the PDF will be: $p_{scaled} = p(x) \cdot R$. The result for the PDF of the $24^{th}Aug$ is reported in Figure

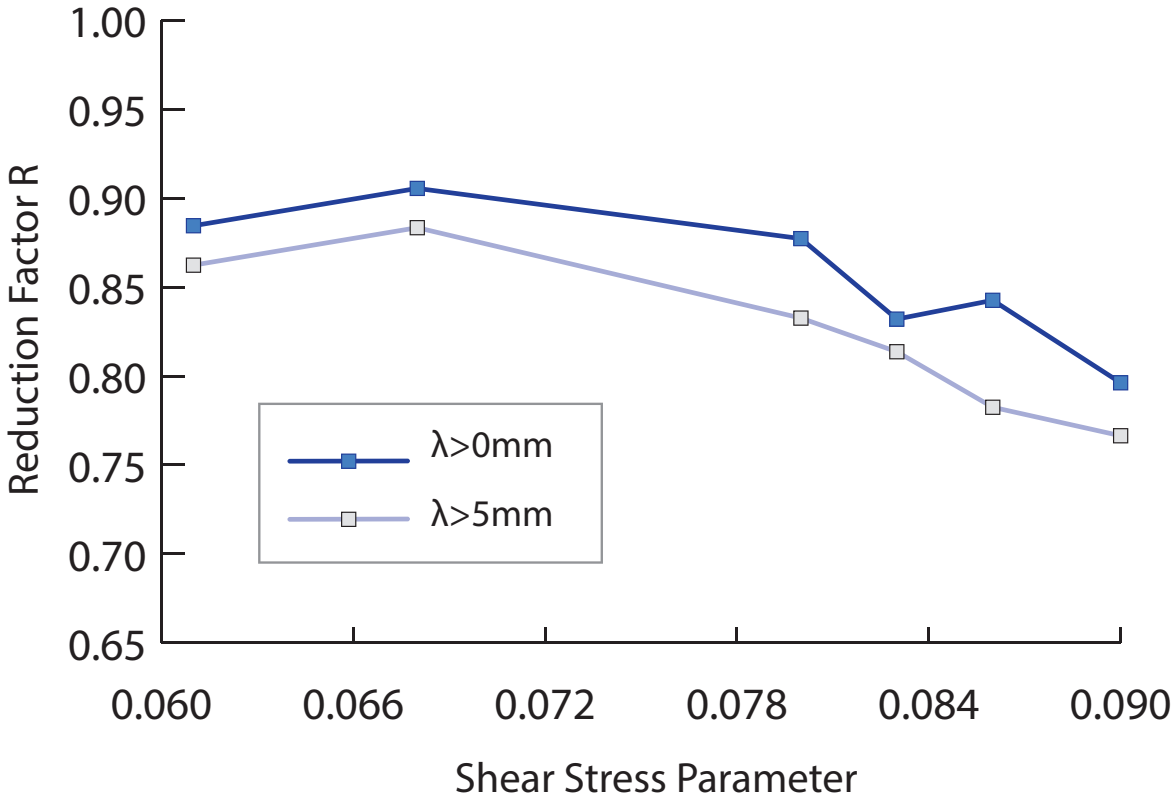

Figure 4.7: Reduction factors vs Shear Stress parameter

After the calculation of the Probability Density Function (PDF) it is possible to calculate the Cumulative Distribution Function (CDF). The points of the CDF can be calculated as the 'Integral' of the area of the PDF. Since the PDF obtained has discrete values the CDF can be calculated by multiplying the value of the PDF with the amplitude of the class dX as reported in Equation 4.6.

$$P(X) = p(X) \cdot dX \tag{4.6}$$

It is important to say that the points of the PDF are divided in classes where all the points have the same value. The CDF instead is calculated in points. If the definition reported in 4.6 is assumed the CDF point will assume the vale $P(X)$ in the point X only, where X represents the higher limit of a class. The CDF obtained for the case of the 24^{th} of August is Reported in Figure 4.9. As can be noticed by the Figure, the maximum value of CDF is lower than the unit. The maximum value for the CDF is the ratio calculated with Equation 4.3.

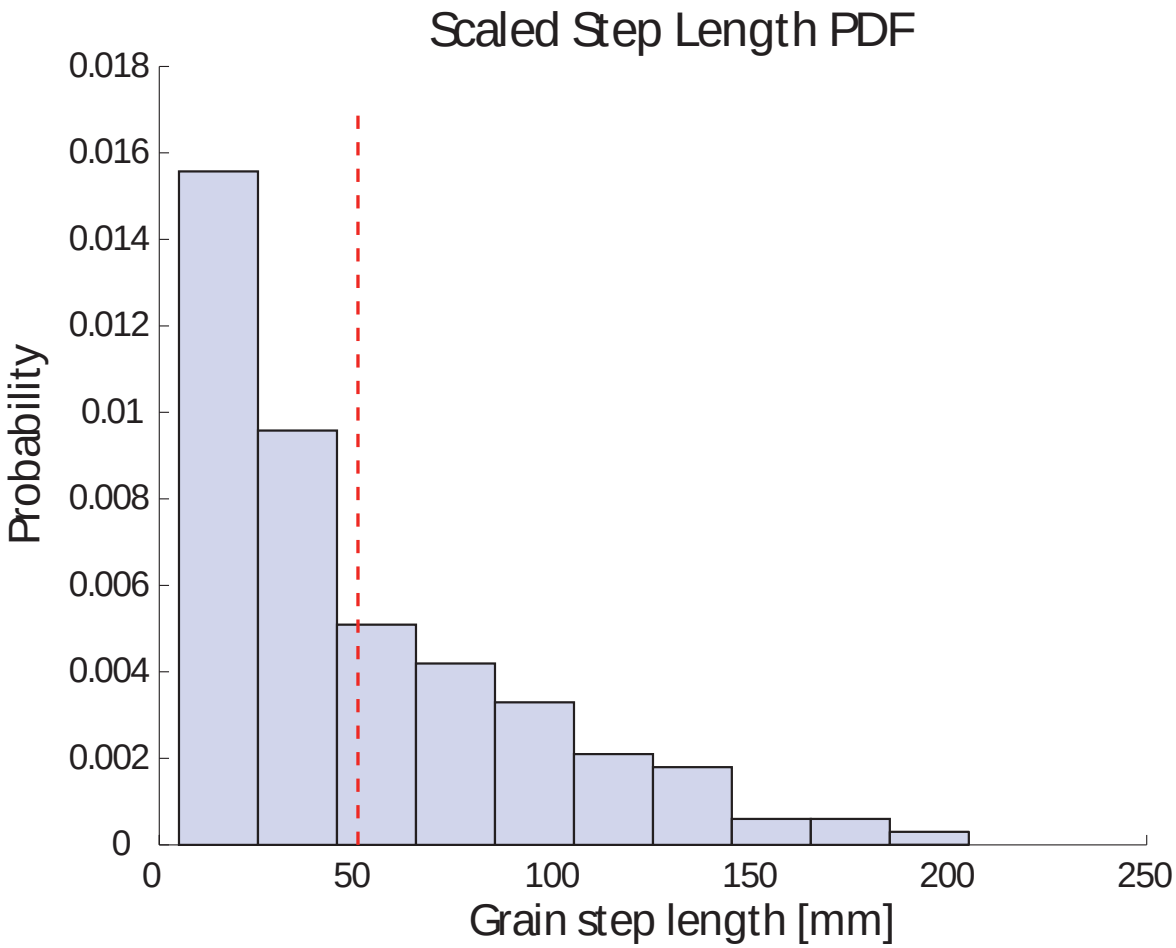

Figure 4.8: Probability Density Function (24^{th} August, 'shakes' excluded)

4.2.5 Statistical Model Fitting

After the calculation of the Cumulative Distribution Function of the Step Lengths it is possible to impose a Statistical Model to the data to obtain a reliable estimation of parameters like mean and variance. This method was necessary because the Grain Movement-type analysis showed that the values of more than 10% step lengths is unknown. The only property known for those step lengths is that their value is higher than 200mm. The model chosen for the step length distributions are reported below:

- Exponential Distribution
- Log-Normal Distribution
- Weibull Distribution

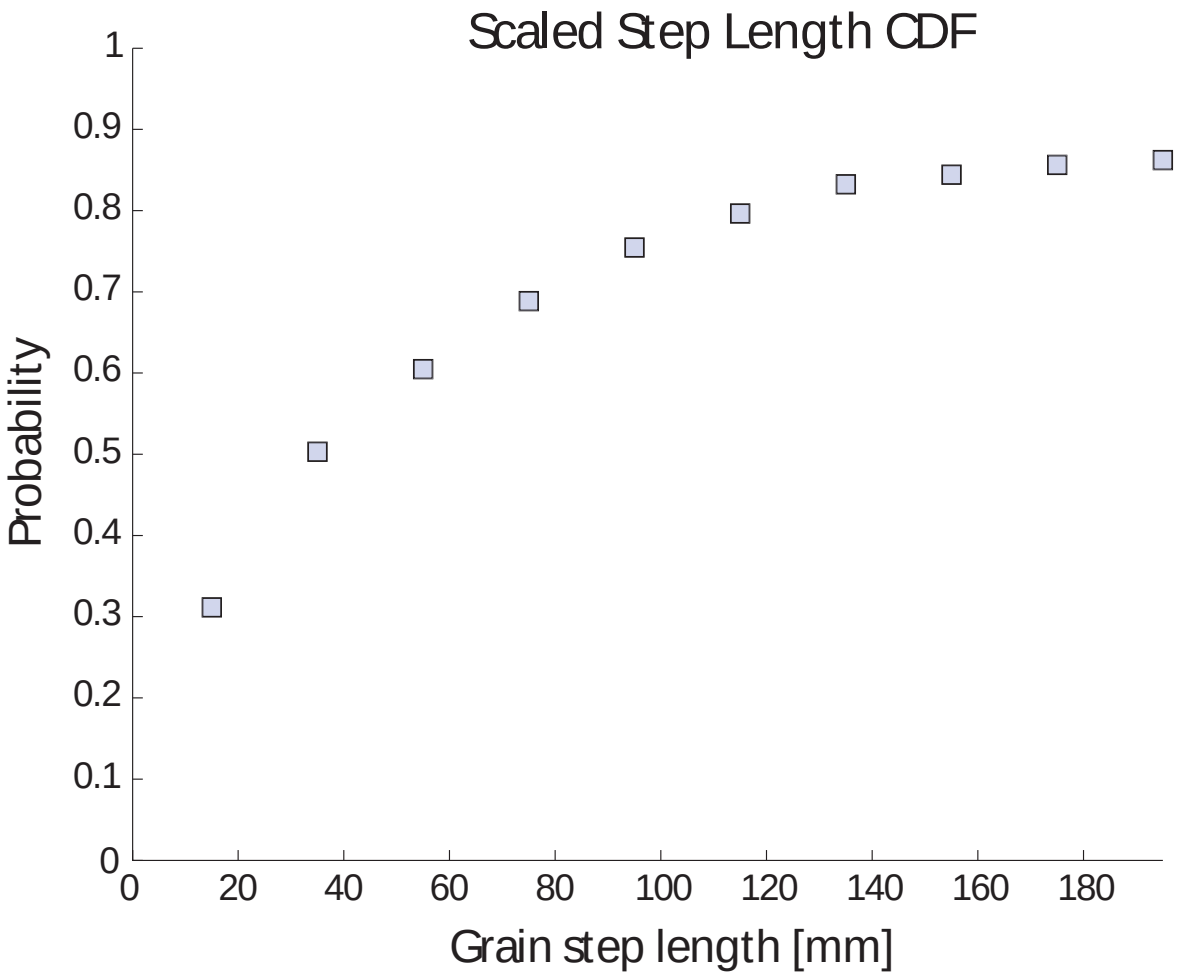

Figure 4.9: Cumulative Distribution Function (24^{th} August, 'shakes' excluded)

- Gamma Distribution

The parameters of the statistical models were found by numerically fitting the CDF curves to the experimental data. The reason to apply a numerical fitting was supported by the fact that the number of data is quite low and their quality is quite poor. The method chosen for the numerical fitting of the distributions was a least squares sum of the residuals. The fitting procedure is divided into steps.

1. A minimum and a maximum value must be assigned for every parameter of the desired ditribution (i.e. $[\alpha_1^{min}, \alpha_1^{MAX}]$ and $[\alpha_2^{min}, \alpha_2^{MAX}]$ in case of two parameters).

2. Each interval is split in a number of 'test' values for the parameters (i.e. if

$\alpha_1^{MAX} = 10$ and $\alpha_1^{min} = 4$ then $\alpha_1 = [4, 4.1, 4.2, ..., 10]$). For each set of test values (in case of two parameters they will be (α_1, α_2)) the CDF curve is calculated.

3. For each set of test values the squared sum of the residuals S is calculated through the following formula:

$$S = \sum_{i=1}^{n} (Y^*(X_i) - Y(X_i))^2 \tag{4.7}$$

Where $Y^*(X_i)$ are the values of the 'test' CDF with parameters (α_1, α_2) calculated in X_i and $Y(X_i)$ is the CDF obtained by experimental observations. Therefore there will be a value for S for each set of 'test' parameters.

4. The minimum value for S is found. This procedure in case of two parameters is reported in Figure .

The reason why the fitting is focussed on the CDF and not on the PDF is that the result obtained for the fitting of the former is satisfying for the latter too. The result obtained from the fitting of the PDF gives a poor estimation of the CDF.

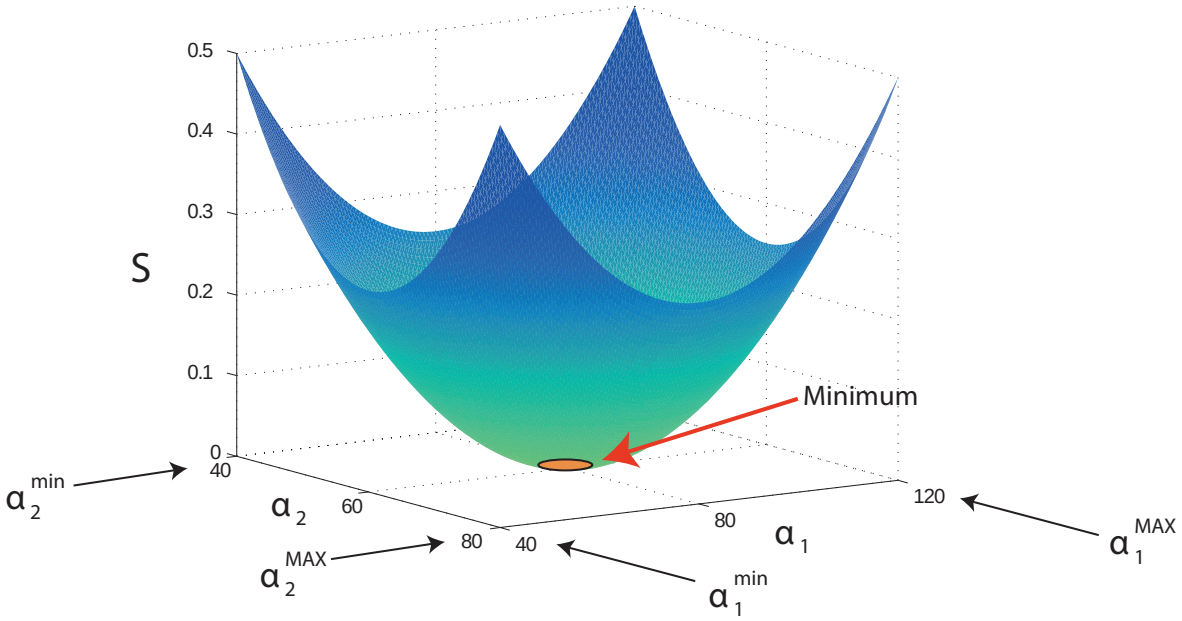

Figure 4.10: Least squares sum of the residuals in case of two parameters

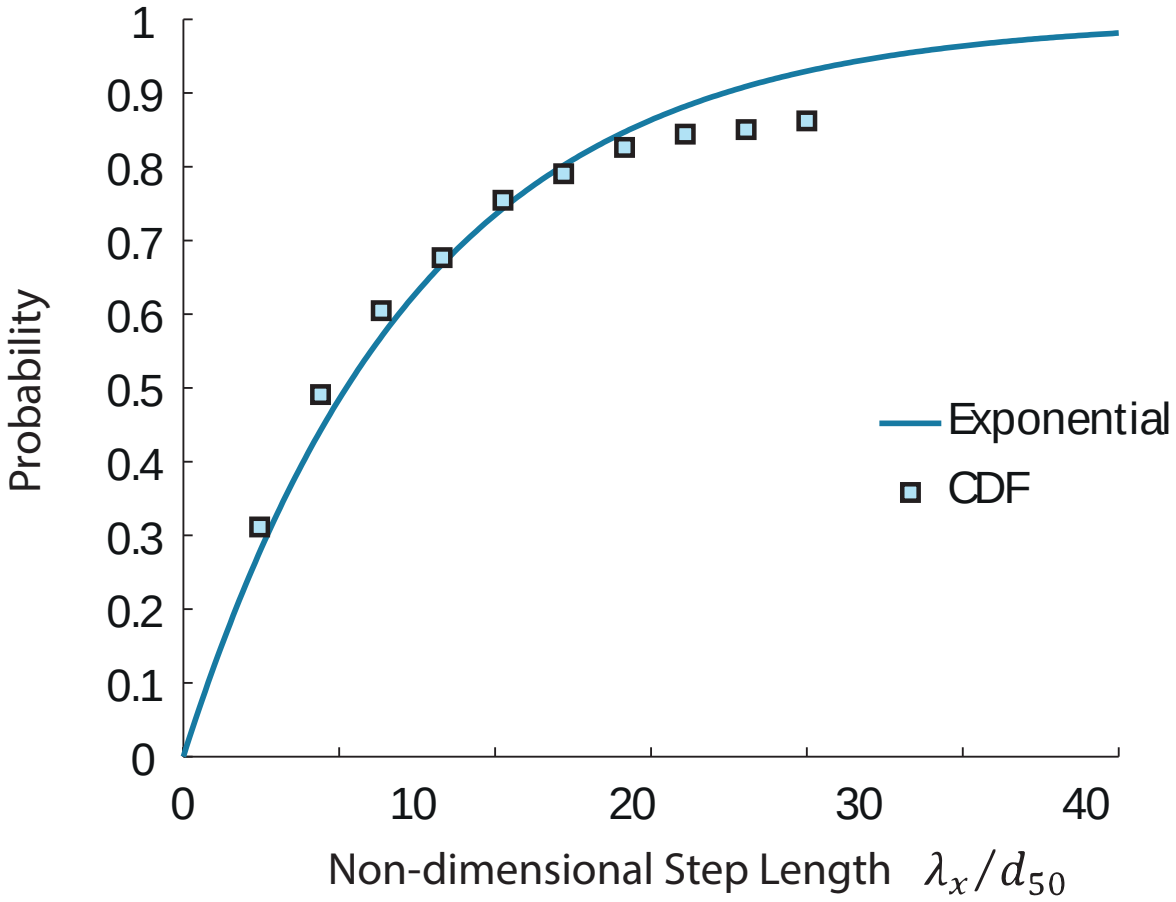

Figure 4.11: Exponential fitting for the case of August 24^{th} - 10 classes (CDF)

4.2.6 Exponential Distribution Fitting

The exponential distribution is a 1-parameter distribution. The formula for the Cumulative Distribution Function is reported in Equation 4.8.

$$P(X < x) = 1 - e^{-\lambda \cdot x} \tag{4.8}$$

The mean value of the Exponential distribution $\mu = 1/\lambda$. For this distribution $\sigma = \lambda$. The parameters that will be fitted numerically will therefore be:

1. μ: Mean value of the distribution

The best-fitting curve for the 24^{th} of August for the case of 'Shakes' excluded is reported in Figure 4.11.

The result of the fitting for all experiments is similar to the one showed in Figure 4.11.The fitting for all other experiments and cases are reported in Figures 7.5, 7.6, 7.7,

7.8 for what regards the CDF. As can be seen the quality of the fitting is quite poor. The use of the exponential distribution is not probabily a good choice to represent the step length distribution. This fact could be related to the nature of the distribution. If the grains follows an exponential distribution there should be a lot of grains that travel very short distances. This feature of the process (if it exists) is impossible to spot in this experiments: Very short displacements of a grain can't be spotted by an human eye.

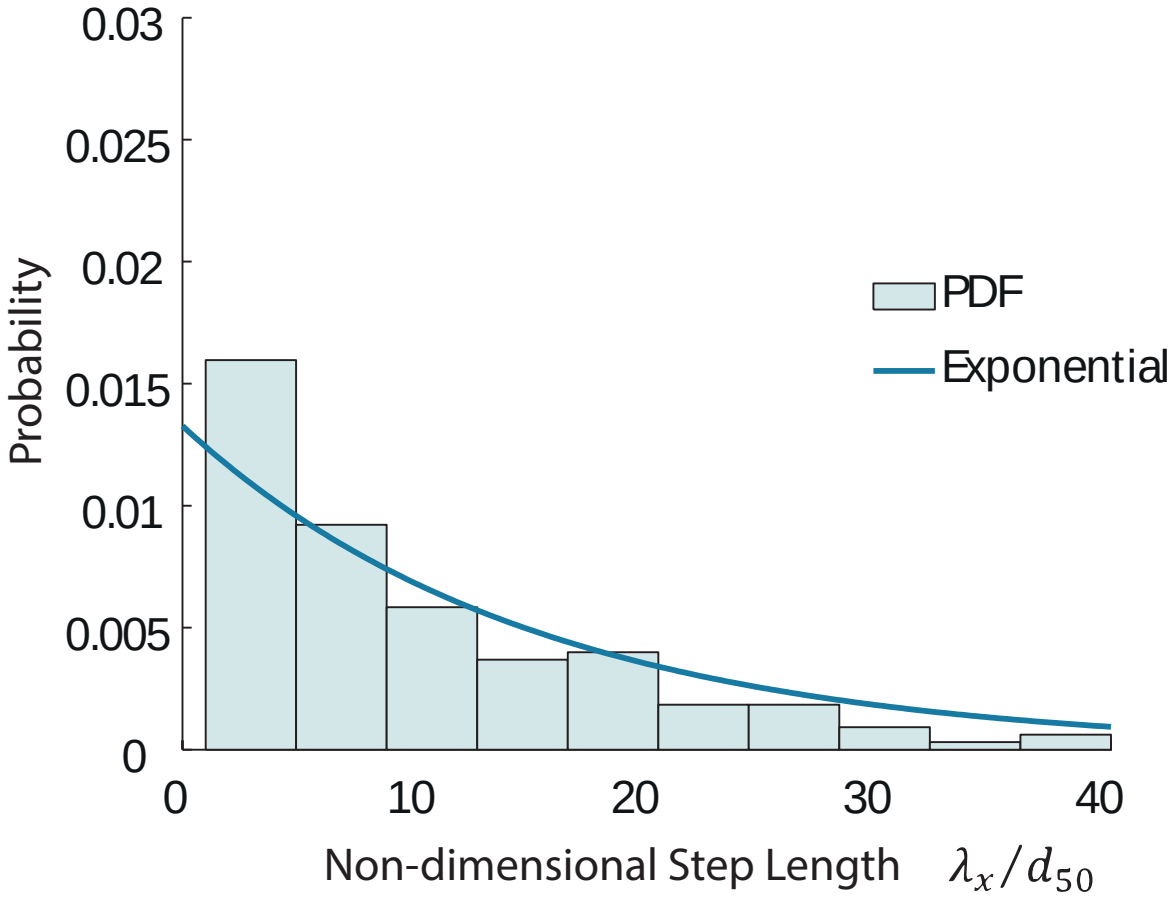

Figure 4.12: Exponential fitting for the case of August 24^{th} - 10 classes (PDF)

The fitted Probability density function (PDF) is reported in Figure 4.12. This probability density function is calculated with the same parameters obtained from the fitting of the CDF. As can be seen from the picture, the result in this case is quite satisfying. The fitting for all other experiments and cases are reported in Figures 7.9, 7.10, 7.11, 7.12 for what regards the PDF.

All databases were fitted with an exponential distribution and the result in terms of mean step lengths is reported in Figure 4.13. The figure shows that the presence or not (in this case) of shakes has a major influence on the results of the fitting. A minor effect is played by the number of classes for the calculation of the PDF. If the 'shakes'

are considered there is not a clear trend in the mean step length versus shear stress. If they are neglected instead a clear trend can be seen. If this statistical model is valid a relationship between the mean step length and the non-dimensional shear stress can be expected.

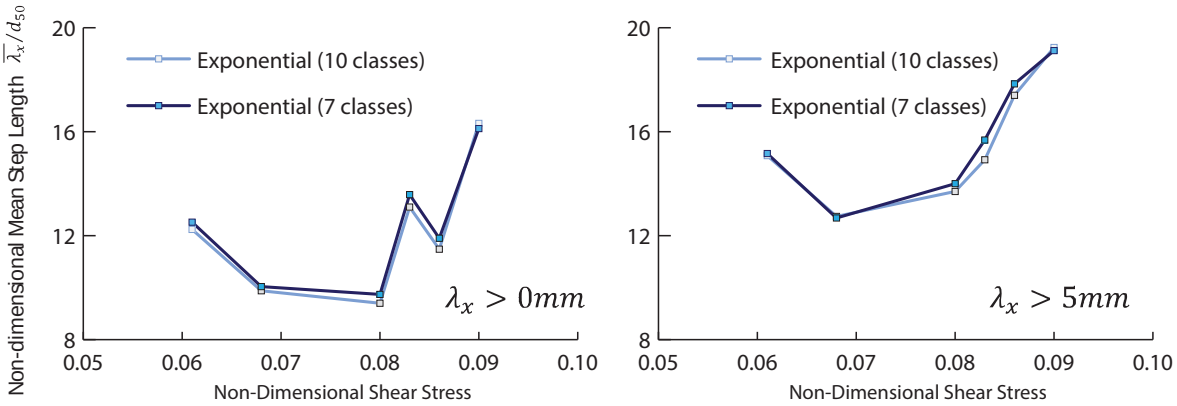

Figure 4.13: Mean Step Length with Exponential Distribution: 'shakes' included (left), 'shakes' excluded (right)

4.2.7 Gamma Distribution Fitting

The gamma distribution is a distribution that is defined by 2 parameters: A shape parameter α and a scale parameter β. The Cumulative Distribution Function can't be expressed algebraically, but can be written as reported in Equation 4.9.

$$P(X < x) = \frac{1}{\Gamma(\alpha)} \cdot \gamma(\alpha, \beta \cdot x) \tag{4.9}$$

Where γ is a known function of the two parameters α, β and x. The two parameters are related to the 1^{st} and 2^{nd} order moments of the distribution through the following relations:

$$E[X] = \mu = \frac{\alpha}{\beta}, \qquad Var[x] = \sigma^2 = \frac{\alpha}{\beta^2} \tag{4.10}$$

The fitting process will be based on the fitting of those two parameters in this case. The parameters that will be numerically fitted in this case will be:

1. μ: Mean of the Distribution

2. σ: Deviation of the Distribution

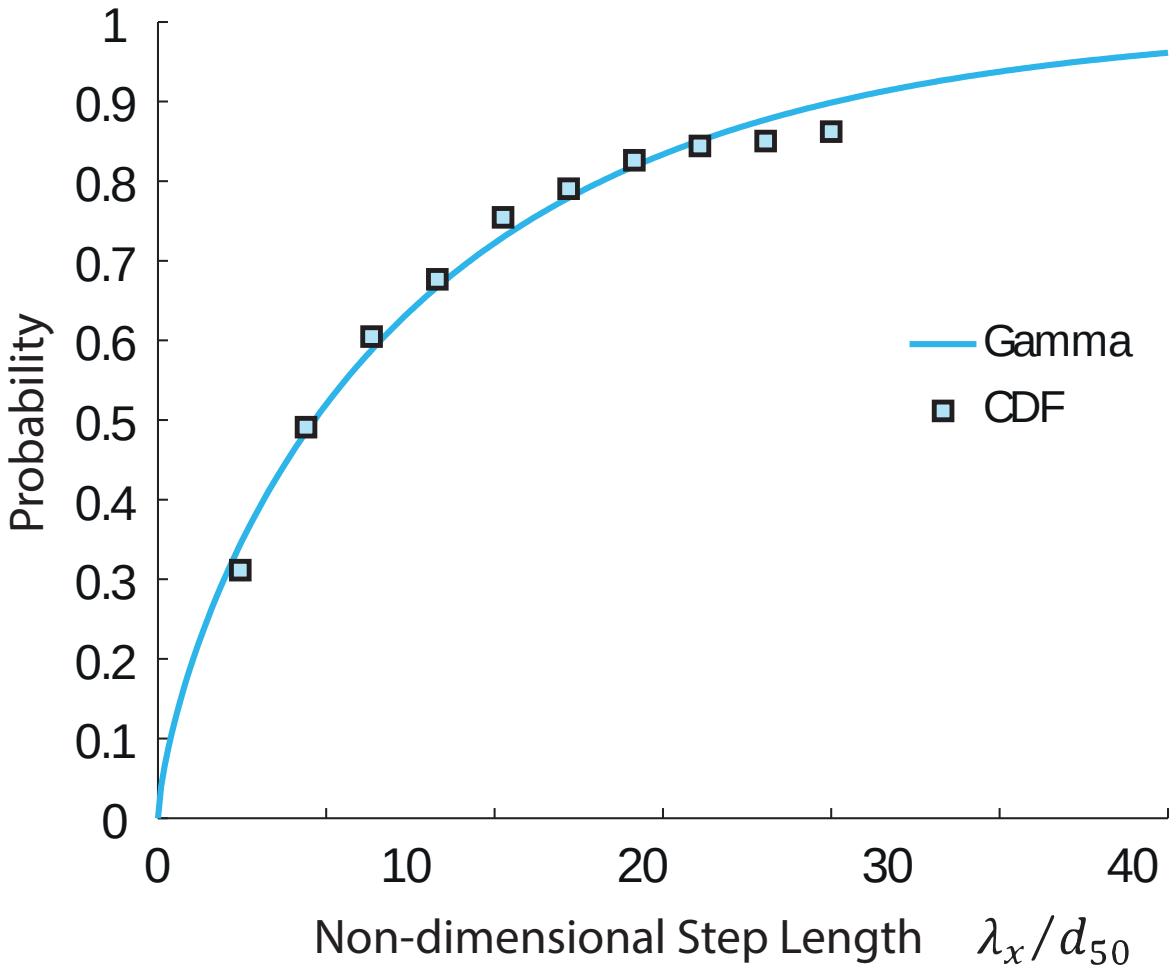

Figure 4.14: Gamma fitting for the case of August 24^{th} - 10 classes (PDF)

When the fitting reaches a satisfying result then the mean and standard deviation are calculated through 4.10. The result for the fitting of the 24^{th} of August with the Gamma Distribution is reported in Figure 4.14. The fitting for all other experiments and cases are reported in Figures 7.5, 7.6, 7.7, 7.8 for what regards the CDF. As can be seen in this case both the low and the high values of the distributions are modelled satisfactorily. However, for what concerns the tails of the distribution, the gamma distributions tends to have higher values respect to the experimental data.

The fitting for the PDF of this particular case is reported in Figure 4.15. As can be seen by the Figure the gamma distribution assumes very high values for low step lengths. In this area the PDF seems to decrease like an exponential function but for higher step lengths the distribution decreases very slowly with a long tail. The fitting for all other experiments and cases are reported in Figures 7.9, 7.10, 7.11, 7.12 for what regards the PDF.

When the fitting is completed it is possible to calculate the mean of the obtained

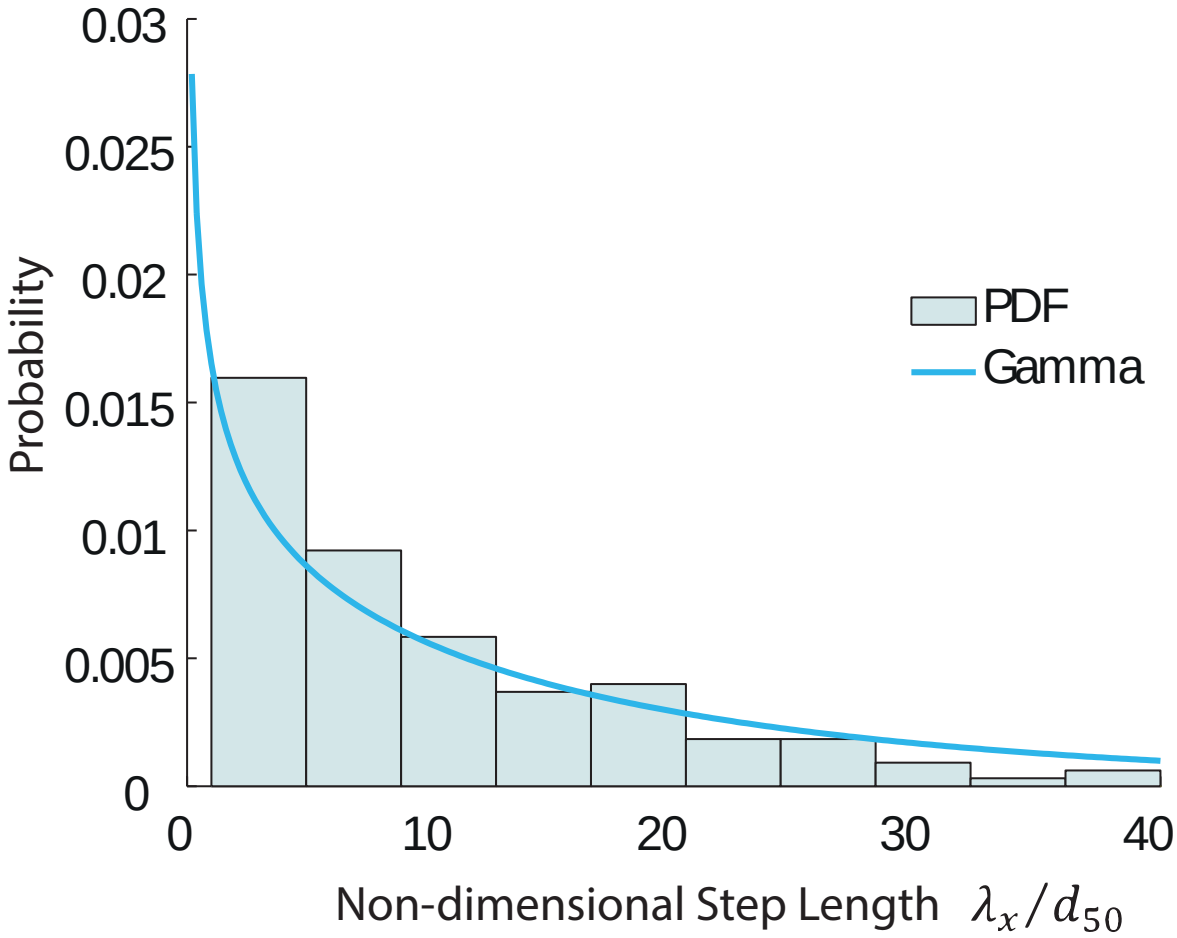

Figure 4.15: Gamma fitting for the case of August 24^{th} - 10 classes (PDF)

distribution through Formula 4.10. The mean value obtained through this procedure is then plotted versus the non dimensional shear stress parameter for each experiment. Four sets of mean values are plotted since two populations are considered ('shakes' included or excluded) and on each population two analysis are performed (7 classes/10 classes). The result obtained is reported in Figure 4.16. As can be seen from this picture a clear trend is present in the 'shakes' included population. A good result can also be seen in case of 'shakes' excluded. In this case too the number of classes seems to have a minor effect on the result in term of mean step lengths. To assess the quality of the fitting the 30 points with lower sum of squared residuals are plotted in a mean-variance plot. The result is reported in Appendix 1 in Figure 7.14.

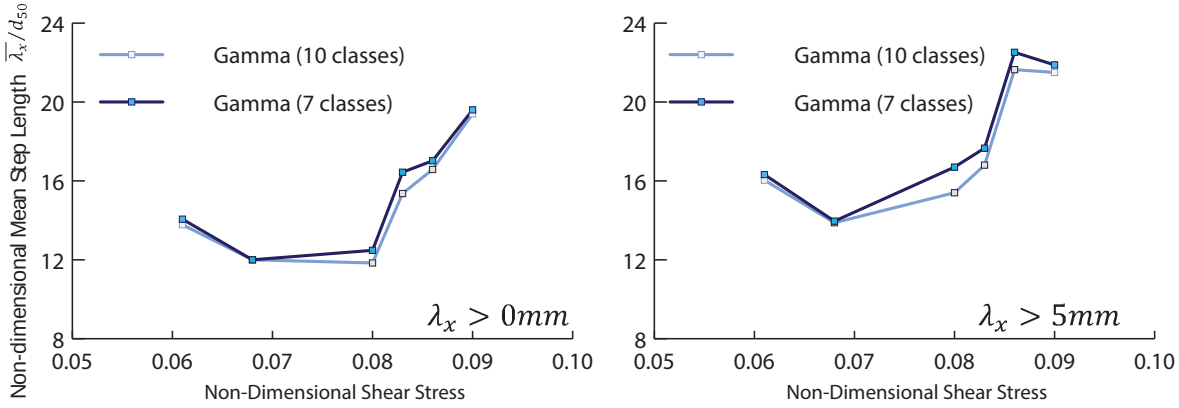

Figure 4.16: Mean Step Length with Gamma Distribution: 'shakes' included (left), 'shakes' excluded (right)

4.2.8 Weibull Distribution Fitting

The Weibull distribution is a distribution that is defined by 2 parameters: A shape parameter k and a scale parameter λ. The Cumulative Distribution Function can be expressed algebraically: the law is reported in in Equation 4.11.

$$P(X < x) = 1 - e^{-\left(\frac{x}{\lambda}\right)^k} \tag{4.11}$$

The two parameters k and λ can be related to the 1^{st} and 2^{nd} order moments of the distribution through Equations 4.12 and 4.13.

$$E[X] = \mu = \lambda \cdot \Gamma\left(1 + \frac{1}{k}\right) \tag{4.12}$$

$$Var[x] = \sigma^2 = \lambda^2 \cdot \left[\Gamma\left(1 + \frac{2}{k}\right) - \left(\Gamma\left(1 + \frac{1}{k}\right)\right)^2\right] \tag{4.13}$$

Where Γ is the gamma function. The parameters k and λ are present in both equations. Therefore they must be calculated by simultaneously solving the two equations through a numerical method. The parameters fitted numerically this time are the follwing:

1. k: The 'shape' parameter
2. λ: The 'scale' parameter

When the fitting is complete, mean and variance are calculated through 4.12 and 4.13. The result of the fitted CDF is reported in Figure 4.17. As can be seen from the Figure the fitting of the CDF is good and it is very similar to the one obtained

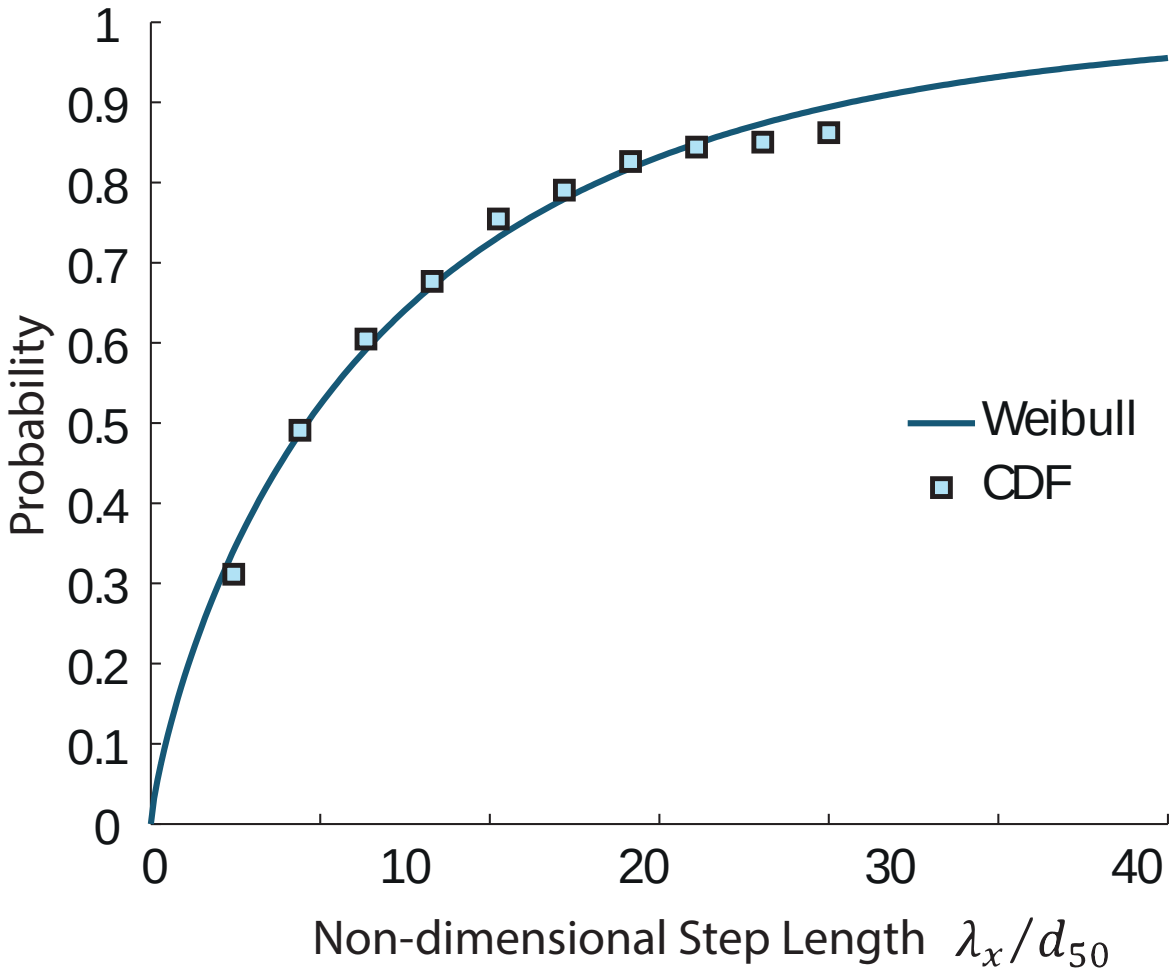

Figure 4.17: Weibull fitting for the case of August 24^{th} - 10 classes (CDF)

with a gamma distribution: The experimental CDF is matched almost perfectly for low values. For high values the match is still good, but the fitted curve tends to have higher value respect to the real curve. The fitting of the CDF for all experiments in the four different analysis are reported in Figures 7.5, 7.6, 7.7, 7.8. The fitted probability density function is reported in Figure 4.18.

In this case the Probability density function has a steep decrease for low values for the step length. For higher step lengths values the decrease is much milder. This kind of shape is assumed for low shape coefficients. As can be seen from the Figure, the quality of the fitting is good in this case too. The fitting procedure is applied to both populations ('shakes' included or excluded) and for both number of classes for the PDF (7 classes or 10 classes). The result in terms of mean step length is reported in Figure 4.19.

As can be seen from Figure 4.19 the behaviour of the mean step length shows a little difference between the cases of 'shakes' included and 'shakes' excluded. In the

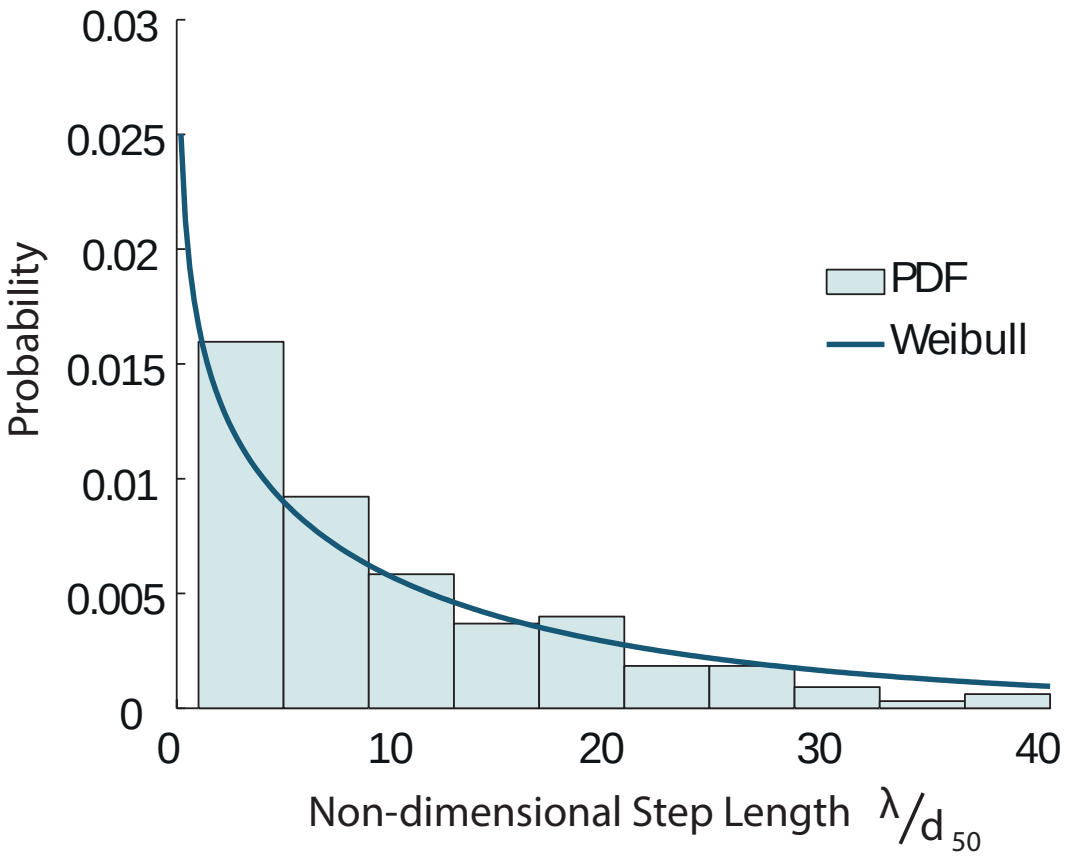

Figure 4.18: Weibull fitting for the case of August 24^{th} - 10 classes (PDF)

previous case the increasing trend can be easily spotted: by increasing the flow intensity (represented by the non-dimensional shear stress) the mean step length increases significantly. If the mean step length values for the experiment of Sept. 2^{nd} (shear stress parameter 0.068) and the experiment of Oct. 1^{st} (shear stress parameter 0.09) are compared, an increase of more than 50% can be observed. The trend is a bit less clear in the case of the latter case. As can be seen by the Figure, there's a little decrease in the last value of mean step length. Therefore a clear trend can't be defined, however a general increase of mean step length with shear stress parameter can be observed. To assess the quality of the fitting the 30 points with lower sum of squared residuals are plotted in a mean-variance plot. The result is reported in Appendix 1 in Figure 7.15.

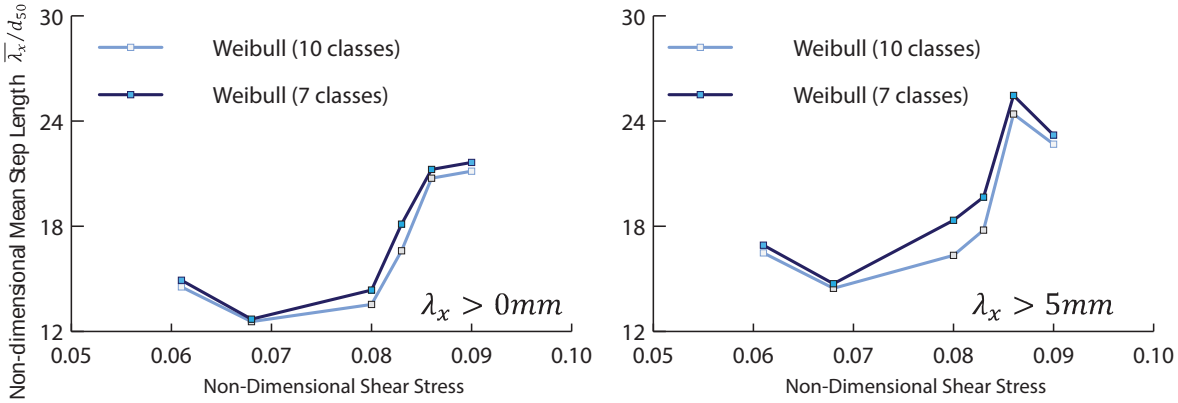

Figure 4.19: Mean Step Length with Weibull Distribution: 'shakes' included (left), 'shakes' excluded (right)

4.2.9 Log-normal Distribution Fitting

The Log-normal Distribution is a continuous probability distribution defined by two parameters: the mean of the associated normal distribution μ and the variance of the associated normal distribution σ^2. Usually a log-normal distribution is defined through an associated normal distribution because the logarithm of the data follows a normal distribution. The Cumulative distribution function (CDF) expressed in function of μ and σ^2 is reported in Equation 4.14.

$$P(X < x) = \frac{1}{2} + \frac{1}{2} \cdot erf\left[\frac{\ln(x) - \mu}{\sqrt[2]{2} \cdot \sigma}\right] \tag{4.14}$$

It is possible to express the mean and the variance of the log-normal distribution as a function of the mean and the variance of the associated normal distribution μ and σ^2. From now on μ_N and σ_N^2 will be used to express the mean and variance of the associated normal distribution, instead μ_{lnN} and σ_{lnN}^2 will be used to express the mean and variance of the log-normal distribution. The first and second moment of the data can be linked to the mean and variance of the associated normal distribution through Equations 4.15 and 4.16.

$$E[X] = \mu_{lnN} = e^{\mu_N + \frac{\sigma_N^2}{2}} \tag{4.15}$$

$$Var[x] = \sigma_{lnN}^2 = (e^{\sigma_N^2} - 1) \cdot e^{2 \cdot \mu_N + 2 \cdot \sigma_N^2} \tag{4.16}$$

Through Equations 4.15 and 4.16 it is possible to obtain the mean and the variance of the log-normal distribution. The fitting of the log-normal distribution is obtained through the use of the following parameters:

1. μ_{lnN}: Mean of the Log-normal distribution

2. σ_{lnN}: Deviation of the Log-normal distribution

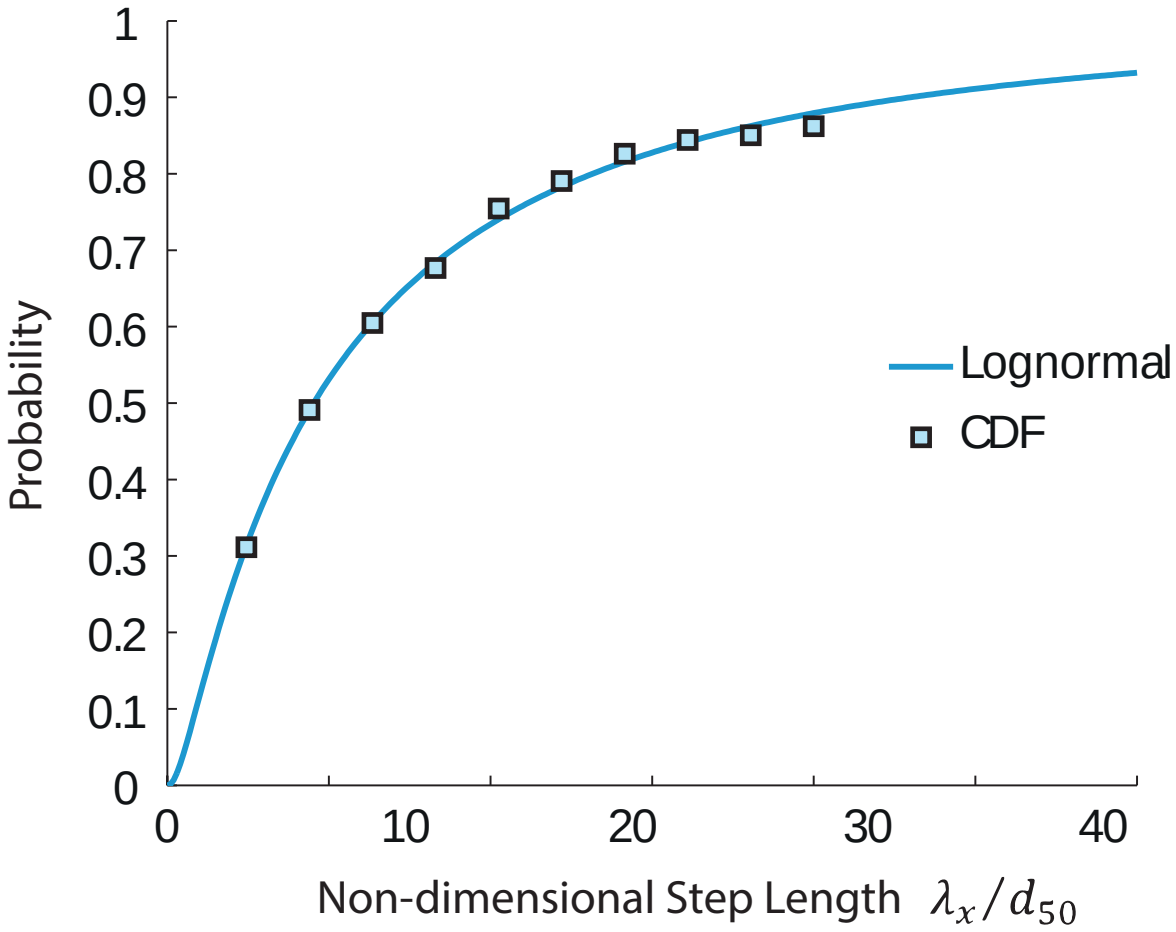

Figure 4.20: Log-normal fitting for the case of August 24^{th} - 10 classes (CDF)

The result of the fitted CDF for the case of Aug the 24^{th} is reported in Figure 4.20. The fitting of the CDF in this case is almost perfect. The distribution accurately esttimate the points for both low step lengths and high step lengths: this is the best distribution so far found to model the long tails of the distribution. The result of the fitting procedure for all other cases is reported in Appendix 1 in Figures 7.5, 7.6, 7.7, 7.8. By examinating all the fits the conclusion is that the most accurate fits are obtained with the population with the 'shakes' included. The fitted PDF is reported in Figure 4.14.

In this case the shape of the Probability Density function is totally different from the ones obtained from the previous distributions. The maximum value for the density is not any more for the value of step length $\lambda_x = 0$. The Probability function in this case assumes a value close to zero for low step lengths, increases quickly and then decreases very slowly, with a long tail. Qualitatively the fit of the PDF looks very accurate for both the low values and the high values of step lengths. The problem with

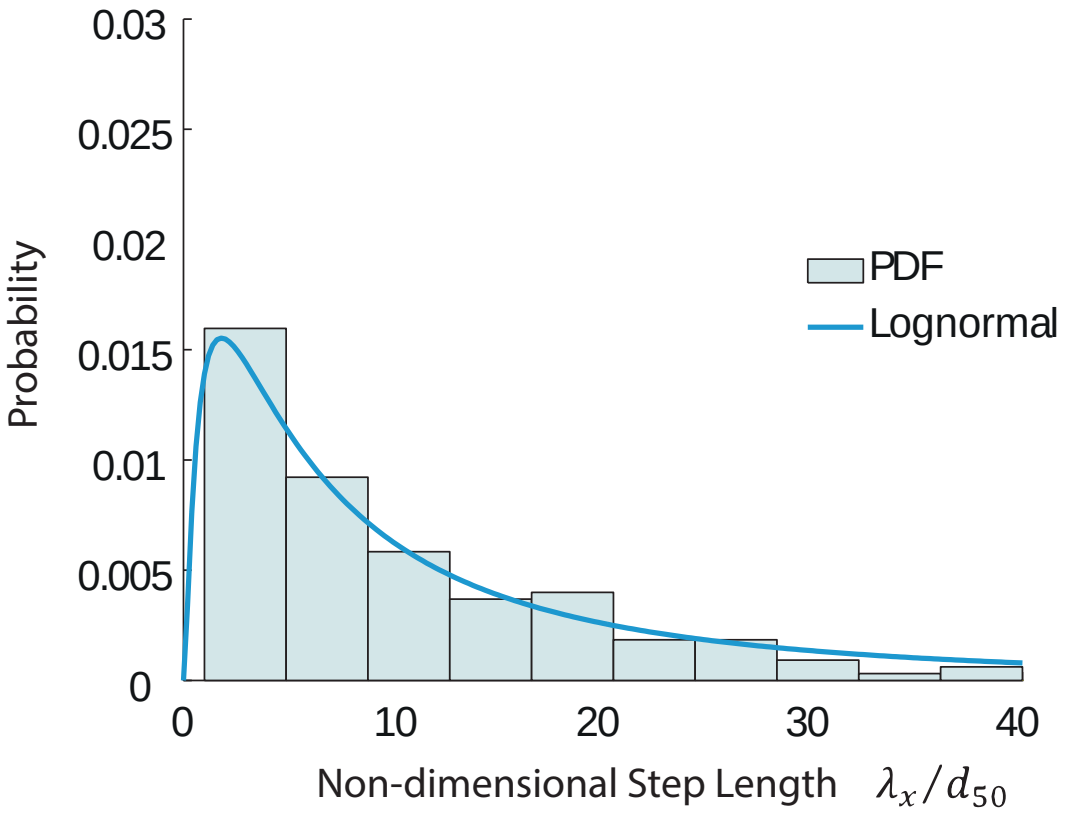

Figure 4.21: Log-normal fitting for the case of August 24^{th} - 10 classes (PDF)

the log-normal distribution is that the values obtained for the mean and variance are considerably higher than the ones obtained with the other distributions. The fitted Probability density functions for all the other cases are reported in Figures 7.9, 7.10, 7.11, 7.12. The result of the mean step length obtained through the fitting for each experiment is reported in Figure 4.22. The Figure shows that for both populations ('shakes' included or excluded) the mean step length generally increases by increasing the non dimensional shear stress parameter. The effect caused by the variation of the number of classes is negligible for the case of 'shakes' excluded. For the case of 'shakes' included instead the result is a bit different. For the experiment of September the 22^{nd} (shear stress parameter 0.080) and September 23^{d} (shear stress parameter 0.083) there's a difference of about the 20% between the mean step length obtained with 10 classes and the mean step length obtained with 7 classes. To assess the quality of the fitting the 30 points with lower sum of squared residuals are plotted in a mean-variance plot. The result is reported in Appendix 1 in Figure 7.16.

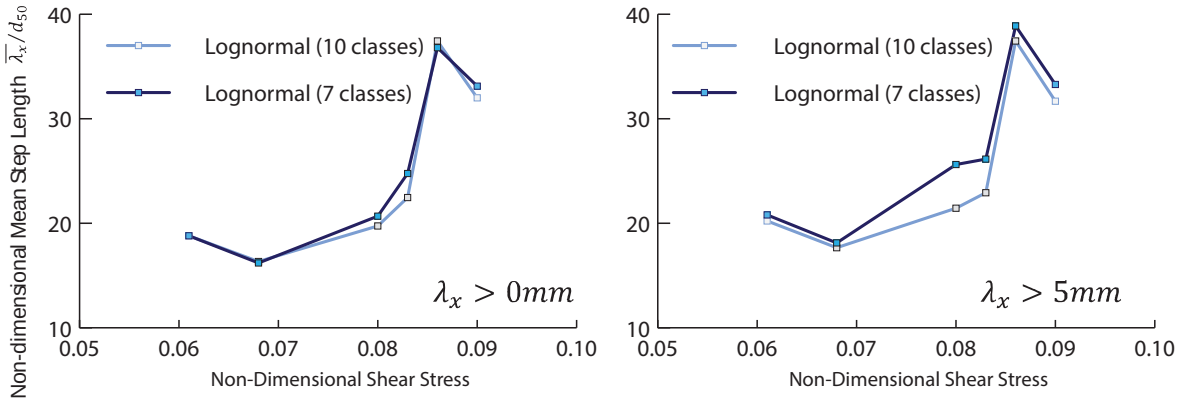

Figure 4.22: Mean Step Length with Log-normal Distribution: 'shakes' included (left), 'shakes' excluded (right)

4.2.10 Results

The fitting procedure showed that:

1. The *Exponential* distribution is not the most suitable statistical model to use to represent the step lengths. The exponential distribution has very short tails, therefore the higher step lengths can't be modelled appropriately. On the other hand, the fitting of the data with this distribution is very quick and simple. The mean step lengths obtained does not show a clear trend with the shear stress parameter if the 'Shakes' are included in the population. If the 'Shakes' are excluded the a clear trend can be observed. The effect of the variation of the number of classes in this case is negligible.

2. The *Gamma* distribution accurately captures some features of the step lengths observed. The fitted curve matches almost perfectly the points obtained by experimental data. However, this distribution seems to loose precision in proximity of the higher values of the step length. An increase in mean step length with the shear stress parameter can be observed for all the cases considered. The variation of the number of classes in this case has a very weak effect on the mean step length obtained.

3. The *Weibull* distribution has a good result in terms of fitting. The Fitted CDF in all experiments is very close to the CDF obtained by the Gamma distribution. The CDF obtained accurately estimates the probability for low values of step lengths. For high values of the step lengths the fitted CDF assumes probability values a bit higher than the ones found through the experimental investigations. For what concerns the link between mean step length and shear stress parameter the trend is clear for both 'shakes' included and 'shakes' excluded. The variation of the number of classes has a minor effect in this case.

4. The *Lognormal* distribution is probably the best distribution to use to fit the data for what concerns both the low values and high values of step length. The fitted CDF for about all experiments accurately matches the points obtained through experimental observations. The PDF has a particular shape respect to the other distributions, but the result of the fitting is very accurate. The mean step length against shear stress parameter shows that those two quantities are probably correlated. The number of classes used for the construction of the PDF in this case has a negligible effect in case of 'shakes' included, but the effect is not negligible for the 'shakes' excluded.

Figure 4.23 shows the sum of errors for the test of the Population without shakes and 10 classes for the histogram. It is clear that the distribution that better fits the experimental data is the log-normal distribution followed by the Weibull distribution. The Gamma distribution is the one that presents the higher sum of errors, except for the exponential distribution which is not plotted: the error relative to exponential distribution was an order of magnitude higher than the error relative to Gamma distribution. The same plot for all experiments is reported in Chapter 7 Figure 7.13.

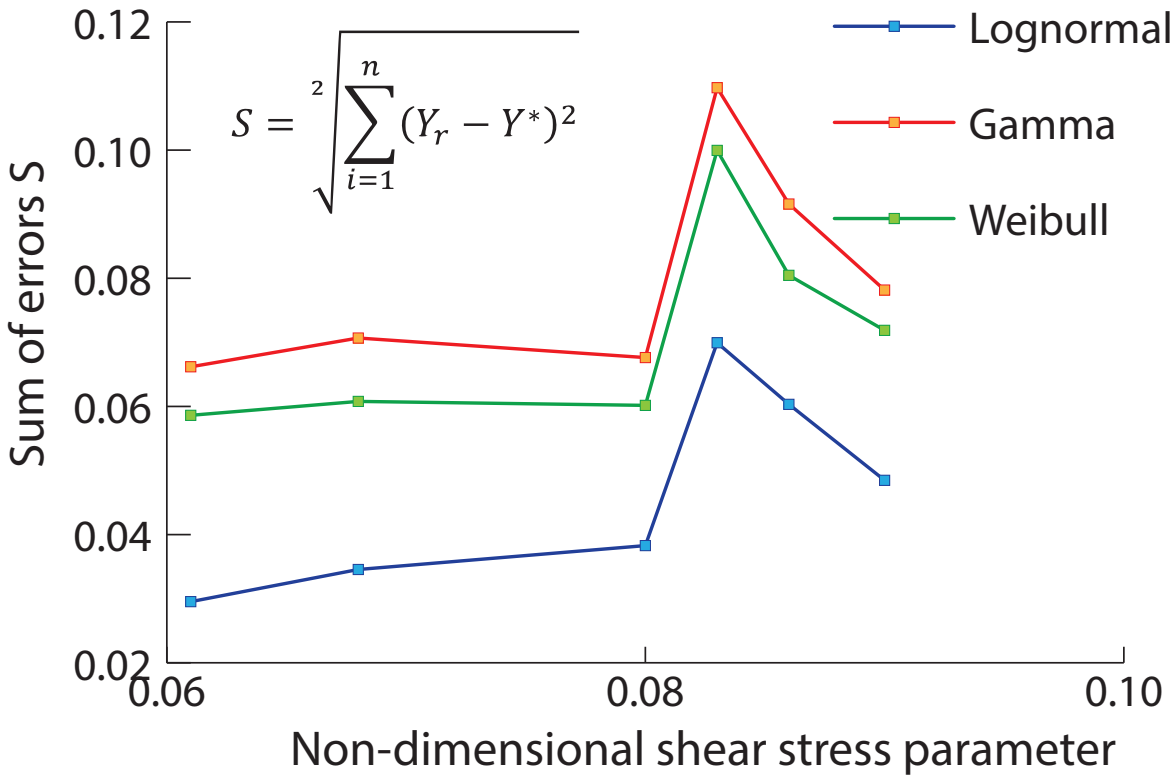

Figure 4.23: Sum of error vs. Shear stress parameter for the case of 24Aug - No shakes, 10 Classes

4.3 Grains Velocity

4.3.1 Analysis

The data obtained through the tracking of the experiments can be used to study the velocity of the grains that are entrained by the flow. The images recorded by the camera are taken with a frequency:

$$f = 45Hz = \frac{1}{\Delta t} \rightarrow \Delta t = \frac{1}{45}s \simeq 0.022s \tag{4.17}$$

The position of a moving grain is recorded in each frame. Therefore the travel distance in the stream-wise direction followed by a grain between two consecutive frames can be calculated as follows:

$$\Delta X = X_{f_i} - X_{f_{i-1}} \tag{4.18}$$

Where X_{f_i} is the position of a grain in the i^{th} frame, and $X_{f_{i-1}}$ is the position of the same grain at the previous frame($(i-1)^{th}$ frame).

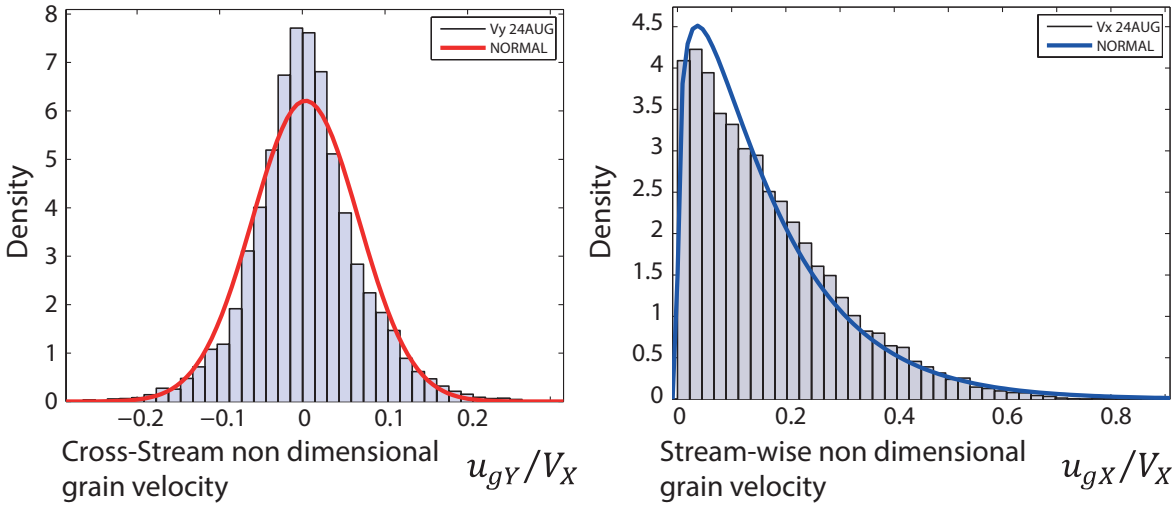

Figure 4.24: Non-dimensional Grain Mean Velocity and deviation vs Shear stress parameter: Streamwise (left), Cross stream (right) for the case of August 24^{th}

With those data available it is possible to calculate the population of the grain velocities as the ratio between travel distance and time. Therefore the grain stream wise velocity component averaged over a time window $\Delta t \simeq 0.22s$ can be calculated as:

$$v_x = \frac{\Delta X}{\Delta t} \tag{4.19}$$

This procedure is applied in the database between those grains that have two or more consecutive 'move' states. When the velocity population is available it is possible to look at the probability distribution function of the stream-wise velocity. The stream-wise velocity component for the case of August the 24^{th} is reported in Figure 4.24. In Figure it is reported the fitting of the PDF. In this case the statistic model used was a Gamma distribution. The same plot for all experiments is reported in Figure 7.17. For the case of grain velocity the population is large enough to have reliable statistics. The stream-wise velocity in all experiments seeems to be described accurately with a Gamma distribution. By fitting all experiments with this distribution it was found that the Grain Velocity seems to be identically distributed and indipendent from the shear stress parameter.

The velocity analysis was performed also in the case of the cross stream direction. In the case of cross stream velocities the data are centred in zero and the distribution is symmetric (as expected). The result for the others experiments are reported in Figure 7.18. The distribution chosen in this case to fit the data was a normal distribution. The PDF obtained trough the fitting with a normal distribution is a good estimation of the cross stream velocity. However the normal distribution seems to underestimate the probability for the values close to zero. The distributions of cross stream velocity seems to be independent from the shear stress parameter.

4.3.2 Results

1. The stream-wise velocity seems to follow a Gamma Distribution. The statistics of the fitted distributions seems to be independent from the shear stress parameter.

2. The cross stream velocity seems to follow a Normal Distribution. The distribution obtained experimentally has a mean value around zero and is symmetric. However, the Normal distribution under estimate the density for values around the mean of the distribution. The statistics of the fitted distributions seems to be independent from the shear stress parameter.

4.4 Grains Rest time

In this section a simple analysis on the particles rest time will be performed.

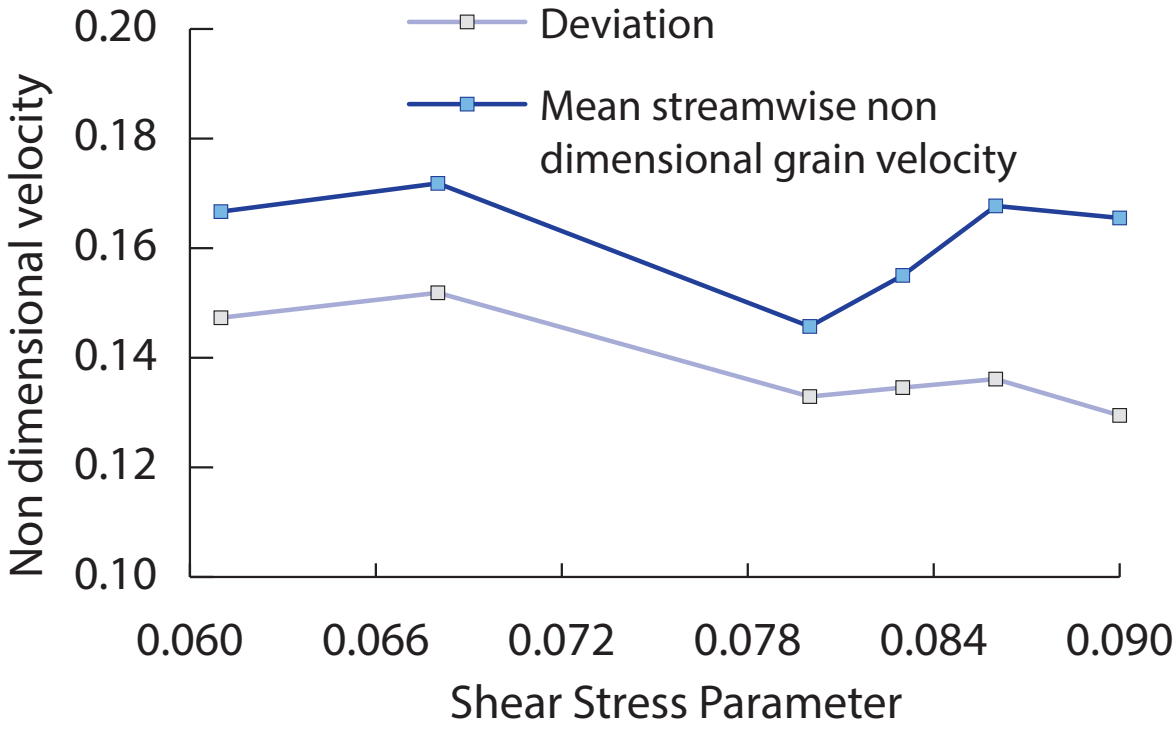

Figure 4.25: Mean and Deviation of the stream-wise velocity vs. shear stress parameter

4.4.1 Analysis

The particles rest time is an important quantity to study in bed load transport processes. The transport of a particle is composed by quick movement phases alternated by long resting phases. A particle has a registered state, position for each frame in which it performs an action. Therefore, by looking at the history of a grain it is possible to estimate the rest time as reported in Equation 4.20.

$$t_R = t_{start} - t_{stop} \tag{4.20}$$

Where t_{start} is for each grain the time in which a grain starts to move (state=1) and t_{stop} is the time of the last recorded stop in the grain history (state=3). If this analysis is applied to the data it is possible to derive the population of the rest times. The derived PDF for the case of $Aug.24^{th}$ is reported in Figure 4.26. The PDF for all other data are reported in Appendix 1 in Figure 7.19.

The red line is the PDF obtained through the fitting of an Exponential distribution. The fitted curve PDF is reported for illustrative purposes only, since the PDF derived for the Rest Times can't be described properly by using the data available. Probably the number of available data is too low for all experiments. The only possible analysis that can be made on the rest times is just the calculation of the mean. In Figure 4.27 it is reported the mean rest time for each experiment plotted against the shear stress parameter. As can be seen from the Figure, no clear trend can be observed. However,

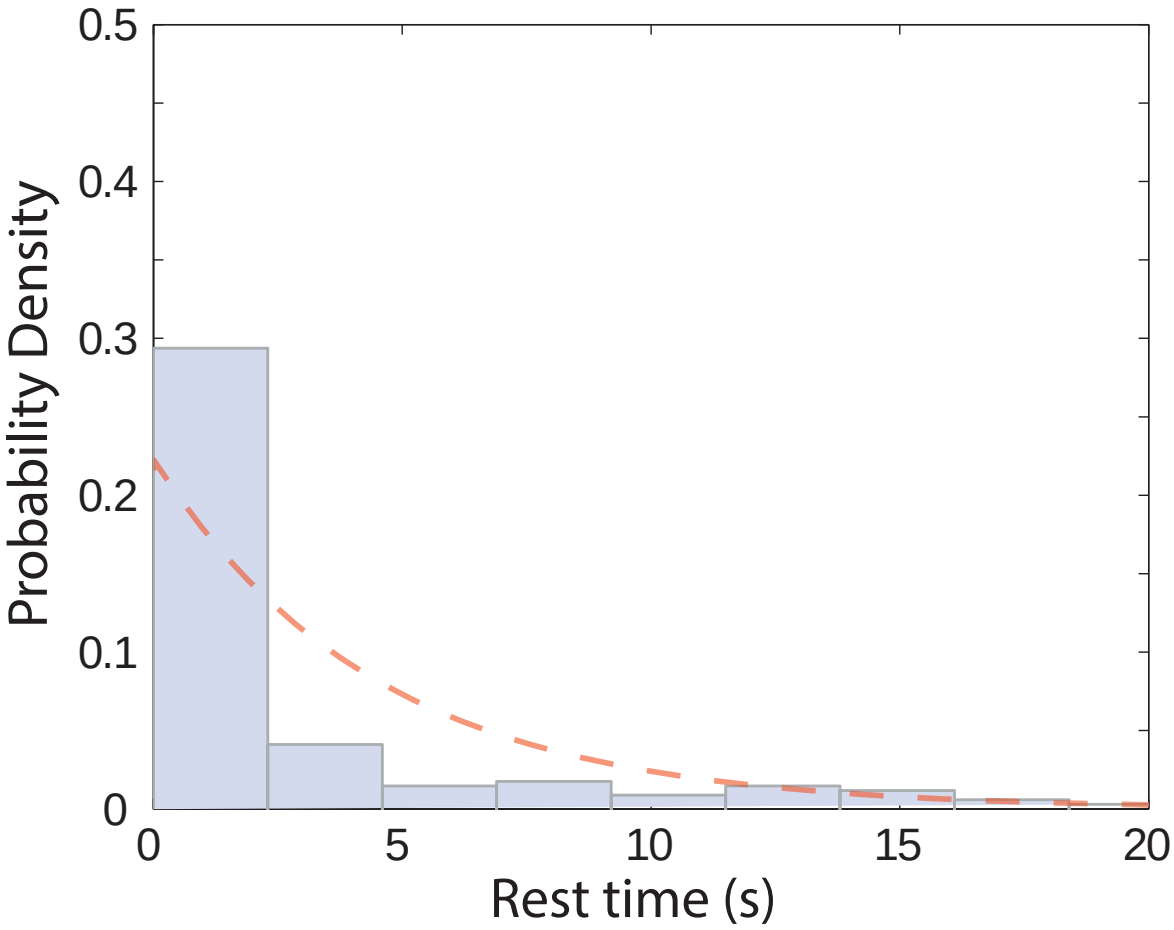

Figure 4.26: Grain rest time for the case of August 24^{th}

the number of data used to describe the population is probably too low, therefore no conclusion can be made for what concerns the rest time.

4.4.2 Results

1. The number of data available to perform the grain rest time analysis is probably too low to have a clear result.
2. The link between the mean rest time and the shear stress parameter can't be described with the present study.
3. The population seems to be characterized by the presence of many low values of grain rest times and few high values.

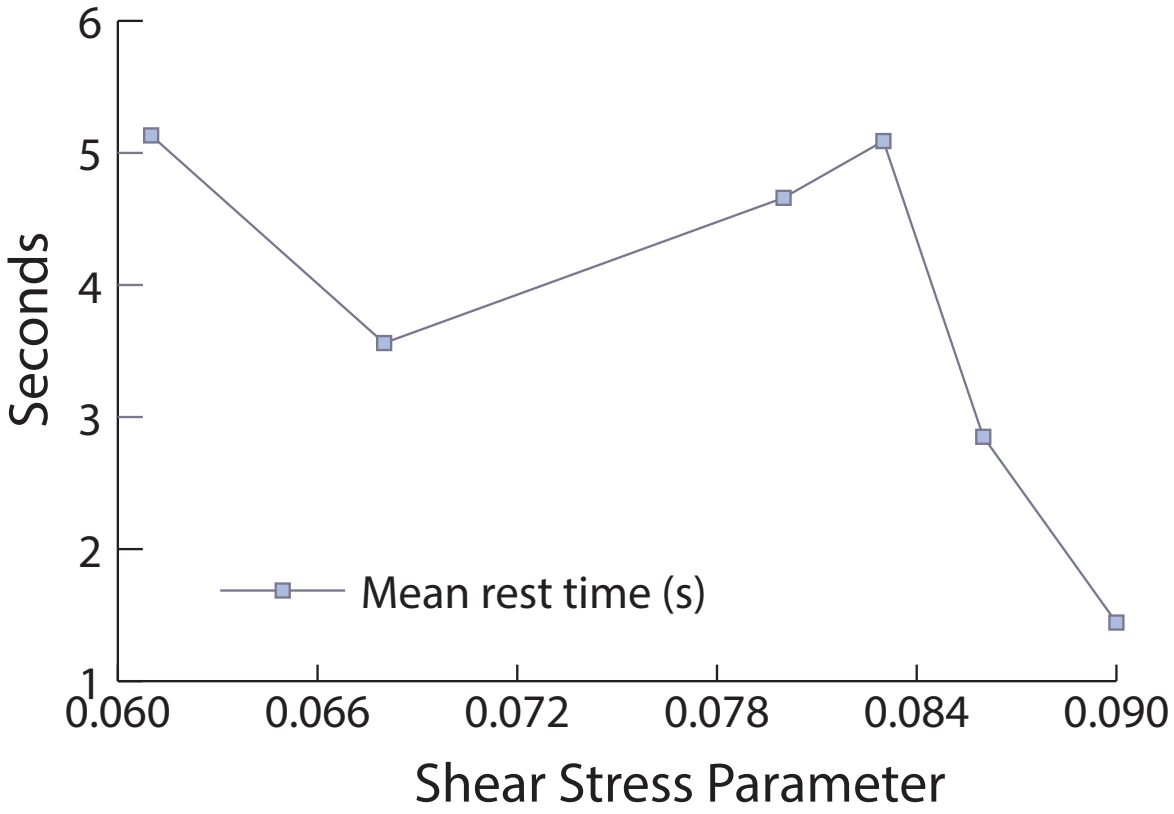

Figure 4.27: Grain rest time vs. shear stress parameter

4.5 Grains Diameter and Step Length

In this section the link between the the grains diameter and the step lengths will be investigated. Theoretically, the grains which have an higher diameter should travel a lower distance and the grains with lower diameter should travel longer. This is due to the fact that in the same flow conditions if the particle diameter increases the weight force will increase faster than the hydrodynamic forces such as lift and drag force. The reason is because of the fact that hydrodynamic forces are proportional to the square of the diameter (d^2) instead weight force is proportional the cube of the diameter (d^3). This means that particles that have a bigger diameter once entrained should tend to deposit more quickly respect to finer particles, therefore the travel distance should be lower.

4.5.1 Analysis

The first step in this analysis is to obtain an estimation of the grain diameters by using the data stored inside the databases. In the grain database there are 3 properties that are linked to the grain diameter:

- area: The value of the grain area enclosed by the tracked border.
- border: The position of the points that defines the border of a grain.
- bbox: The value of the two sides of the rectangle that encloses the grain.

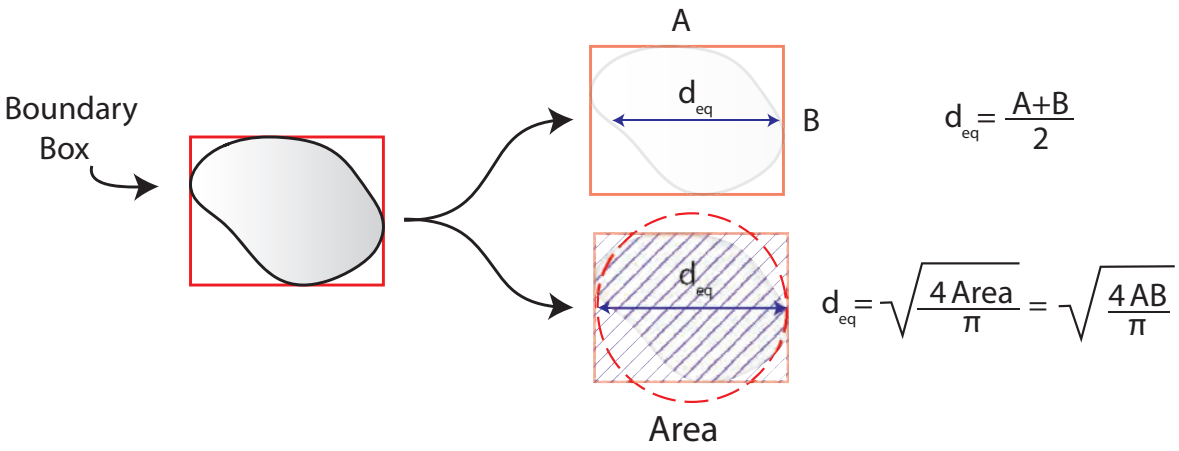

Figure 4.28: Estimation of the equivalent diameter d_{eq} from the boundary box

For more detailed explanations about these quantities consult Chapter 3 in Figure 3.8. The choice in the present study was to use the boundary box to define the diameter. Two different methods were used to estimate the diameter value:

1. : Mean side: The diameter d_i is calculated as the mean value between the two sides of the boundary box, therefore if one side is called A and the other B then $d_{eq} = (A + B)/2$.
2. : Equivalent Area: The diameter d_i is calculated as the diameter of the circle that has the same area, therefore $d_i = [(4 \cdot A)/\pi]^{1/2}$.

The two procedures to calculate the diameter are reported in Figure 4.28. Both of those methods, however, will lead to an over estimation of the grain diameter. As stated previously the boundary box assumes a different value in every frame in which a grain is moving. Therefore for each grain registered the equivalent diameter will be calculated as the mean value between all the calculated diameters. Therefore:

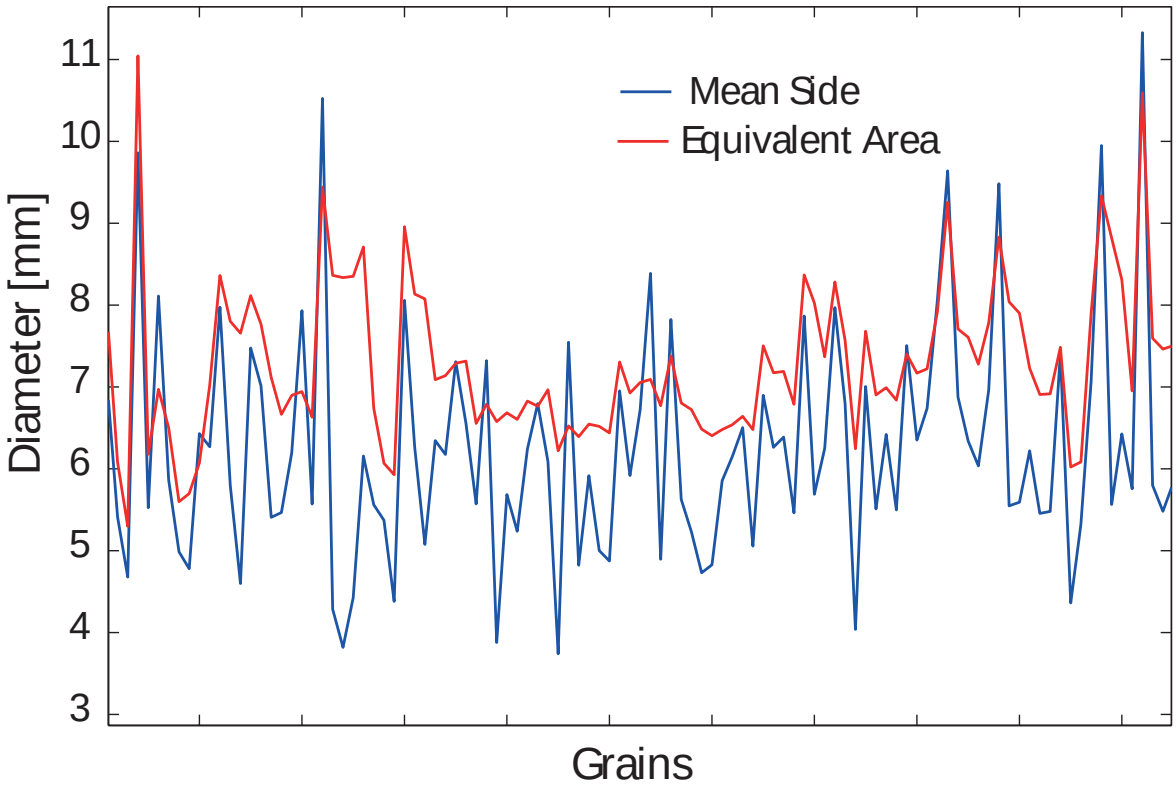

Figure 4.29: Values of equivalent diameters obtained for the two methods proposed (case:$Aug.24^{th}$)

$$d_{eq} = \frac{\sum_{i=1}^{i=n} d_i}{N} \tag{4.21}$$

Where d_{eq} is the equivalent diameter for each grain and d_i is the diameter calculated in every frame. The series of d_{eq} constitutes the grain population. Therefore there will be a value of d_{eq} for each grain that is recorded. On those data it is possible to calculate the granulometric curve (or the Probability Function) to compare the estimated diameter with the real one.

The effect of the two different methods used to estimate the diameter is reported in Figure 4.29. The picture shows that the diameters obtained through the second method has a lower 'peaks' and higher 'droughts'. This effect is probably related to the intrinsic property of this mean (the former method is an algebraic mean and the latter can be seen as a geometric mean). The grains diameter obtained for each experiment can be used together to describe the population. The result is reported in 4.30.

As can be seen by the Figure, both methods fails in giving a good estimation of the actual grain diameter. The wrong estimation of the diameters is primarily due to the method of calculation and secondarily by manual tracking of the particles. However in this section it is not important to estimate the diameter population accurately.

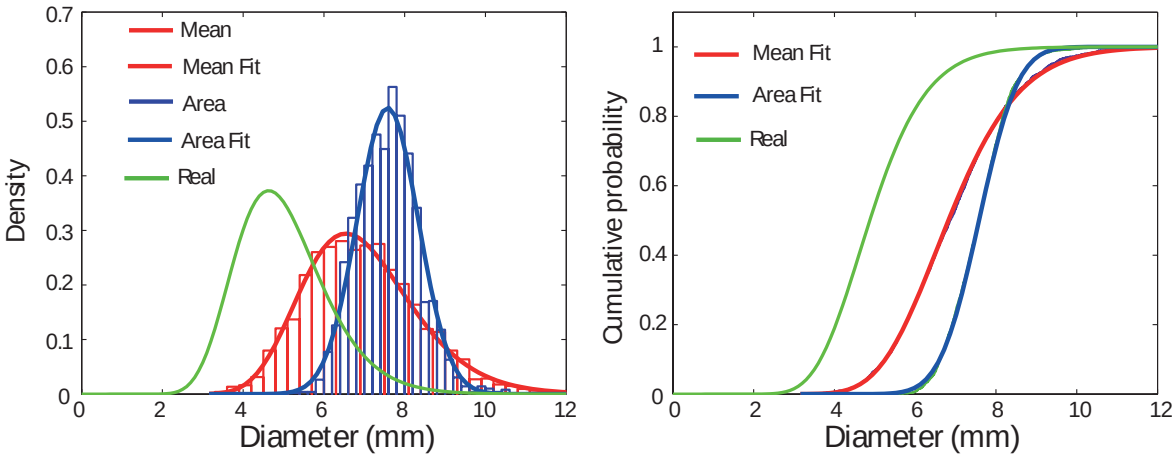

Figure 4.30: Grain diameter PDF and CDF (real case, mean of the sides, equivalent area)

To study if there is some sort of relationship between the grain diameters and the step length the diameter associated to each step length was calculated for each experiment. The mean μ and the standard deviation σ of the diameters were then calculated. Three classes of diameters were defined:

1. 'Low diameters' with diameter $d_i < \mu_d - \frac{\sigma_d}{2}$

2. 'Medium diameters' with diameter $\mu_d - \frac{\sigma_d}{2} < d_i < \mu_d + \frac{\sigma_d}{2}$

3. 'Low diameters' with diameter $d_i > \mu_d + \frac{\sigma_d}{2}$

With this definition three sets of data $(d_i;\lambda_i)$ are available for each experiment. On each set of data the mean step length was calculated and plotted in a diameter over step length chart. A graphical description of these operations is reported in Figure 4.31. The result of this analysis is reported in Figure 4.32. By observing this Figure it is clear that with the available data it is not possible do define any link between the mean step length of a group of grains with a defined mean diameter. It can be stated that no clear trend can be observed. This can be explained because of the fact that the material chosen to simulate the bed is quite uniform. Therefore at this scale an appreciable discrepancy between the behaviour of the grains with different sizes can not be observed. In Appendix 1 Figure 7.20 it is reported a plot with the standardized step length (x axis) against the standardized diameter (y axis). It is clear by observing those diagrams that it is impossible to define a link between these two quantities.

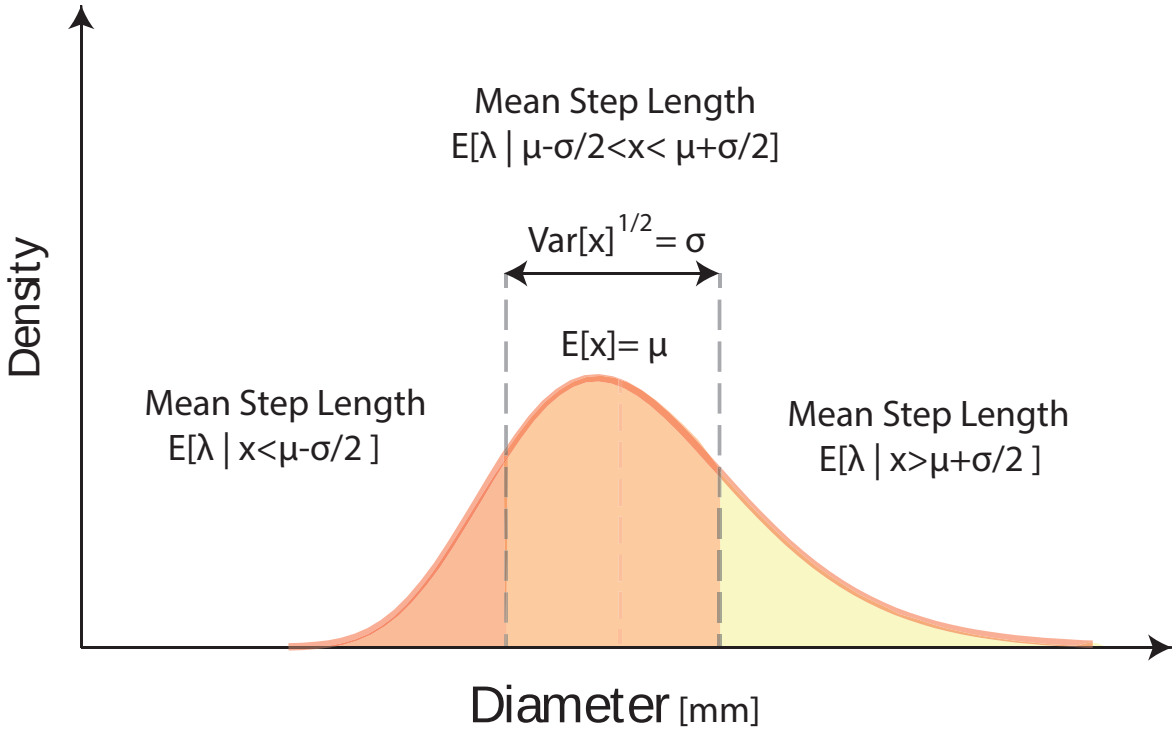

Figure 4.31: Grain diameter classes definition

4.5.2 Results

The investigation about the link between step length and diameter led to the following results:

1. The use of the boundary box to define the diameter of a particle did not give a reliable result. Two methods were used to calculate the diameter: a 'geometric' mean and an 'algebraic' mean. Strong discrepancies were observed for both methods between the resulting PDF and the real PDF of grain sizes.

2. No clear trend was found between the diameter of a particle and the step length of a particle for both methods.

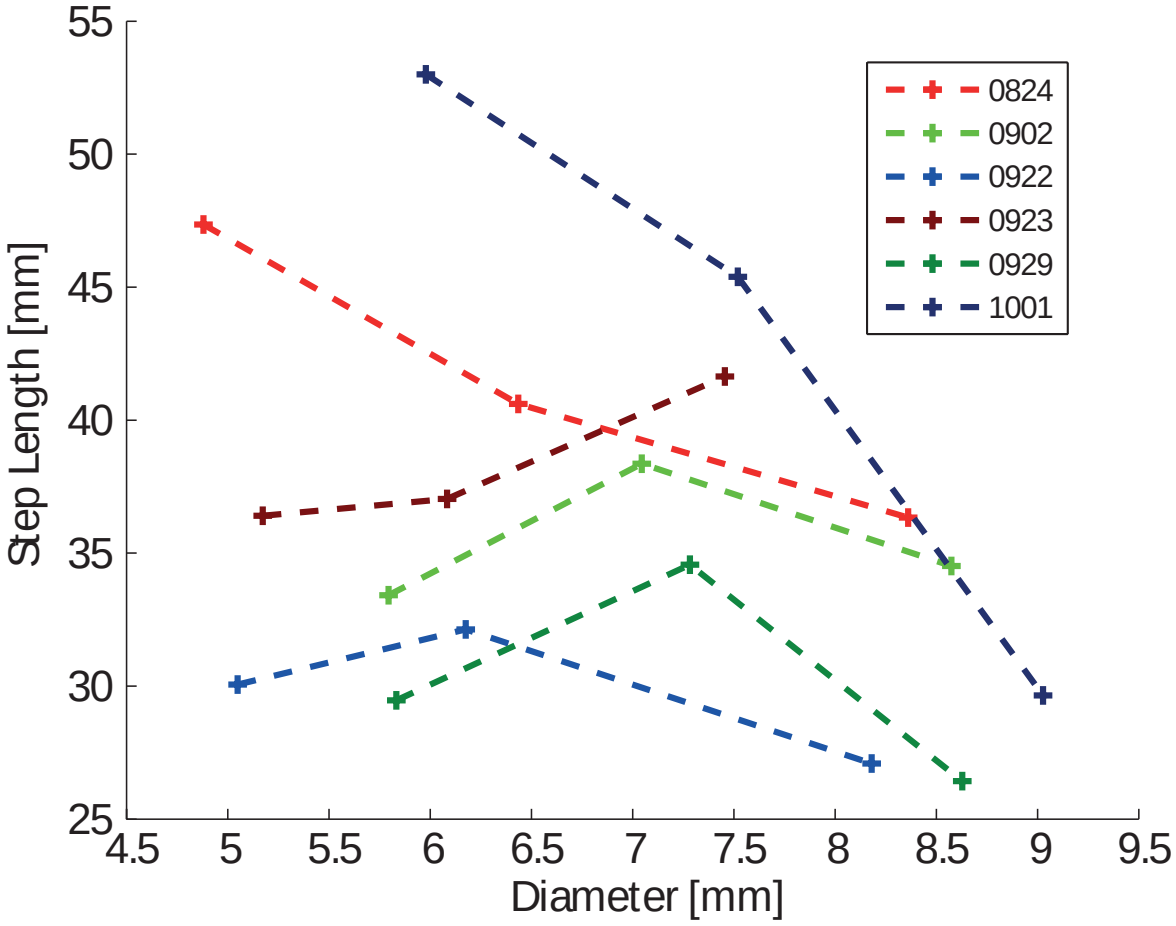

Figure 4.32: Mean Step Length vs Mean Diameter (Mean side (left), Equivalent Area (right))

4.6 Entrainment Rate

The entrainment rate is a fundamental quantity that is of primary importance to define the Sediment Transport. The sediment transport can be estimated through the definition reported in Equation 4.22 (McEwan et al. 2004).

$$q_b = \phi \cdot \lambda \tag{4.22}$$

Where ϕ is the entrainment rate and λ is the step length. In this section the investigation of the entrainment rate in the experiments will be performed.

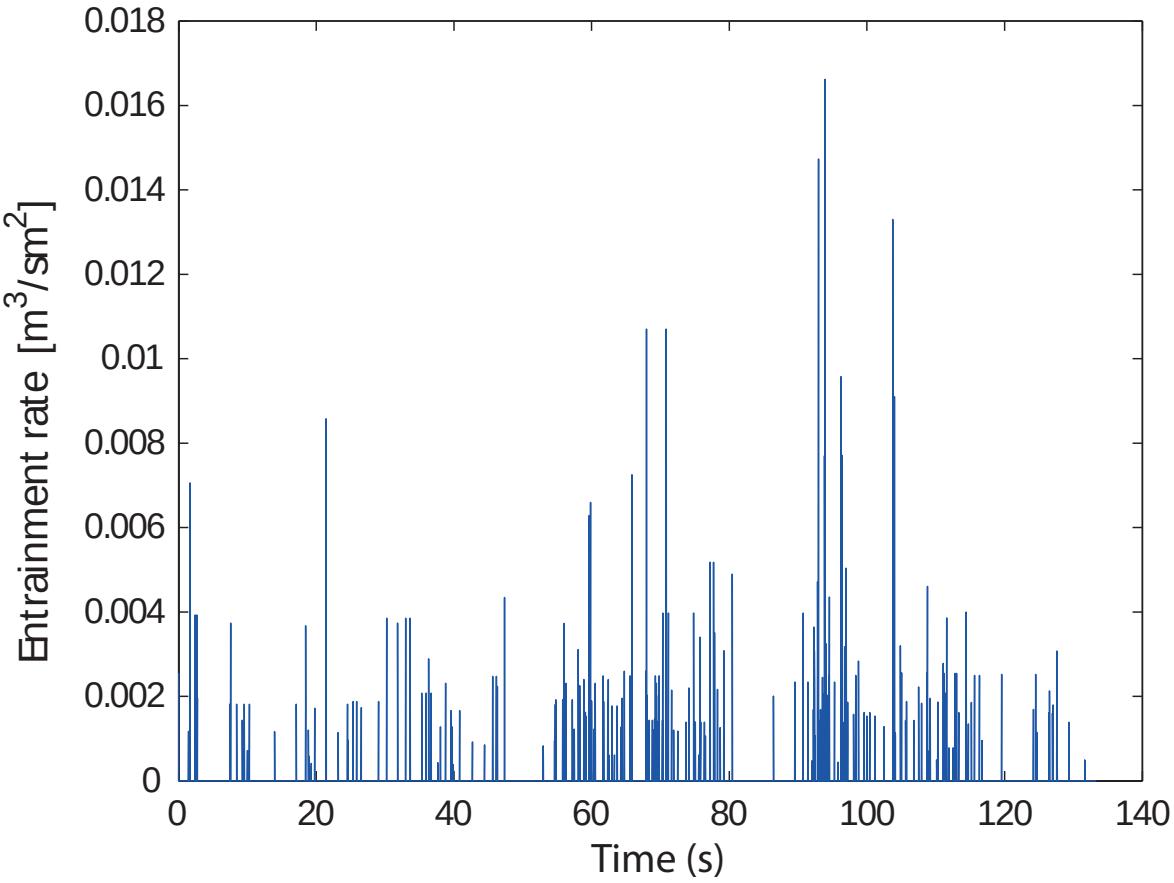

Figure 4.33: Istantaneous Entrainment Rate (Case: $Aug24^{th}$

4.6.1 Analysis

The Entrainment rate is a value that represents the intensity of the bed load. In the present study the entrainment rate can be calculated as the the volume (or mass) of bed material entrained in the area under examination A in a time interval Δt. Under those assumptions it is possible to calculate the Entrainment Rate as reported in Equation 4.23.

$$\phi = \frac{V_{particles}}{\eta \cdot A} \cdot \frac{1}{\Delta t} \tag{4.23}$$

Where $V_{particles}$ is the Volume of the particles that are entrained in the area under examination in the time interval Δt. The volume of the particles that leaves the area can be calculated as reported in Equation 4.24

$$V_{particles} = n_{particles} \cdot V_{sphere}(d = 5mm) = n_{STATE=1} \cdot \frac{4}{3} \cdot \frac{\pi \cdot d_{mean}^3}{8} \tag{4.24}$$

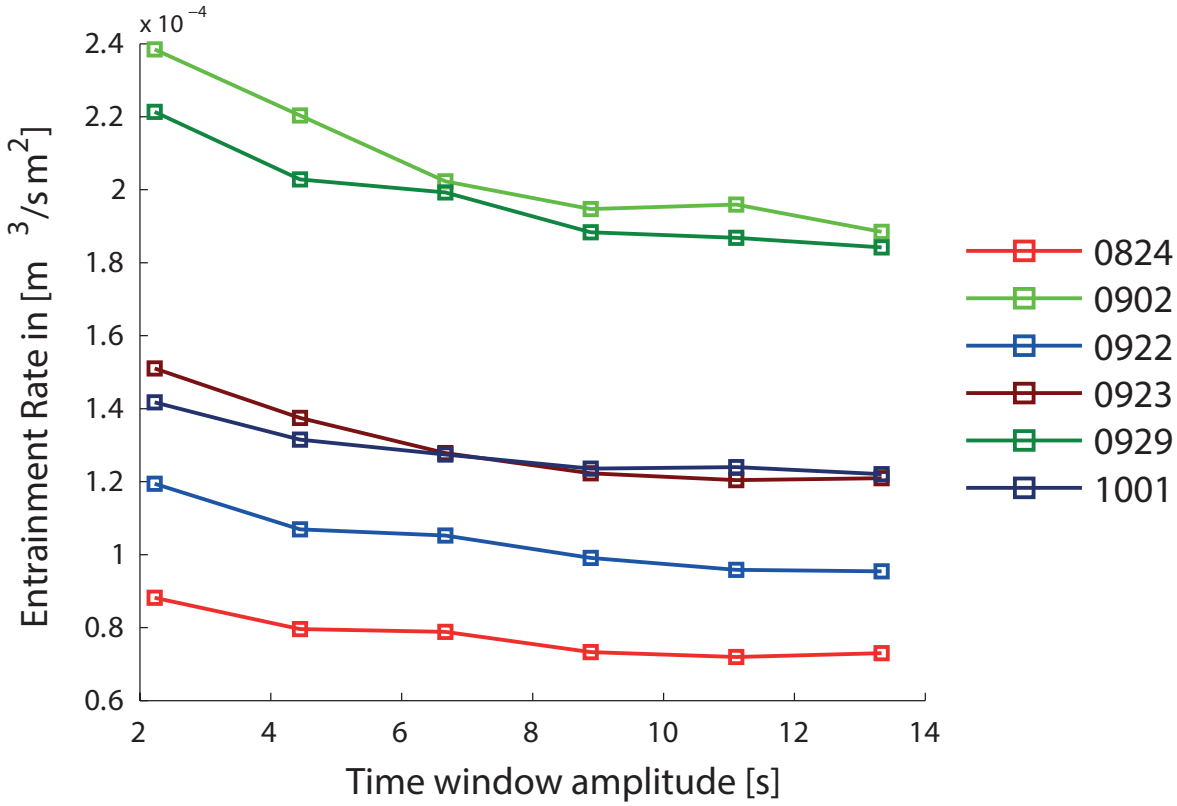

Figure 4.34: Entrainment Rate against Time window amplitude

Where $n_{particles}$ is the number of particles that are entrained. This number is exactly equal to the number of particles that assume state=1 (start) in the selected time window. The volume of each particle entrained was approximated as the volume of the mean particle (d=5mm). The only thing left to define is the time window. The number of particles entrained by the flow is a quantity highly intermittent, as shown in Figure 4.33. To estimate the Entrainment rate from Equation 4.23 it is necessary to average this quantity on a time window Δt. For this purpose different values for the time window were assumed. The time windows used were: { 2.22s, 4.44s, 6.66s, 8.88s, 11.11s, 13.33s } corresponding to { 100, 200, 300, 400, 500 , 600 } frames. The purpose was to estimate which is the minimum value for time window to achieve the 'stability' of the average entrainment rate. This could be estimated through the comparison between the entrainment rate obtained in function of the time window amplitude. The result is reported in 4.34. As can be observed the mean entrainment rate tends to stabilize for high values of the time window. Therefore in order to grant more stability the time window was fixed to 13.33s (or 600 frames). The Entrainment Rates obtained with a time window of 600 frames are reported against the shear stress in Figure 4.35. As can be noticed by the figure no clear trend can be spotted. However, the nature of this experiment is too dependent on the human sensibility. The entrainment rate as calculated in the present study depends on how much grains can be detected and

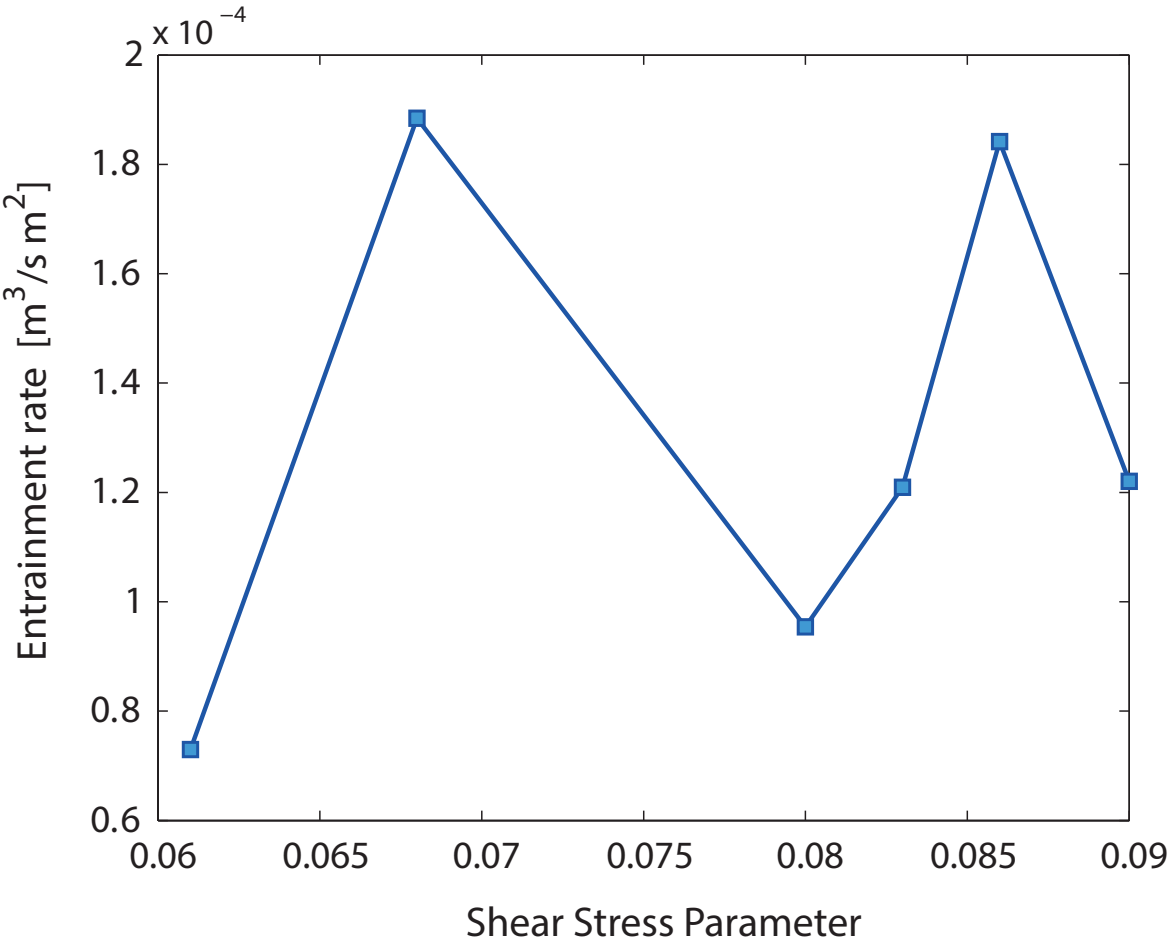

Figure 4.35: Entrainment Rate against Shear stress parameter

tracked manually in each experiment. Therefore the more time is spent on tracking a database the higher number of grains will be detected: this can significantly bias the data. For that reason the estimation of the entrainment rate presented in this experiment has a low reliability.

4.6.2 Results

1. The entrainment rate in the present study is an impulsive variable. This variable must be averaged in short time windows and then averaged again on the whole time of observation. The increase of the time windows amplitude leads to a stability in the result. Therefore the time window selected was 600 frames (13.33s).

2. The values of entrainment can be affected by a biasing due to the manual tracking of the particles.

3. No significant link was found between the shear stress parameter and the entrainment rate, since this latter quantity depends primarily on the time spent in the particle manual tracking.

Chapter 5

Bed particle diffusion

5.1 Introduction

The previous chapter studied the interactions between the properties of the bed particle (such as step length, rest time and grain velocity) and the flow conditions. Those quantities can be useful to describe the motion of the bed load particle on a diffusive perspective. The motion of a bed particle can be described as follows:

1. Step Length: A particle (when it is not resting) is entrained by the flow travels a distance λ. This distance can be described stochastically through the use of a statistical model.

2. Grain Velocity: During a particle journey between two resting position the grain velocity usually is not constant (especially in the acceleration phase when a particle is starting and the deceleration phase when a particle is stopping).

3. Rest Time: The time t between two moving condition can be described through the use of a statistical model.

If a good estimation of those three quantities is obtained the motion of bed load particles can be idealistically described as a series of quick steps followed by long resting period. The purpose of this chapter is to analyse the longitudinal trajectories of the moving grains.

5.2 Theoretical Background

5.2.1 Grain Movements Types

The grain movements can be studied on the basis of the time scale in which they are observed. A grain which is moving along the bed is characterized by three different phases. The first phase is when the grain movement is observed while it is performing a motion between a start and a stop. In this phase the trajectory is composed by quick fluctuations in position and velocity. This trajectory can be referred to as *local trajectory*.

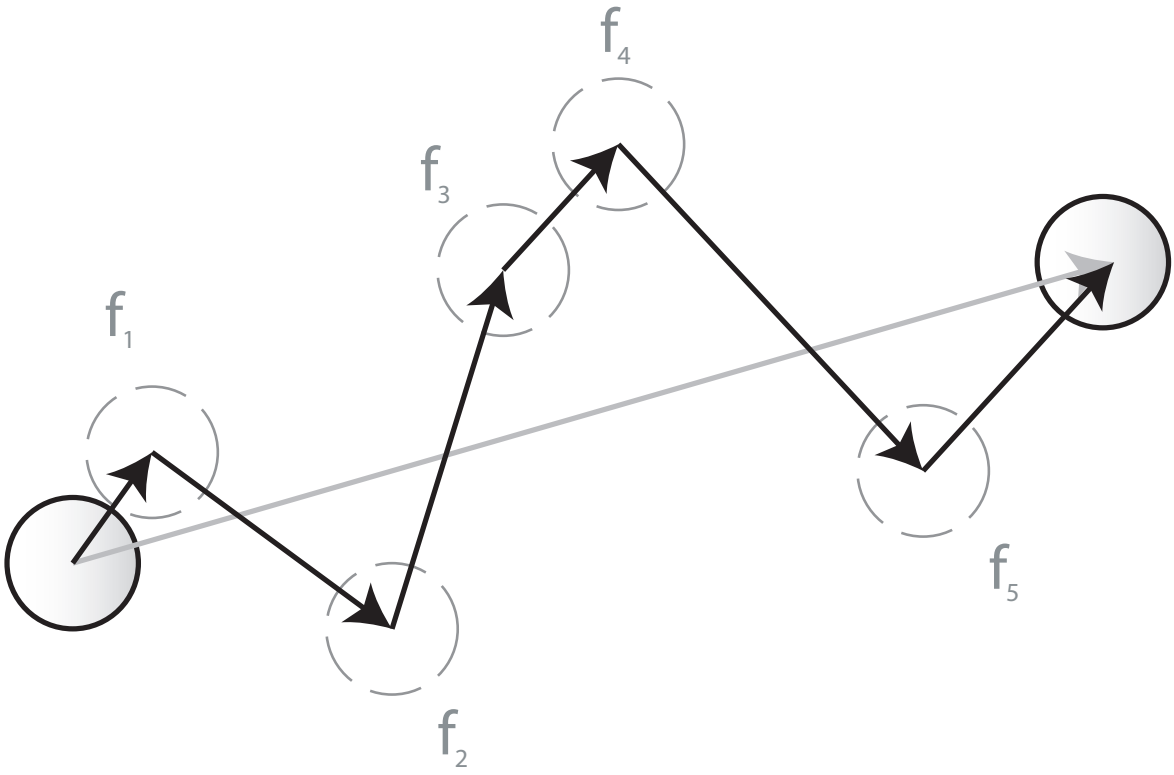

Figure 5.1: Local trajectories (Black)

A graphic representation of the local trajectory is reported in Figure 5.1. As can be seen the local trajectories can be represented as an instantaneous fluctuation on the mean trajectory between a start condition and a stop condition. An accurate detection of the local trajectories is a result that is quite hard to reach experimentally, since an high frequency position detection is required. In the present study the local trajectory is considered as the distance travelled by a particle between two following frames.

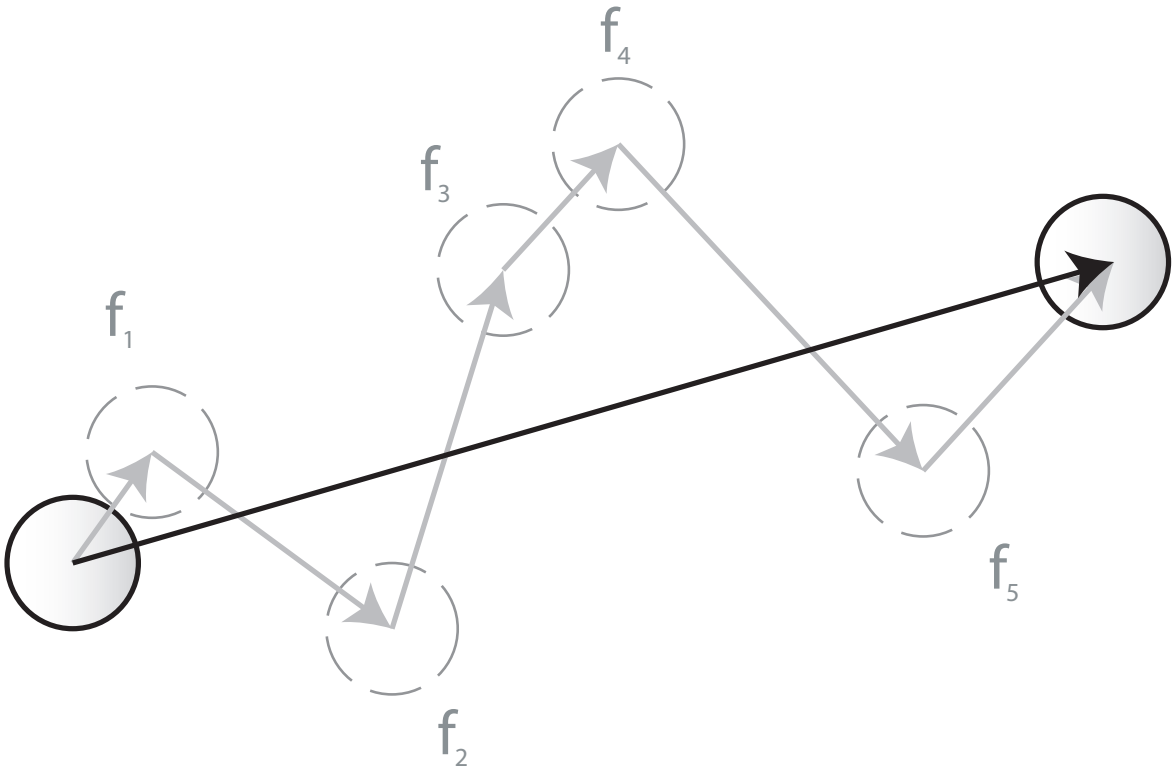

Figure 5.2: Intermediate trajectory (Black)

When a particle alternates quick movements to long resting phases this is called an *intermediate trajectory*. This trajectory is the sum of all the local trajectories. In this experiment the intermediate trajectories are defined as the difference between the positions recorded as a 'start' (state=1) and 'stop' (state=1). This kind of trajectory was named as 'step' and it was extensively treated in Chapter 4 in Section 4.2. The intermediate trajectory is reported in Figure 5.2. The average time that a particle needs to complete this trajectory is (on average) an order of magnitude lower than the average rest time.

A third category is composed by the *global trajectories*. The global trajectory is the distance travelled by a grain in long time scales. It is composed by the sum of several intermediate trajectories. Therefore the global trajectory is the travel distance made by a particle after several steps and resting phases. A graphical representation of this kind of trajectory is reported in Figure 5.3. It is important to state that the global trajectory is made by several intermediate trajectories just as the intermediate trajectories are made by several local trajectories.

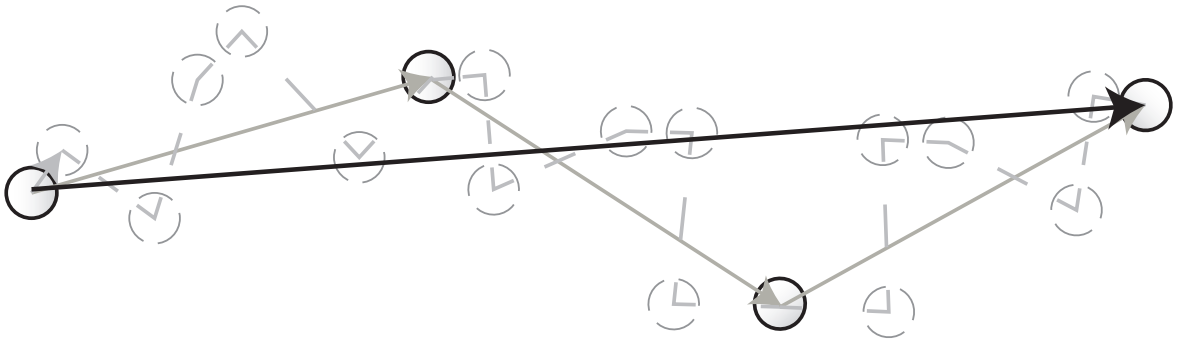

Figure 5.3: Global trajectory (Black)

5.2.2 Particle Diffusion

The Pure diffusion phenomenon is often modelled with the use use of the concept of the 'random walk'. Let us imagine the case of fluid particle in still water. The particle will start to move around randomly according to a distribution due to Brownian motions. The random walk is constituted by a sum of a sequence of steps $\overrightarrow{\lambda_i}$ which are distributed according to a probability density function. The position of the particle can be described as:

$$\overrightarrow{X} = \sum_{i=1}^{n} \overrightarrow{\lambda_i} \tag{5.1}$$

This arrow in $\overrightarrow{X}$ and $\overrightarrow{\lambda}$ means that they are vectors. This case can be simplified by reducing the dimensions. An example of 2D random walk is reported in Figure 5.4. A particle is supposed to start in the position $(x, y) = (0; 0)$. After $i = 100$ random steps the position of the particle is the one marked by the end of the red arrow. The diffusion can be modelled by studying the behaviour of a wide population of particles which are moving randomly.

For example, the case of the drop of ink in water can be studied by representing the drop as a 'cloud' of particles which have the same starting point and move randomly. The average properties of the cloud of particles can be studied. If the position of each particle in every instant is known then the centre of a cloud can be calculated as:

$$\overline{X} = \begin{pmatrix} \overline{x} \\ \overline{y} \\ \overline{z} \end{pmatrix} \tag{5.2}$$

Where $\overline{x}$, $\overline{y}$, $\overline{z}$ are the mean of the coordinate of a the position o each particle. The mean position $\overline{X}$ represents the position of the center of the cloud. To assess the radius of the cloud the standard deviaton of the coordinate of the points can be used. The deviation of the cloud points in a direction can be calculated as:

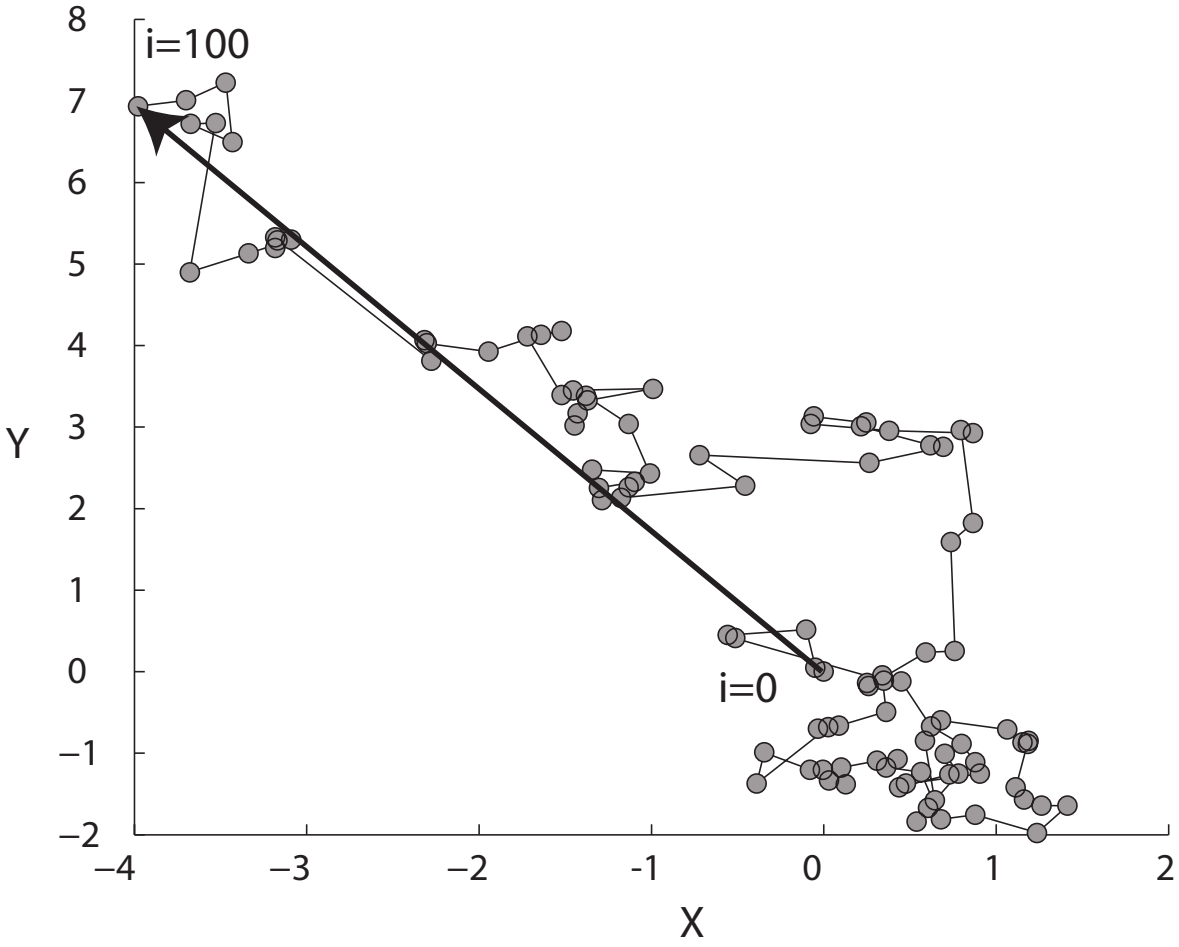

Figure 5.4: Random walk of a particle in two dimensions

$$\sigma_x = \sqrt[2]{\frac{\sum_{i=1}^{n}(x_i - \overline{x})^2}{N}} \tag{5.3}$$

If the x direction only is considered the spreading of a cloud can be calculated simply through Equation 5.4. In Equation 5.4 it is written that for the case exposed the variance of the points is linearly proportional with the time. An example of 2D 'normal' diffusion is reported in Figure 5.5. Three series of points are plotted corresponding to three different amount of time steps considered. As can be seen the point cloud expands when more steps are performed. In Figure 5.5 (right) it is plotted the variance of the distribution as a function of the time elapsed. As can be seen for high values of the time the relation between time and variance is linear.

$$\sum_{i=1}^{n}(x_i - \overline{x})^2 = 2 \cdot D \cdot t \tag{5.4}$$

The 'normal diffusion' expression is used to define those phenomena whose variance

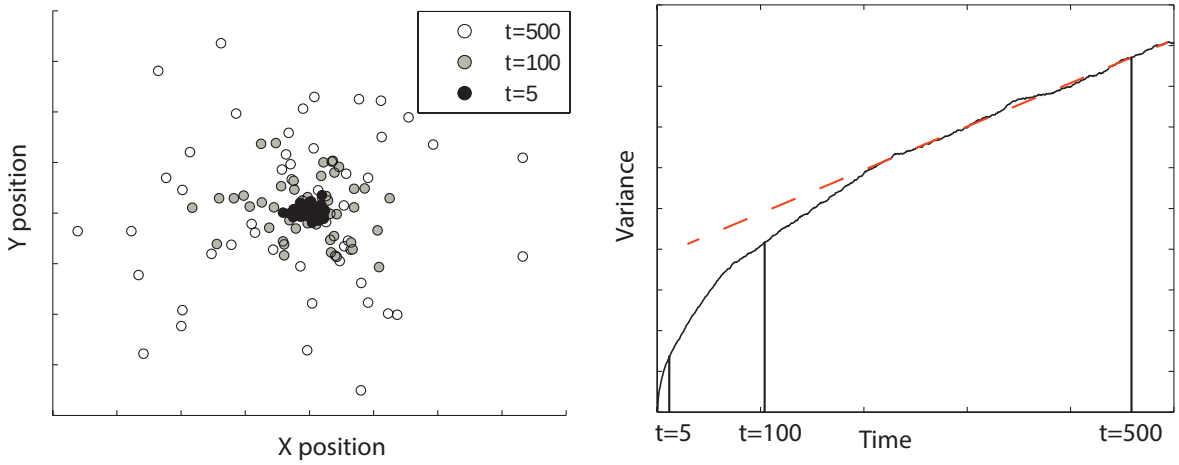

Figure 5.5: Normal diffusion of particles released in the same point

increases linearly with the time. The normal diffusion case is also known as 'normal' diffusion. In this case, the probability distributions of the steps are independent and have short tails (no 'long-range' correlations are present). In those conditions the Central Limit Theorem (CLT) holds. The Central Limit Theorem states that the mean of a sequence of independent and identically distributed random variables distributes like a normal distribution. A graphic representation of the CLT is reported in Figure 5.6. The Figure shows the sum of independent identically distributed random variables that distributes as a gamma distribution. As can be seen after a sum of more than 12 variables the resulting distribution can be assumed as normally distributed. The direct implication of the CLT is that for 1-D 'normal' diffusion the statistical distribution of the particles position for large times follows a normal distribution.

5.2.3 Grain diffusion in the case of bed-load

The purpose of this section is to treat the particles position in the stream-wise direction as a diffusion problem. The conditions applied for the Flume Experiments at the University of Bradford in 2009 however have some relevant differences from the 'normal' diffusion model. In particular:

1. In the case of normal diffusion the particles are in a state of constant motion, without interruption in their path. When speaking about bed load instead, a particle alternates quick moving phases and long resting phases. A better description of this phenomenon is a "diffusion among traps" (Bouchaud & Georges 1990), in which a particle performs a sequence of steps then stops for a long time that distributes according to a probabilistic law.

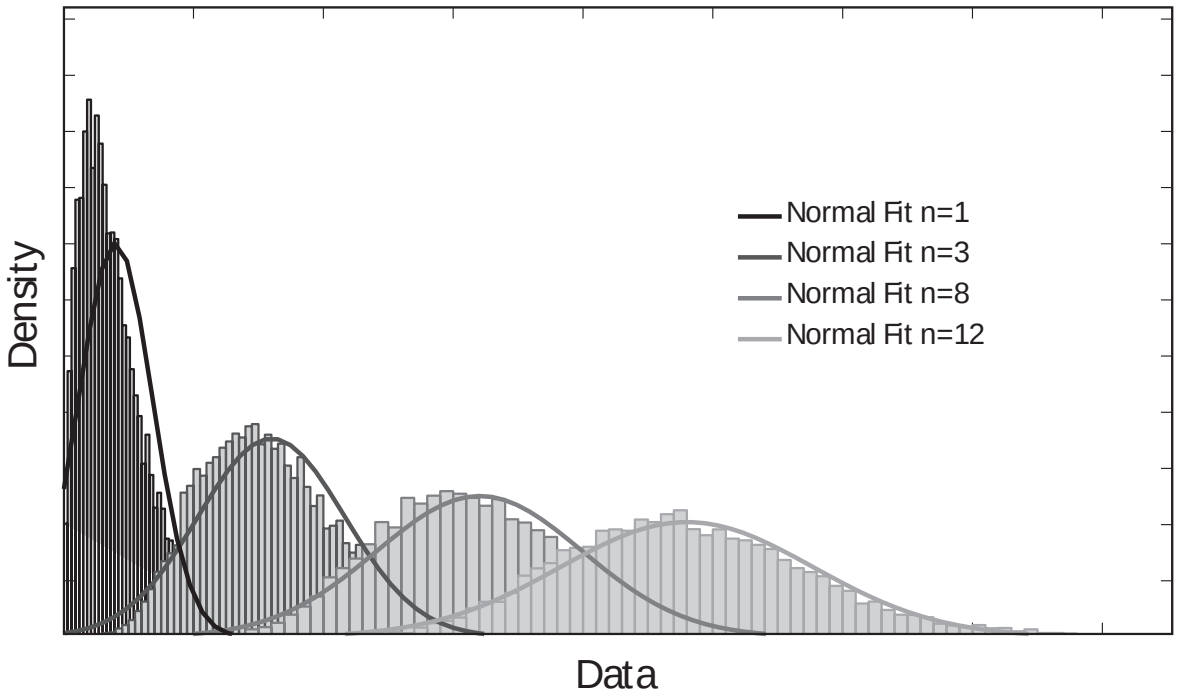

Figure 5.6: Central Limit Theorem for gamma distributions

2. The step lengths probability distribution for high values of step lengths is still an unknown quantity. The result obtained in the present study is obtained through an extrapolation of the known points of the step lengths PDF.

3. In the normal diffusion an absence of 'broad' distributions and 'long-range' correlations is supposed to occur. In the case of flume experiments these mechanisms can't be excluded a priori. For example some 'long-range' correlations in the flow turbulence or some 'broad' distributions due to long extremely resting times may occur (Nikora et al. 2002).

For all these reasons the bed load can be described as a case of anomalous diffusion.

5.3 Nikora's Approach (2001)

5.3.1 Introduction

In this approach the bed load particles were studied by focussing on the statistical properties of the particles trajectories. The position of each moving particle is dependent on time therefore the moments of the particles positions distribution will evolve through time. In 'normal' diffusion the second order moment of particle position is linearly depended with time. In a 2D case the regime of the diffusion process in a specific direction X can be studied through Equations 5.5.

$$\overline{X'(t)^q} \propto t^{q\gamma(q)} \qquad \overline{Y'(t)^q} \propto t^{q\gamma(q)} \tag{5.5}$$

Where $X(t)$ and $Y(t)$ indicate the position of a particle along stream-wise and cross-stream direction respectively, $X'(t) = X(t) - \overline{X}$ and $Y'(t) = Y(t) - \overline{Y}$ indicates the fluctuation around the mean of each particle. The quantities reported in Equation 5.5 are the moments of the particles position distribution. The moments are proportional to the time through an exponent $\gamma(q)$. The exponent $\gamma(q)$ leads to the description of the diffusion in three different categories.

1. $\gamma(q) > 0.5$: This behaviour is called *super-diffusive*. In this case the cloud of particles spreads out in a more rapid way than the normal diffusion mechanism. The case of $\gamma(q) = 1$ is called *ballistic diffusion*.

2. $\gamma(q) = 0.5$: This is the classical 'normal' diffusion mechanism as described in the previous sections. In this case the second order moment (variance) grows linearly with time.

3. $\gamma(q) < 0.5$: This behaviour is called *sub-diffusive*. In this case the cloud of particles spreads out very slowly.

For all the reasons reported in Section 5.2.3 the process studied will probably behave as a 'anomalous' diffusion. The probability distributions of step lengths and rest time is of primary importance to estimate the stream-wise diffusion, since the nature of those distributions may play an important role on the definition of the diffusion mechanism. Nikora studied the diffusion behaviour of bed particles in two papers (2001 and 2002). The former one used computer simulations of bed load movements through a Finite Particle Model. In the latter some experimental data were used. Three different diffusion regimes can be spotted.

A ballistic diffusion was supposed to act in the first stages of transport, where the bed particles follows the 'local trajectory'. The 'local trajectories' in the 2002

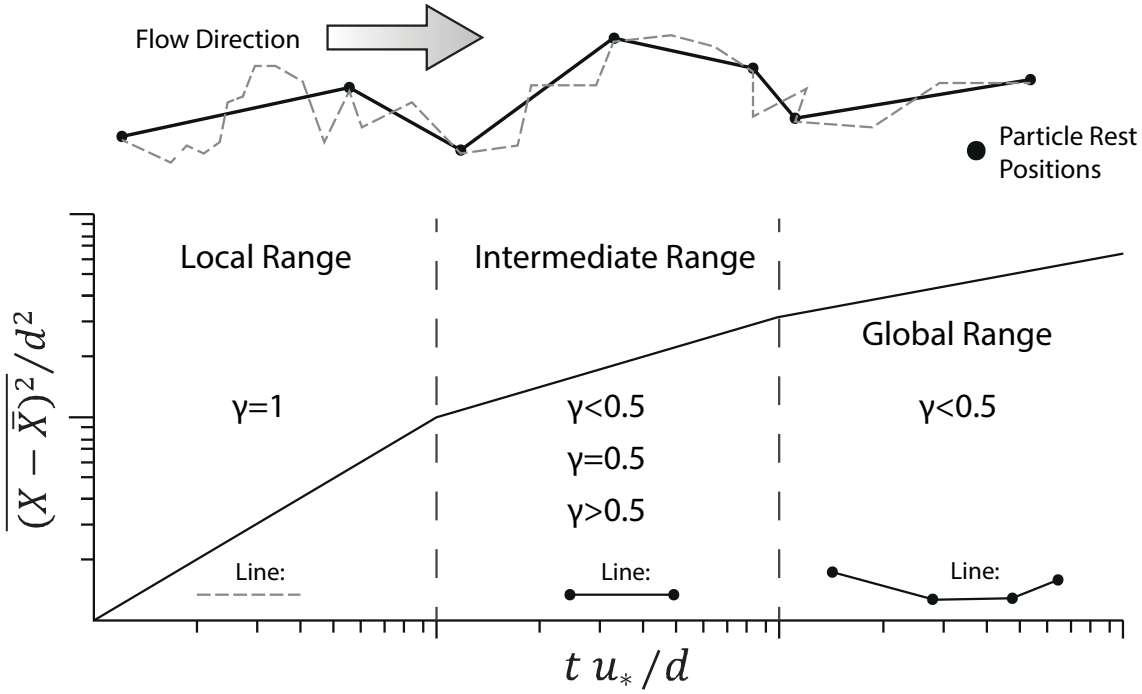

Figure 5.7: Diffusion Regimes (from Nikora, 2001)

paper was defined for saltating particles. This trajectory could be obtained as the path followed by a particle between two consecutive collision events. Those category of trajectories should be smooth and non fractal. When the regime is mainly caused by 'intermediate trajectories' the diffusion could be either sub-diffuse, normal or super-diffusive depending on which process dominates. For example bed topography and near bed turbulence could have opposite effects on the diffusion process. The 'global trajectories' should be characterized by a sub diffuse behaviour because the effect of the resting times are included in those trajectories.The diffusion mechanism described are supposed to occur also for other transport modalities, such as rolling and sliding.

5.3.2 Analytical Description

The problem of bed load transport can be theoretically described with the use of eight variables: u_* shear velocity, g gravity acceleration, d particle diameter, D characteristic dimension for roughness, ν fluid viscosity, t particle travel time including rest period, ρ_w the density of water and ρ_s the density of the particle. Therefore the moments of the distribution can be expressed as a function of those parameters as reported in Equation 5.6.

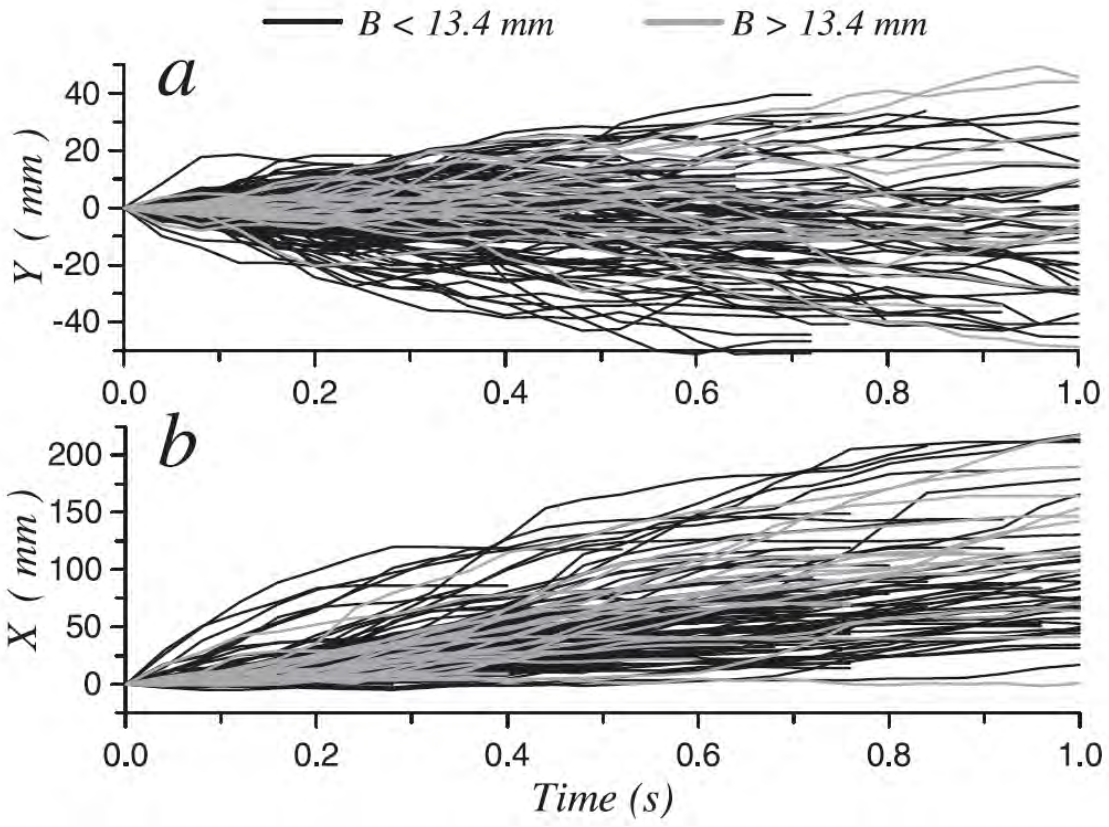

Figure 5.8: Trajectories scaled to zero (from Nikora, 2002)

$$\overline{X'^q}, \overline{Y'^q} = f_q(u_*, g, d, D, \nu, t, \rho_s - \rho_w) \tag{5.6}$$

By manipulating this equation it is possible to obtain the second order moment as a function of the variables of the problem. In Equation 5.7 the second order moment is expressed as a function of groups of non dimensional numbers.

$$\frac{\overline{X'^2}}{d^2}, \frac{\overline{Y'^2}}{d^2} = f_{2a}\left(\frac{u_*^2}{gd}, \frac{d}{D}, \frac{u_* d}{\nu}, \frac{t u_*}{d}, \frac{\rho_w}{\rho_s - \rho_w}\right) \tag{5.7}$$

Equation 5.7 can be furtherly simplified by introducing an hypothesis of incomplete self-similarity with respect to tu_*/d and by neglecting viscous effects (when $u_* d/\nu \geq 100$). In addition if the roughness characteristic length D is assumed to be equal to the mean diameter d Equation 5.7 becomes:

$$\frac{\overline{X'^2}}{d^2}, \frac{\overline{Y'^2}}{d^2} = \frac{t u_*}{d}^{2\gamma_x, 2\gamma_y} \cdot f_{2b}\left[\frac{\rho_w u_*^2}{(\rho_s - \rho_w) g d}\right] \tag{5.8}$$

The exponent of the diffusion coefficients γ_x, γ_y should be determined through experimental investigations. The term between squared brackets is the Shields shear

stress parameter and the parameter f_{2b} takes into account the relative particle size. The diffusion regimes were studied in the case of an experiment with an irrigation canal. The area under examination had a dimension of $20cm \times 23cm$ and the frequency of image capture was 25Hz. The average grain diameter was $d = 13.4mm$. The images acquired were analysed through a semi-automatic image processing. Particles move from all the positions inside the window. In order to consider the same origin, the coordinates of the first recorded point were subtracted to the coordinates of all points in the trajectory. Therefore the new coordinates become:

$$X_i^* = X_i - X_{0i} \qquad and \qquad Y_i^* = Y_i - Y_{0i} \tag{5.9}$$

Where X_{0i} and Y_{0i} are the coordinate of the first trajectory point recorded. The result of this transformation is reported in Figure 5.8.

5.3.3 Results

The diffusion was studied for two cases: the first is focussed on studying the 'intermediate' range, and the second to study the 'global' range. For what concerns the first case the diffusion process was studied for a time interval of about T=0,7s. The study of the statistics of particle trajectories were preformed on two different populations split between 'large' particles ($d > d_{50}$) and 'small' particles ($d < d_{50}$). The diffusion was evaluated trough the calculation of the second order moment of the particle positions. The result expressed against time is reported in Figure 5.9. The figure is plotted in a logarithmic scale, therefore any power relationship between the second order moments of particles positions and time is represented in this diagram as a line.

The linear relationships are clear and well defined. The exponent found showed that for the cross-stream direction (Y) the kinetic of the diffusion is the same for large and small particles ($\gamma_Y \simeq 0.83$). For what concerns the cross stream direction (X) there is a little difference between the small and the large particles. For large particles ($d > 13.4mm$) the exponent assumed the values of $\gamma_X \simeq 0.87$, for small particles instead ($d < 13.4mm$) the exponent resulted $\gamma_X \simeq 0.77$. In this regime the diffusion appeared to be isotropic for large particles and weakly anisotropic for small particles.

A second study was conducted to assess the diffusion regime in the global range. In this case the data used were taken by an experiment by Drake et al. (1988). The experimental data of this experiment were plotted in a logarithmic scale. The result showed that the diffusion in global range acts as supposed by the author: the regime is strongly sub-diffusive (γ_X and $\gamma_Y < 0.5$). In particular $\gamma_X = 0.33$ and $\gamma_Y = 0.19$. The normalized data were plotted. The result is reported in Figure 5.10. The two regimes seems to be clearly defined by a well defined change in slope. The time scale between the Global range and the Intermediate range seems to be the same for both stream-wise direction X and cross-stream direction Y. However, the two series of data

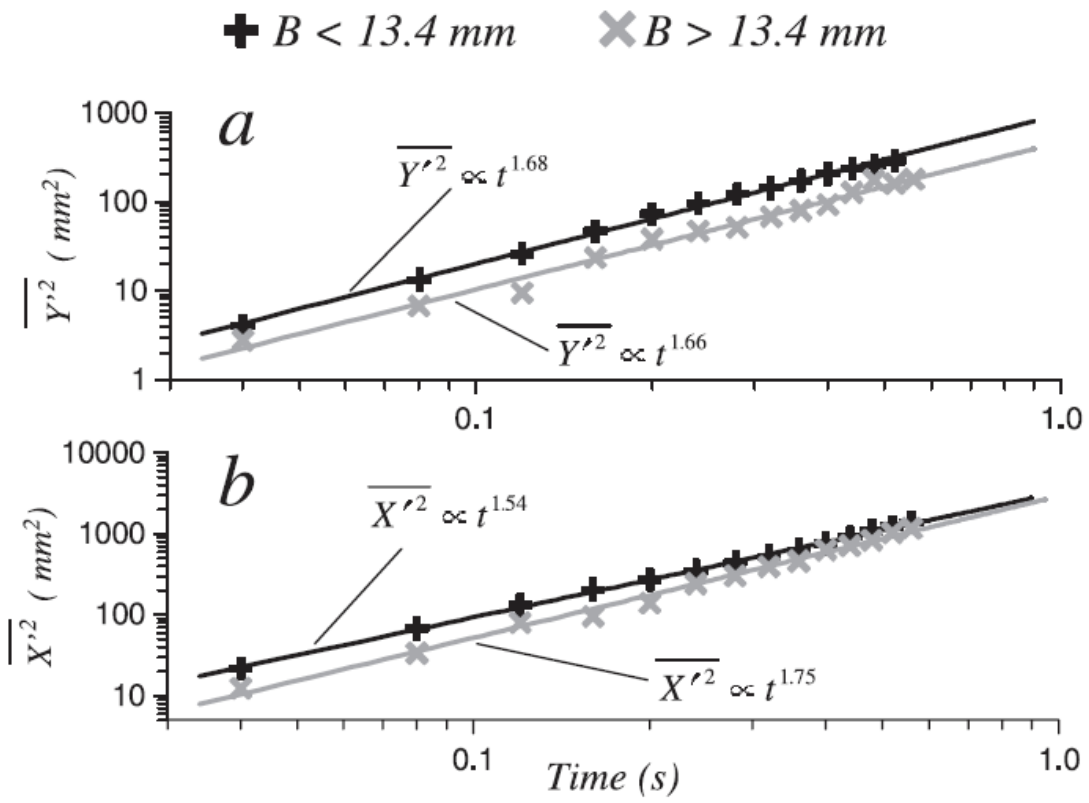

Figure 5.9: Second order moments of particle positions against time (from Nikora, 2002)

presents a discontinuity for the non-dimensional time parameter with value between 10 and 100.

5.4 Diffusion Analysis

In this section the study of the particles trajectories for the six experiments will be performed. The second order moment of the particles positions will be calculated and normalized. This quantity will be plotted against the normalized time as described in Section 5.3.2. The trajectory considered will be the stream-wise direction only.

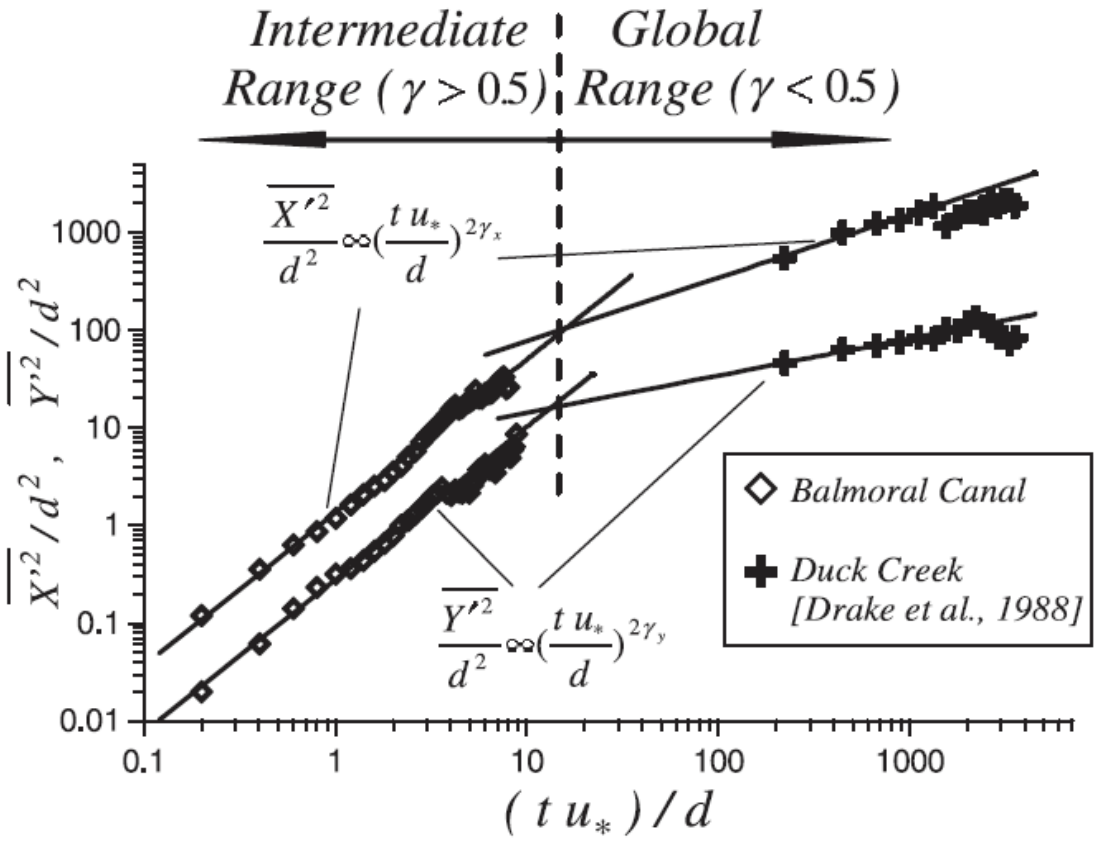

Figure 5.10: Diffusion regimes: Intermediate and Global (from Nikora, 2002)

5.4.1 Trajectories calculation

The same procedure described in Section 5.3 is applied to the tracked databases. The first step to study the particles diffusion is to calculate the trajectories. In the database available the position of each particle is registered for every frame. To construct the trajectories the first position recorded and the first frame in which a particle was found were saved. Then those values were subtracted to the the other positions or frames. Therefore, under the new 'reference' system, the x position, y position and time of recording becomes:

$$\begin{cases} X_i^* = X_i - X_0 & \text{for stream-wise direction} \\ Y_i^* = Y_i - Y_0 & \text{for cross-stream direction} \\ t_i^* = t_i - t_0 & \text{for time} \end{cases} \tag{5.10}$$

This procedure was applied to the data present in the databases with some difficulties related to the continuity of the data. The database presented some discontinuities

due to the fact that the grains which stop does not have a registered position until they are re-entrained. This problem was quickly solved by assigning to each grain the coordinate of the last position recorded before the re-entraining. The definition of which trajectories should be used for the analysis was a second issue. The first assumption was to study every trajectory present in the database without making any hypothesis on the first recorded state and the last recorded state. The result is reported in Figure 5.11.

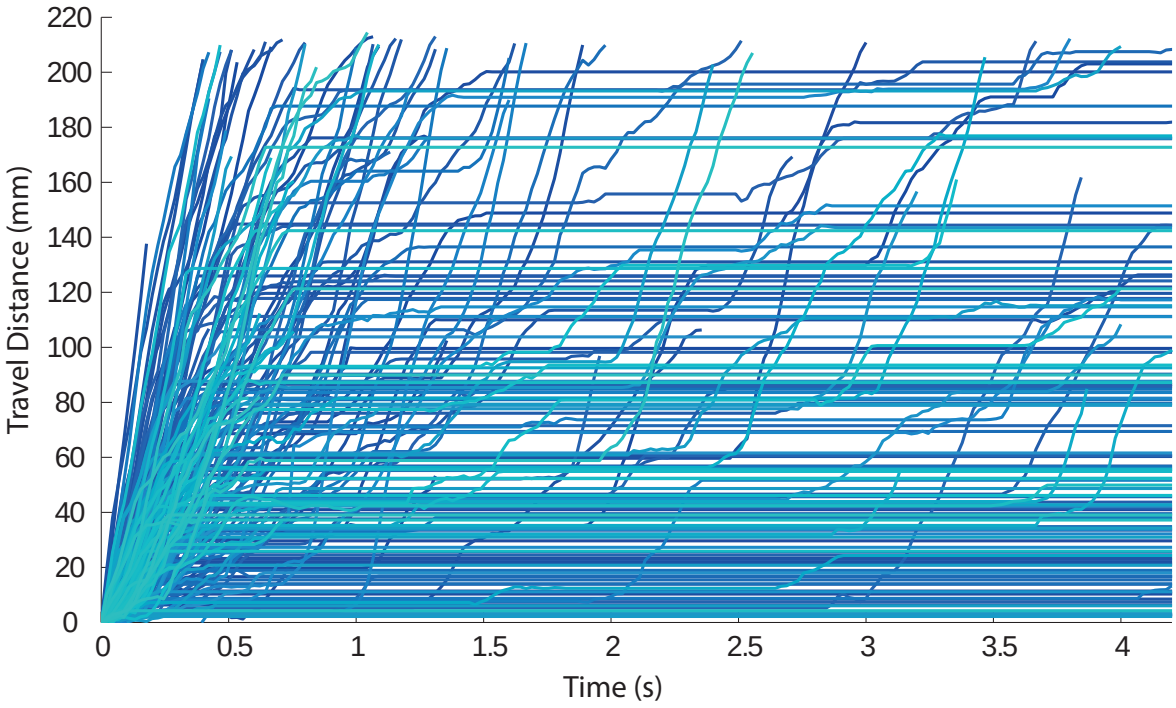

Figure 5.11: Streamwise Trajectories for the experiment of Aug 24^{th} - All trajectories

In this figure the analysis is carried to a maximum of T=4 seconds. In the trajectory calculation it is assumed that if a particle travels outside the window the particle is 'lost'. This assumption can be noticed in the Figure by looking at the truncated trajectories. This effect is particularly relevant at the very beginning of the analysis, it appears that many particles are lost in a time lower than 1 second (45 frames). Those trajectories are probably the ones followed by the grains that doesn't start and stop inside the window. However, the assumption of considering all grains should be taken carefully: the disappearance of the grains from the trajectories may bias the data for the reasons explained in Figure 5.12.

By following this first approach it is clear that the statistics of the particles distribution will be strongly affected by the grains that leave the window. For example, in Figure 5.12 the grains marked by an arrow have a stream-wise coordinate with an high value (almost $x = 200mm$). This coordinate when the grain definitively leaves the window will be lost, therefore the mean position will move to lower values. A second

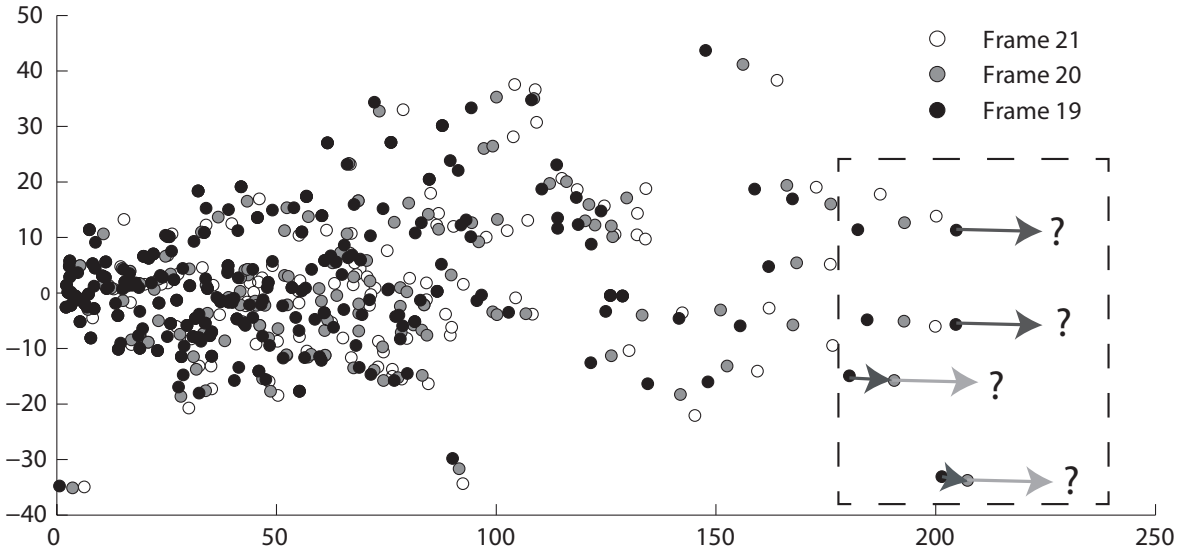

Figure 5.12: Missing Particles for the experiment of Aug 24^{th} - All trajectories

population of trajectories was considered to solve this problem. To be sure to achieve the stability of the data through time two considerations were made.

- Starting Condition: If a grain is entrained by the flow the first stages of its motion will be characterized by a low velocity. Then with the increasing of the exposed area the Drag Force will increase and the grain will accelerate. If a grain enters the window from outside, it will travel inside the window with a velocity that is higher respect to the velocity of a 'starting' grain. Therefore the movement of the grains that enters window should be neglected.

- Stopping Condition: The purpose of the second trajectories data is to grant stability to the statistics by avoiding the loss of grains. The only assumption that can be made to achieve this result is to study the diffusive behaviour of only the grains that stop inside the window.

The effect of the application of those assumptions on the trajectories population is reported in Figure 5.13. From this Figure it is clear that the exclusion of all movements that does not respect the hypothesis has a major role on the trajectories. One of the most important effects that can be noticed 'by-eye' is the exclusion of the grains that does not start or stop inside the window. After the calculation of the trajectories it is possible to start the analysis.

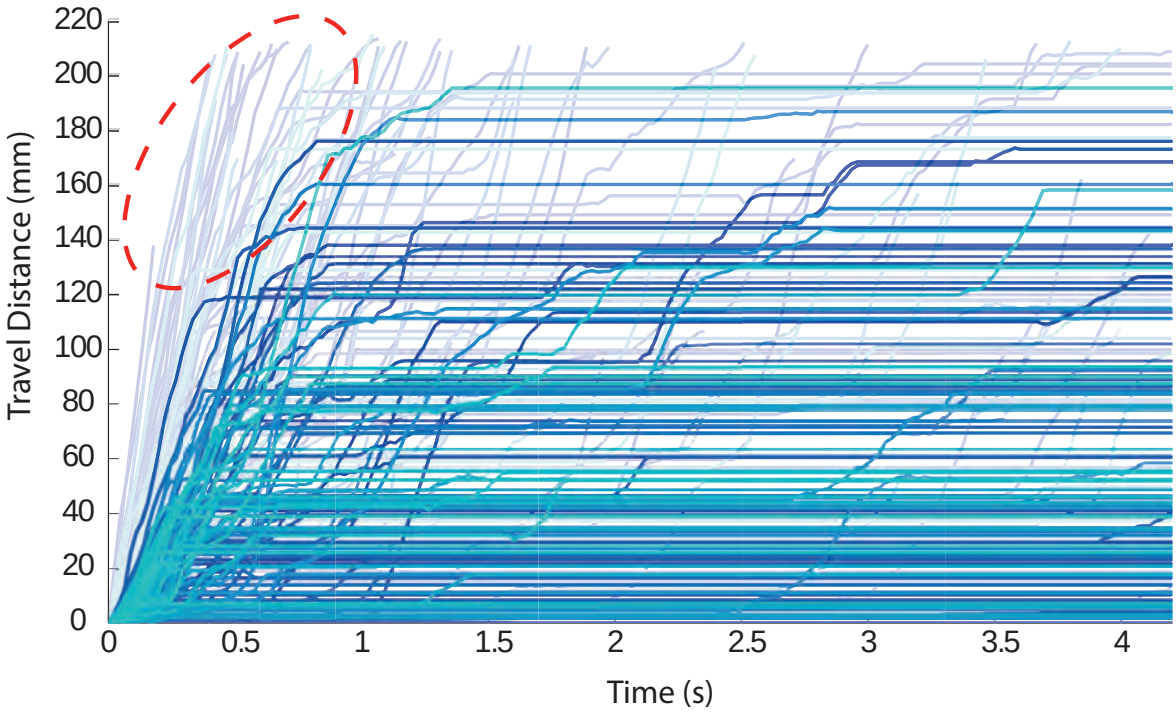

Figure 5.13: Start-Stop Trajectories for the case of Aug 24^{th}

5.4.2 Trajectories analysis

The trajectories are a sequence of (x,y) points that a particle assumes in function of time t. The first thing to define to perform the analysis is the maximum time t_{MAX}. The definition of t_{MAX} is arbitrary and the value chosen was $t_{MAX} = 4s$. This means that the computation of the statistics will be performed until this threshold only: the grain movements correspondent to values that exceed t_{MAX} are neglected. The following parameters are calculated for each frame (or $\forall t$):

$$\text{Mean position: } \overline{X} = \frac{\sum_{i=1}^{n} X_i}{N} \qquad \text{Variance: } \overline{X - \overline{X}^2} = \frac{\sum_{i=1}^{n} \left(X_i - \overline{X}\right)^2}{N} \tag{5.11}$$

The graphical representation of the parameters calculated is reported in Figure 5.14. The red line indicates the standard deviation which is the root of the variance. Those two quantities are calculated for all the points between 0 and t_{MAX}. To follow the approach described by Nikora the time values and the variance must be normalized in order to obtain non-dimensional parameters. Therefore the following normalizations are made:

$$\text{Non-dimensional variance : } S = \frac{\overline{X - \overline{X}^2}}{d^2} \tag{5.12}$$

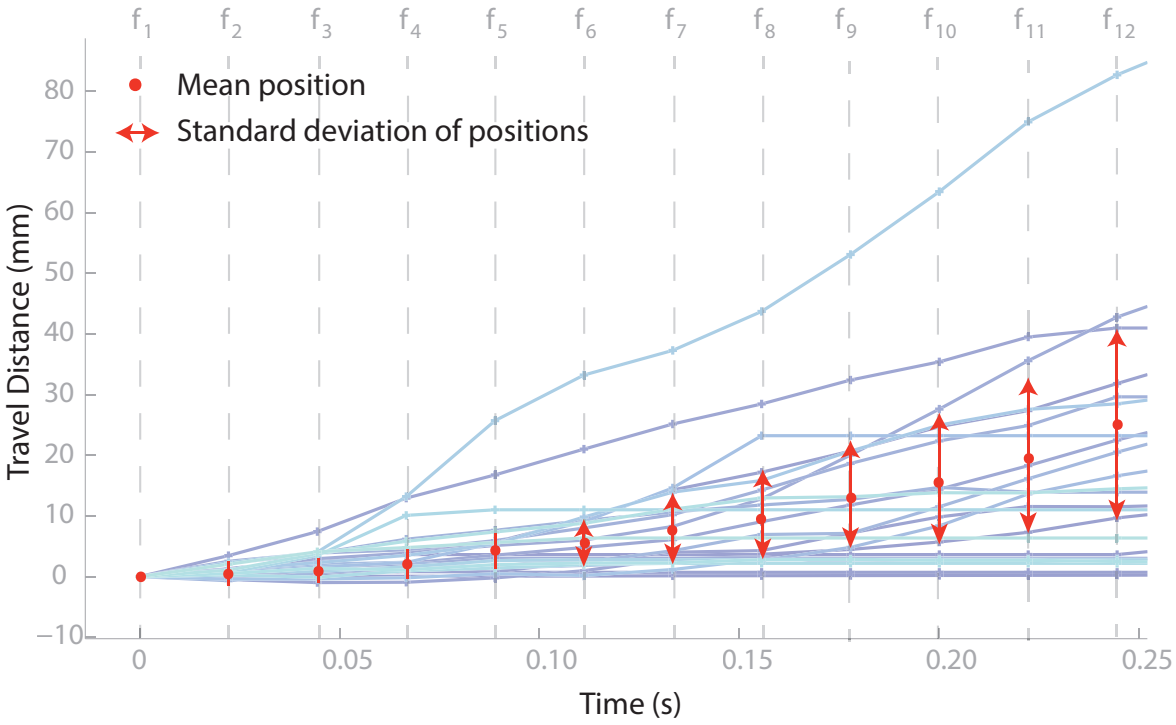

Figure 5.14: Mean and standard deviation of grain positions by frame

$$\text{Non-dimensional time} : T = \frac{t \cdot u_*}{d} \tag{5.13}$$

The theory says that the non-dimensional variance is proportional to the non-dimensional time with a power law. Therefore, in order to estimate if those relations are verified it is useful to plot the data in a double logarithmic scale. Figure 5.15 shows the the result in logarithmic scale for the case of Aug. 24^{th}. The Figure shows that the effects of the grains that disappear from the window is particularly marked for high values of the non-dimensional time parameter. However, the increase of the fluctuations seems to be the same for both cases for high time parameter. A major effect can be spotted for low time-parameter: the steepness of the curve for the start stop case (left) is qualitatively higher than the steepness of the curve for all trajectories (right). For low time parameter the main difference between the two populations is constituted by the particles that does not start or stop inside the window (as reported in Figure 5.13. As explained in the previous sections the 'move-move' trajectories are different in nature from the trajectories of the 'start-stop' grains. Therefore, the analysis should be carried on the latter trajectories population and the former should be neglected. Surprisingly it appears that the diffusion is stronger if the 'move-move' trajectories are neglected. All the diffusion curves for all experiments are reported in Appendix 7 in Figure 7.21.

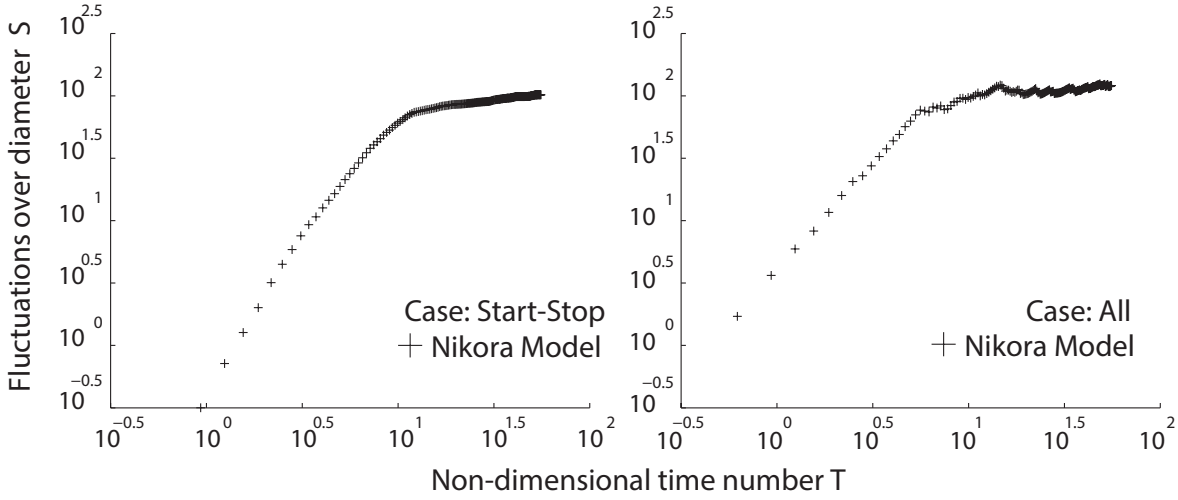

Figure 5.15: Diffusion regimes for the Aug 24^{th} (All trajectories (right) start-stop (left)

5.4.3 Diffusion regimes

From the analysis of the diffusion curves it appears that there's a difference between the result obtained in the present study and the analysis exposed by Nikora. The diffusion curves for almost all experiments have a trend which seems to be linear for the early stages of the diffusion, linear for the last stages and a transitional regime between the two. From the diffusion curves of the six experiments it seems that only two well-defined diffusion regimes can be observed. A third regime is present between the two, but the diffusion curve seems to not follow a linear proportionality with time. Qualitatively the two regimes seems to be joint with 'knee' type of curve. The difference between the theoretical model for the diffusion proposed by Nikora and the diffusion curves obtained by the present study is reported in Figure 5.16.

After the calculation of the diffusion curves it is possible to estimate the diffusion regimes by evaluating the slope of the two 'linear' regimes. To assess the slope the experimental points were interpolated with a line in the double-logarithmic plot. By the observation made from the experimental data two linear fitting were applied: one from the 'head' of the point series and one from the 'bottom'. The procedure adopted to fit the data consists in the following steps:

1. The first point (S_0,T_0) is added to the data sequence.

2. The maximum threshold for sum of squared residuals is fixed.

3. The next point (S_{i+1},T_{i+1}) is added to the data sequence.

4. The data series is fitted with a line.

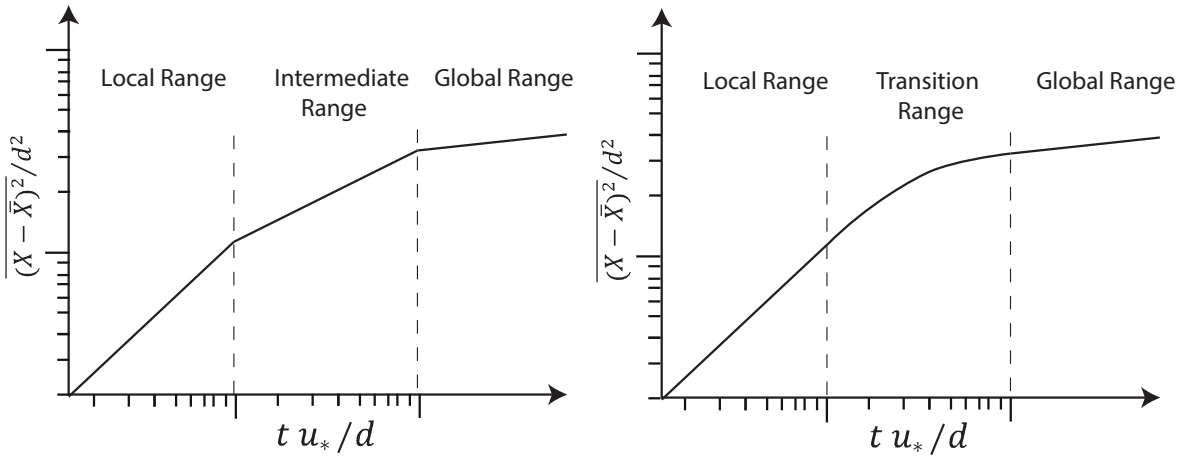

Figure 5.16: Diffusion regimes: Nikora's model (left), Experimental results (right)

5. If the sum of squared residuals is grater than the threshold stop the process. If not, back to point 3 and increase i.

The purpose of this procedure was to set up an automatic fitting of the data based on a steep increase of the sum of squared residuals when the curve can't be approximated as linear any more. However, for all experiments there was not a well defined increase in sum of squared residuals, therefore the definition of the threshold for the squared sum has to be done manually. The fitting must be considered as made 'by-eye'. The result for the fitting of the Aug 24^{th} is reported in Figure 5.17. The coefficients obtained for the fitting are slightly greater than the unit for the low values of the time parameter and are close to a decimal for the high values. This behaviour is respected in the fitting of all other experiments (Reported in Appendix 7 Figure 7.22).

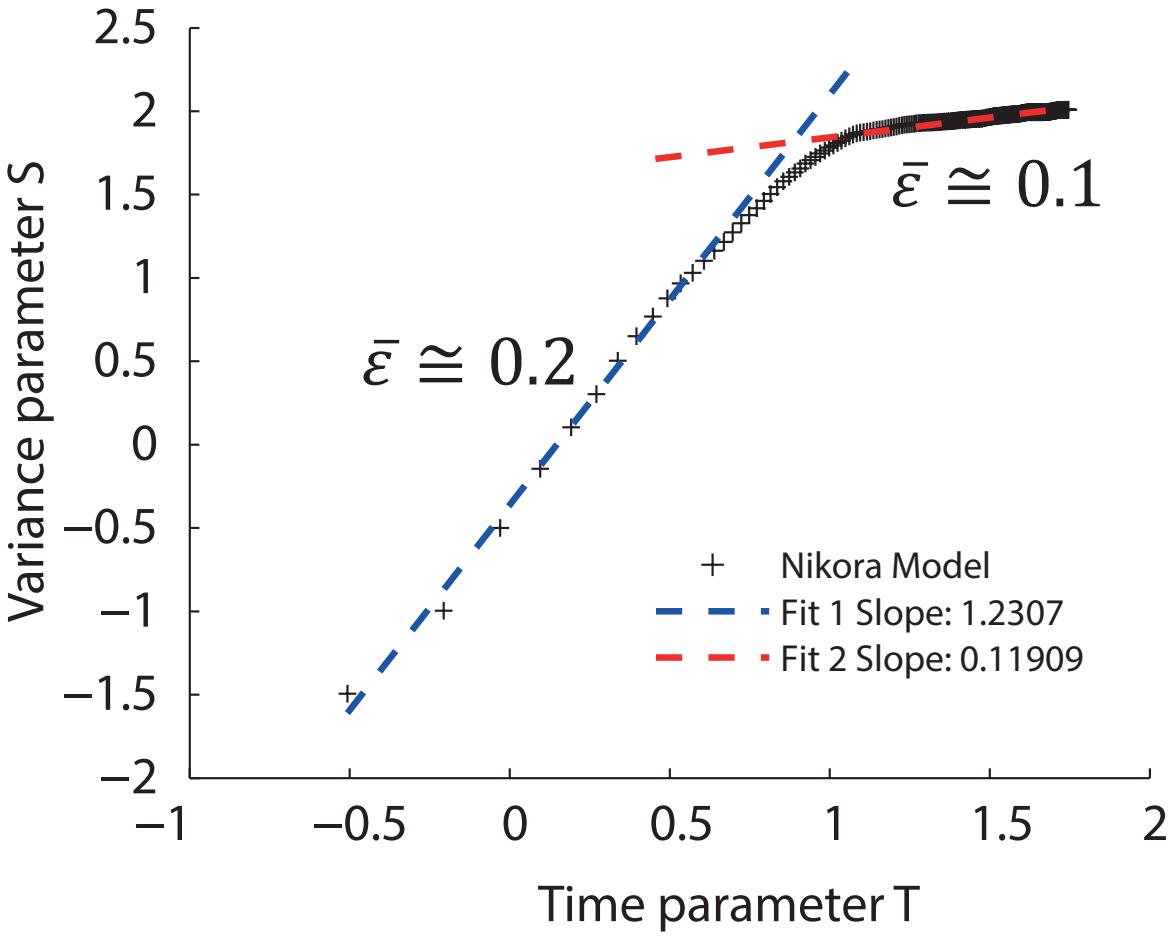

Figure 5.17: Fit of the diffusion curve of Aug 24^{th}

5.5 Result Discussion

The quantities reported in Table 5.1 are the slopes of the two clear linear behaviour of the diffusion curves and the time of intersection between the two regimes. The linear behaviour was spotted for two parts of the curve: for low values of time parameter (lower than 5) and for high values (higher than 11). The average error in Logarithmic scale with the linear fitting resulted is extremely low: $\overline{\varepsilon} \simeq 0.2$ for the linear trend correspondent to low values of the time parameter and $\overline{\varepsilon} \simeq 0.1$ for the linear trend correspondent to high values of time parameter. The slope found for the diffusion regime with low time parameter are in the range $\gamma_X = 0.93 \div 1.23$. Therefore in the very beginnings of the particles motion the diffusion process (local-range) can be assumed as ballistic, according to the model described by Nikora. For high values of time parameter the exponent found was $\gamma_X = 0.10 \div 0.12$. This is considerably lower than the exponent found by Nikora, but indicates that for high time values the regime

Date	τ_0^*	γ_{local}	γ_{global}	T	u_*
Aug 24^{th}	0.061	1.23	0.12	7.67	0.070
Sept 2^{nd}	0.068	0.93	0.12	9.83	0.074
Sept 22^{nd}	0.080	1.16	0.10	8.66	0.080
Sept 23^{d}	0.083	1.08	0.12	8.16	0.081
Sept 29^{th}	0.086	0.93	0.12	9.77	0.083
Oct 1^{st}	0.090	1.08	0.12	8.34	0.085

Table 5.1: Results from the diffusion regime fitting

(global-range) is strongly sub-diffusive. The intermediate range is not well defined. It can be stated that in this case there is a 'transition regime' from the local range and the global range. This transition regime occurs for values in a range of time parameter $T = 7.5 \div 10$. The results obtained suggests that even if the step lengths distributions scales with the shear stress parameter, the diffusion regimes seems to be less affected by that parameter. This can be attributed to both the fact that the diffusion is the composition of three processes (entrainment, travel and deposition) and to the 'weakness' of the fitting procedure.

Chapter 6

Results Discussion and Future developments

6.1 Results

The purpose of the present study was to investigate the properties of bed load under different flow conditions. The experimental procedure for the gathering of reliable bed-load data showed the existence of technical issues that makes the analysis tedious and biased from human errors. The reasons are reported below:

- The quality of the frames taken by the camera was extremely poor. In those condition it was either hard to spot grains that are moving and to run an automated tracking of grains.
- The poor quality of the images led to the necessity of a manual tracking. The manual tracking implied some intrinsic issues in the procedure such as:
  - It is not clearly recognisable the condition of when a grain stops.
  - The tracking procedure is heavily time demanding and greatly biased by possible human mistakes.
  - The trajectory of many grains can not be tracked properly due to the poor image quality.
- The spatial amplitude of the window examined is probably too short to assess the bed load statistics with sufficient reliability.

However, despite the issues presented previously some important results were achieved in the present study. The analysis of the bed-loads statistics performed in Chapter 4 revealed that:

[1]: The flow condition have a major effect on the grain step lengths. This effect was recognised after the calculation of the Probability distribution functions obtained through the analysis of the step lengths. The effect of the short amplitude of the window led to the necessity of the imposition of a statistical model to study the step lengths. This was necessary to involve the relevant effect of the grains that have a step length longer than the window. Four models were applied: Log-normal, Exponential, Gamma and Weibull. The model were fitted to the observed distributions obtained by experiments by means of a least squares method. The distribution that better matched the observed data was the Log-normal, followed by the Weibull, Gamma and Exponential respectively. The intrinsic properties of the Log-normal distribution could describe the bed-load transport in a complete different manner than the other distribution. A log-normal distribution implies that the probability that a grain performs very short displacements is close to zero. This could mean that once a grain is detached from the bed the hydrodynamic forces overcomes a static friction which is higher than the dynamic friction. A grain is then allowed to deposit only after having performed a relevant distance. On the other hand the use of a log-normal distribution led to unrealistic values for the deviation and was the most complex distribution to fit numerically. The mean of the fitted distribution showed a good correlation with the shear-stress parameter in all cases.
[2]: The experimental data allowed a simple and quick analysis of the velocity of the grains. The stream-wise and cross-stream velocities showed almost no correlation at all with the flow conditions. It seems that the grain velocities are independent and identically distributed in every experiment. However, the velocity data are biased both to human perception and the procedure adopted for the manual tracking. The stream-wise grain velocity can be approximated accurately by a Gamma distribution while the cross stream velocity was found following a Normal distribution.
[3]: For what concerns the grains rest time, no relevant difference was found between the six experiments analysed. This is due to the fact that the data available to study this variable have a poor quality since the spatial window examined is too short to observe many depositions and re-entrainment of the same grain. A second reason could be that every experiment was analysed for a maximum of 2 minutes ($\simeq 3000 frames$).
[4]: The link between the grain step length and the grain size was investigated. However, the present study reveals that at this scale no correlation between the flow intensity (expressed as Shields shear stress parameter) could be observed. This could be caused by three reasons. The first is that the quantity of data does not allow to have exhaustive statistics on this phenomenon. The second is reason is that there are some issues involved in the estimation of the diameter from a 3-dimensional quantity to a 2-dimensional representation (the camera images). A third effect is probably due to the fact that the bed composition is quite homogeneous and a relevant effect can't be observed at this scale.
[5]: The Entrainment Rate can't be properly assessed by means of a manual tracking. This is due to the fact that the Entrainment Rate defined as the number of grains entrained by the flow over an unit of time depends strongly on the quantity of grains

tracked by the investigator. Therefore the more time is spent on the tracking the higher the Entrainment rate will be. A second problem is due to the fact that the amplitude of the time window on which the Entrainment rate is averaged has a major effect on the value of this quantity. However, the effect is the same for all experiments, therefore the amplitude of the time window has a minor effect on a possible trend of the Entrainment rate.
[6]: The diffusion can be described as a sum of singular steps. In the case of bed load transport the diffusion can be described as a case of "anomalous diffusion" with a particle that performs a series of steps then it is "trapped" and stays still for some time. The aim of the study was to assess if the link between step length and shear stress parameter is present also in the study of the diffusion. The approach followed was described in some literature papers (Nikora et al. 2001),(Nikora et al. 2002). The result obtained confirmed that in the beginning of the diffusion the particles follow a super-diffusive process. In particular the analysis showed that the diffusion follows a "ballistic" process. For large time intervals the process becomes sub-diffusive. However, in this area the effect of the short window examined have a major effect and the effect of the grains that exit from the window is not present in the analysis. This leads probably to an underestimation of the intensity of the diffusion. No relevant differences between the diffusion linear phases between the experiments was found. In the present study what was defined as "intermediate-range" could not be spotted. However it was possible to asses the time scale that is characteristic for the ballistic range. This quantity (assessed with the non-dimensional time parameter $T = u_* \cdot t/d$) was found in a range between T=7.5 and T=10. Therefore future studies on the global behaviour of the bed-load diffusion must be carried on for time intervals which are longer than the characteristic time.

6.2 Future Developments

The future developments in this topic can be focused only on the overcome of the technical issues that are present in the experiments of 2009 at the University of Bradford. Once those problems are fixed the repetition of the analysis performed in the present study could lead to more exhaustive results. The three main technical problems to solve are:

1. The amplitude of the window examined: The present study allowed to assess the mean step length distance and the deviation on the basis of hypothesis made on the statistical distribution followed by the grain step lengths. To assess properly this quantity it is suggested to increase the examined area. The increase of the area could relevant have positive effect in terms of number of data available for the study of: Step length, Diffusion, Rest time.

2. Quality of the images: One of the main issues encountered in the present study was the poor quality of the images due to the presence of seeding particles in the flow. It is suggested to improve the quality of images for the purpose of the study of the bed-load statistics.

3. Automatic computer-based tracking procedure: The tracking procedure performed in the present study is heavily time demanding and the obtained results are strictly dependent on the sensibility of the investigator. Therefore it is suggested to implement an automated tracking procedure for the moving grains based on image analysis.

The next experiment on those topics is currently object of further studies at the University of Sheffield. The device that will be used for those investigations will be a Rotating annular flume reported in Figure 6.1.

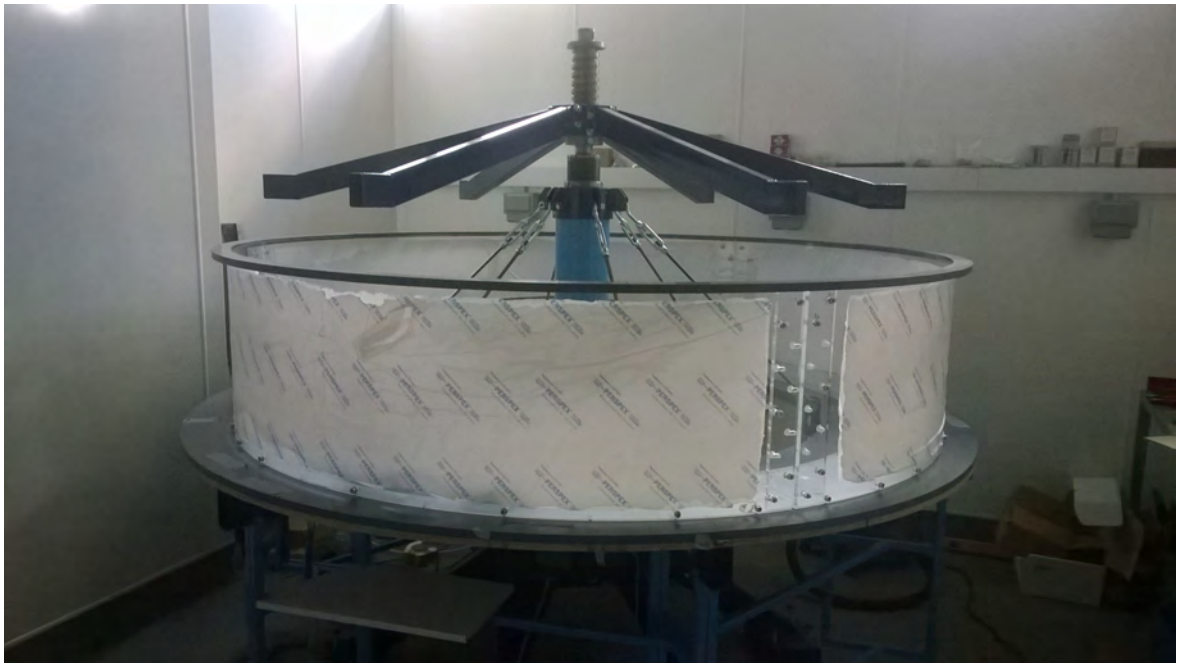

Figure 6.1: Rotating annular flume under construction at the Laboratory of Hydraulics of the University of Sheffield (May 2015)

Chapter 7

Appendix 1: Complementary Graphs

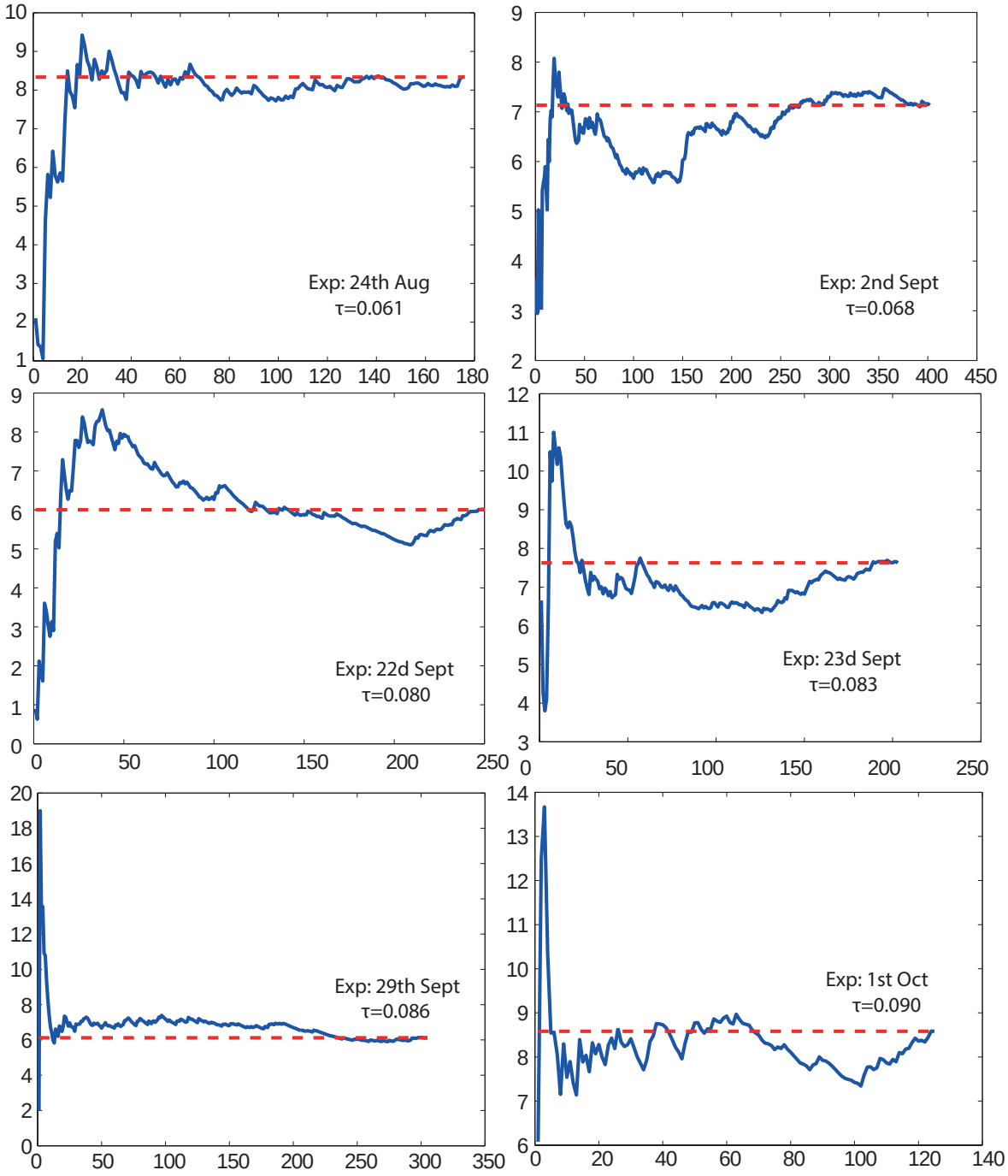

Figure 7.1: Non-dimensional mean step length vs Number of steps for all experiments (Shakes Included)

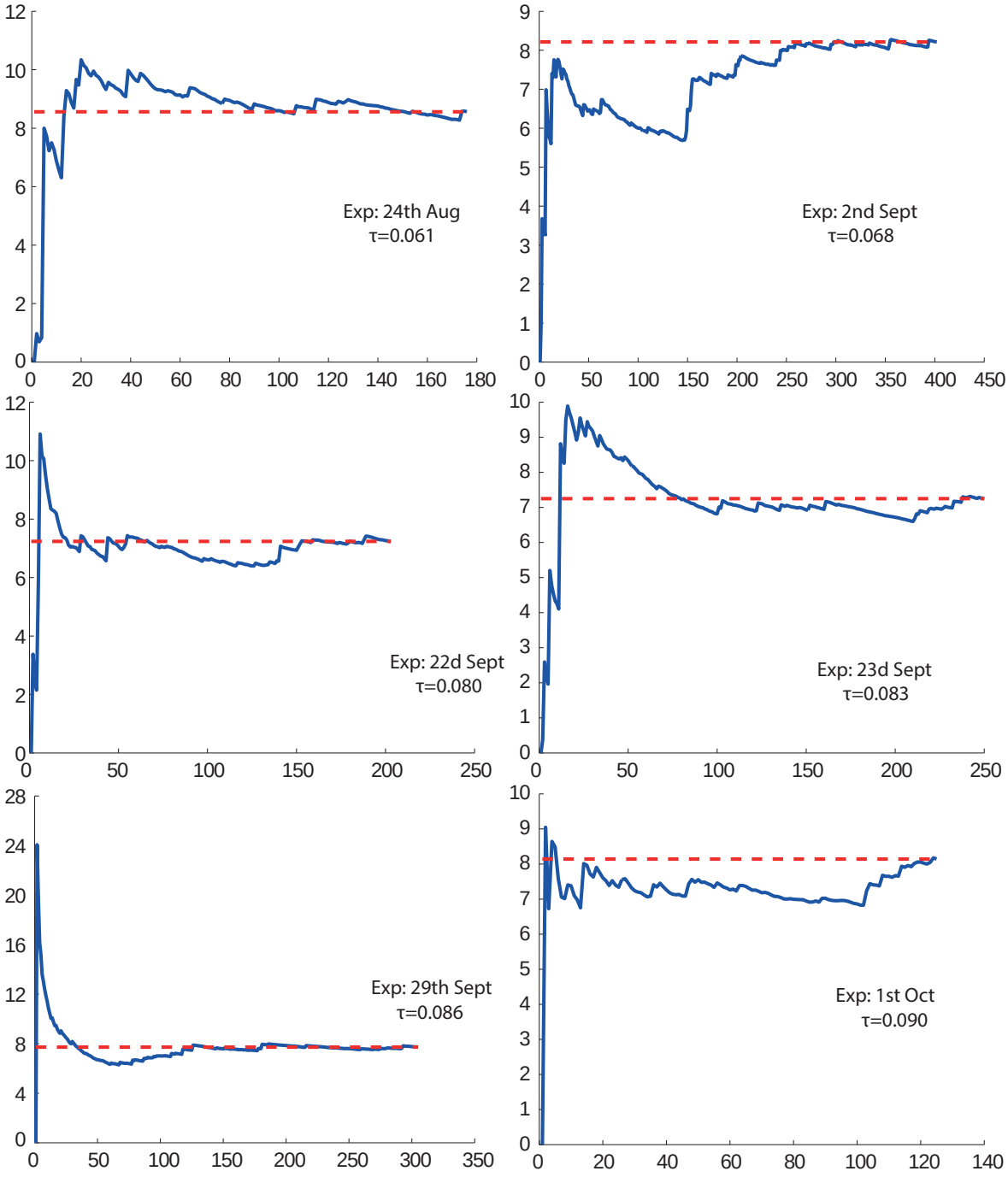

Figure 7.2: Non-dimensional step length standard deviation vs Number of steps for all experiments (Shakes Included)

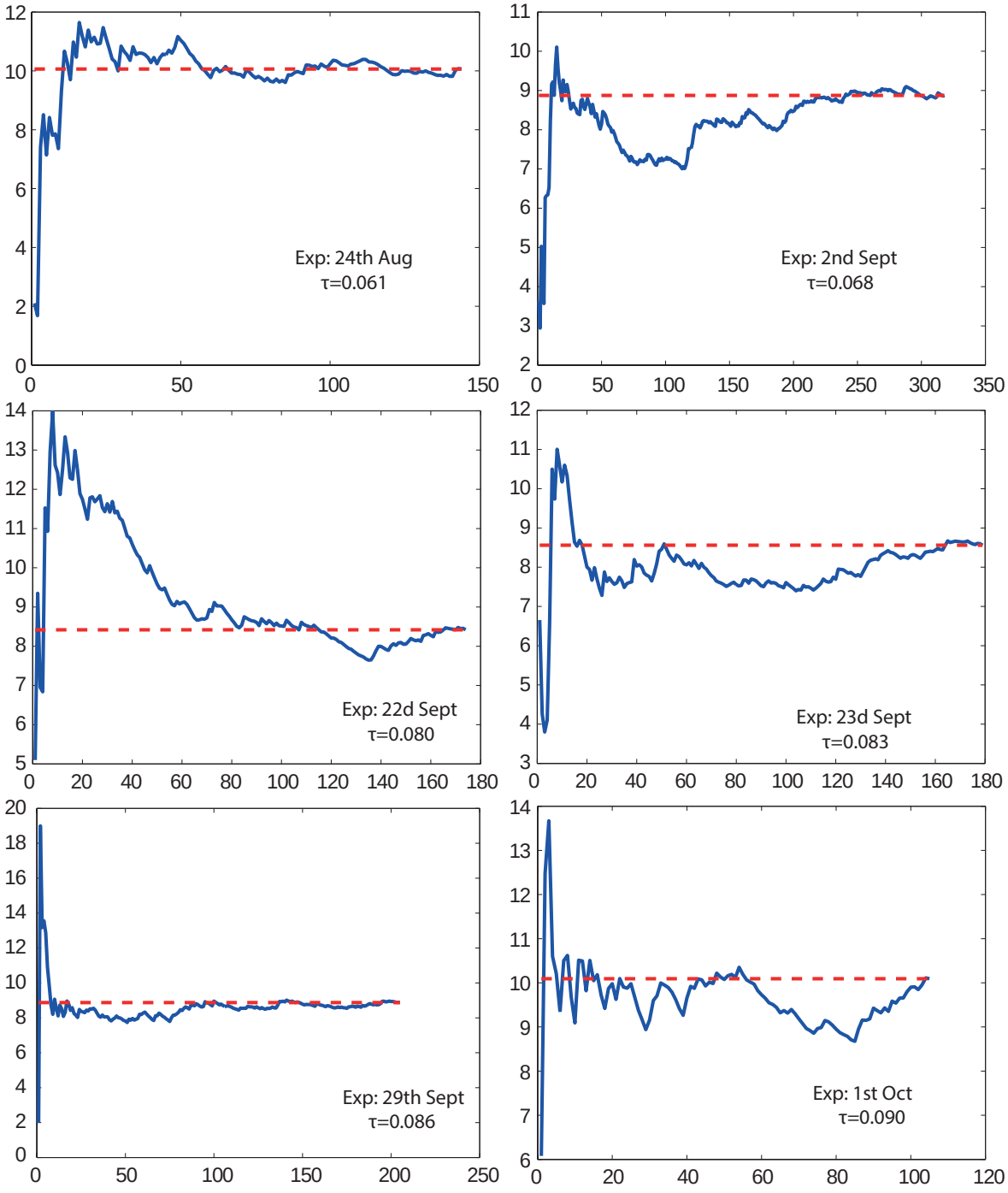

Figure 7.3: Non-dimensional mean step length vs Number of steps for all experiments (Shakes not Included)

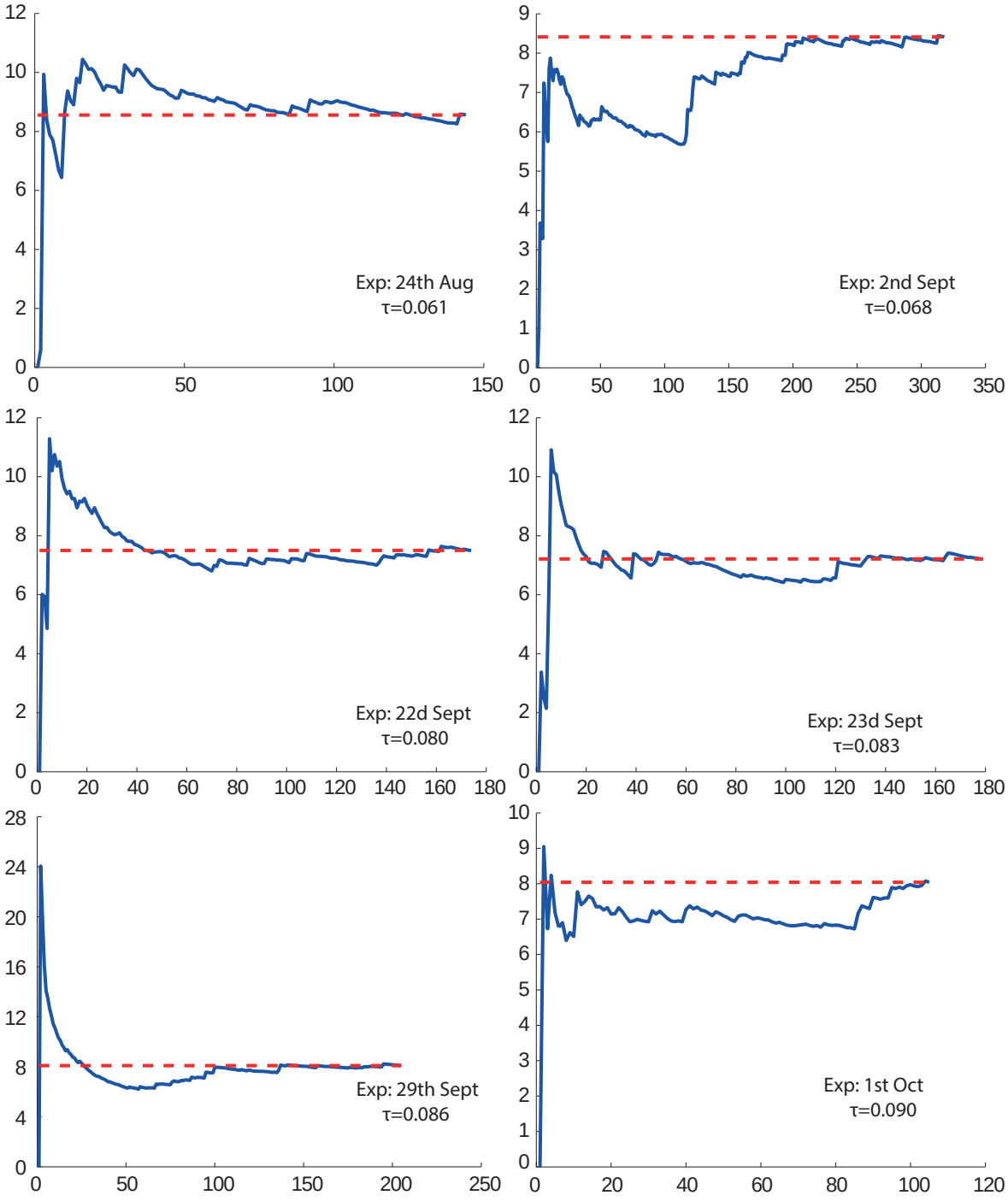

Figure 7.4: Non-dimensional step length standard deviation vs Number of steps for all experiments (Shakes not Included)

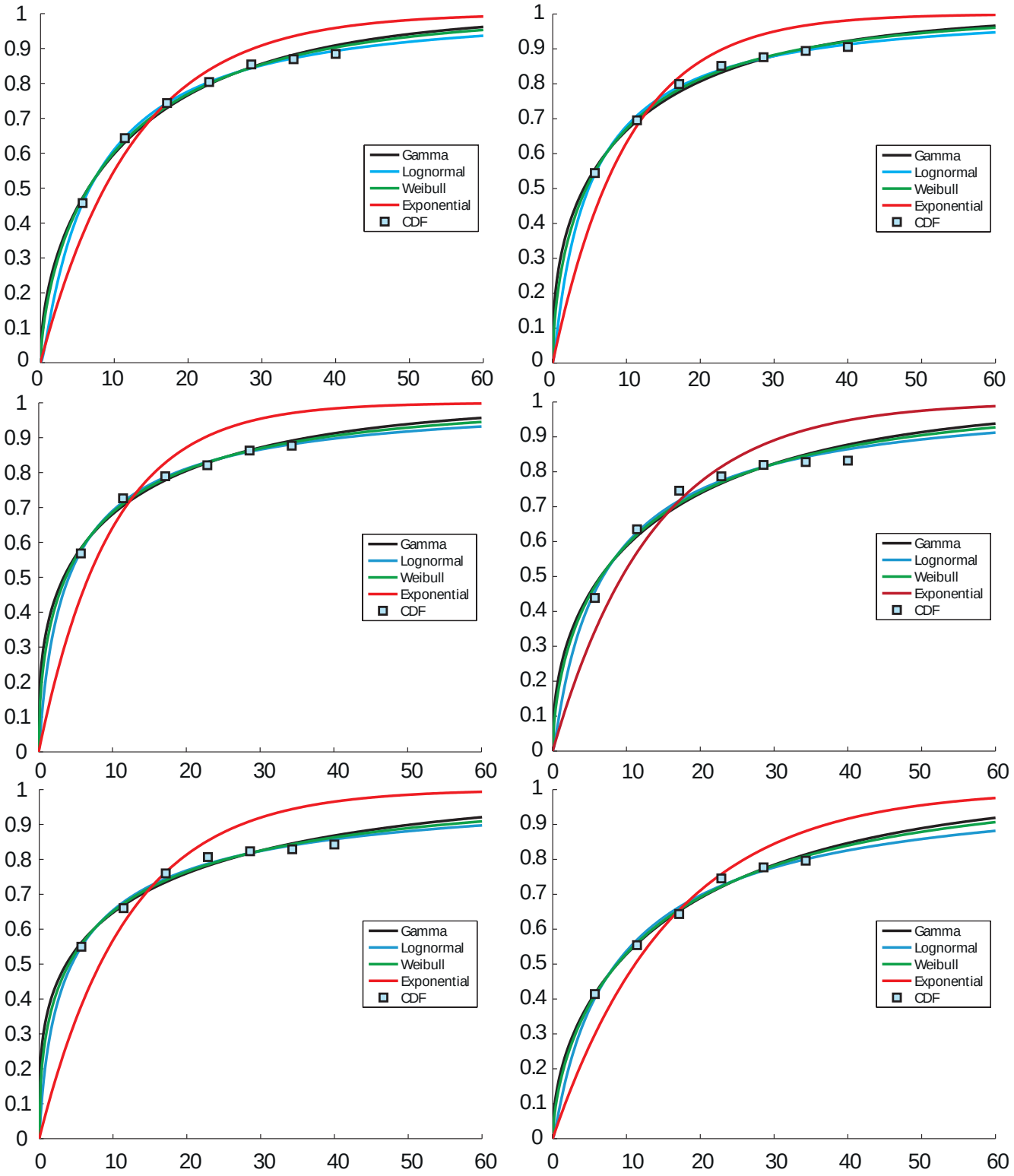

Figure 7.5: Non-dimensional step lengths (mm) CDF fits for all experiments: Case 'Shakes' included-7 Classes (TOP: 24^{th} Aug (left), 2^{nd} Sept (right); MID: 22^{nd} Sept (left), 23^{d} Sept (right); BOT: 29^{th} Sept (left), 1^{st} Oct (right);

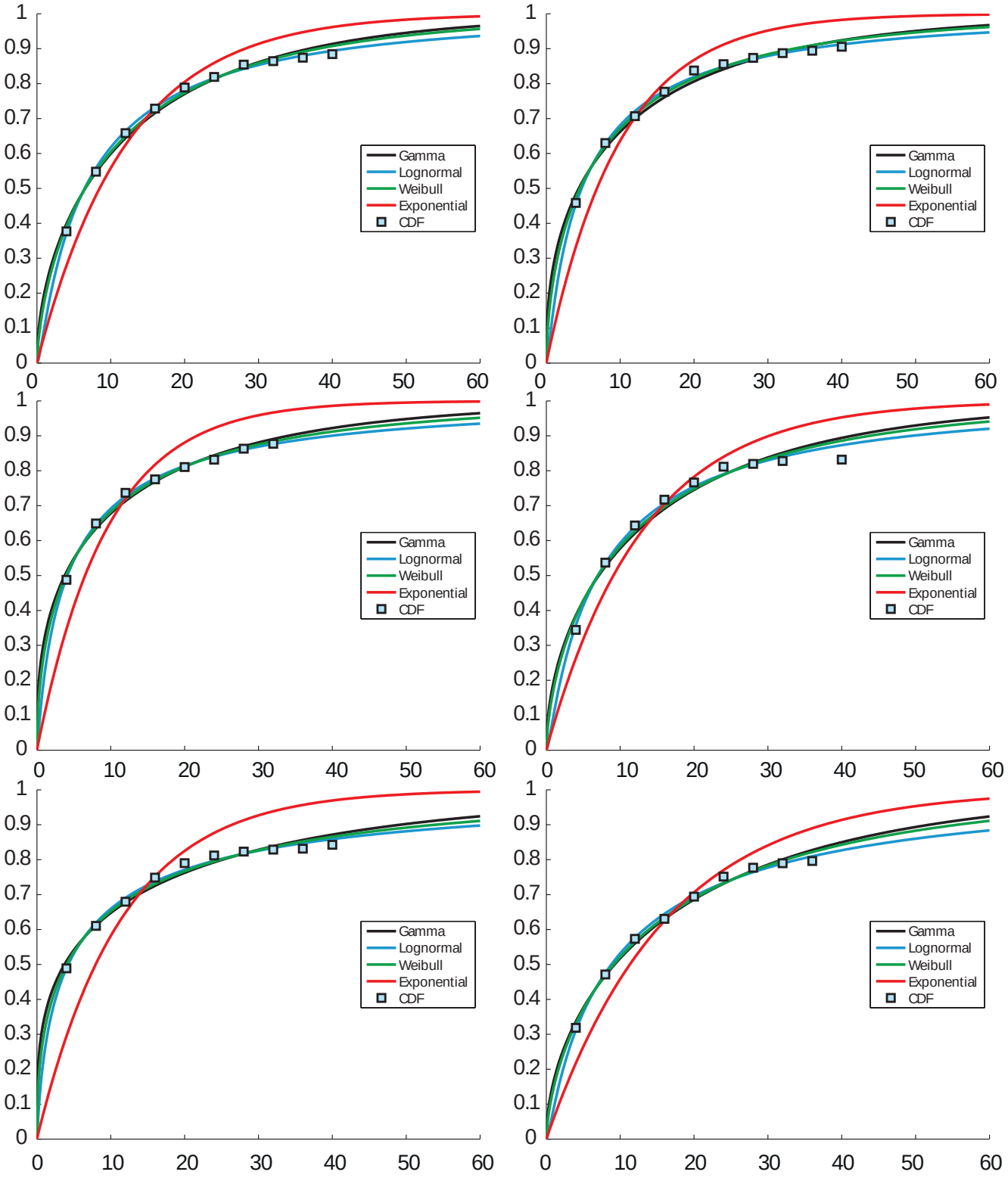

Figure 7.6: Non-dimensional step lengths (mm) CDF fits for all experiments: Case 'Shakes' included-10 Classes (TOP: 24^{th} Aug (left), 2^{nd} Sept (right); MID: 22^{nd} Sept (left), 23^{d} Sept (right); BOT: 29^{th} Sept (left), 1^{st} Oct (right);

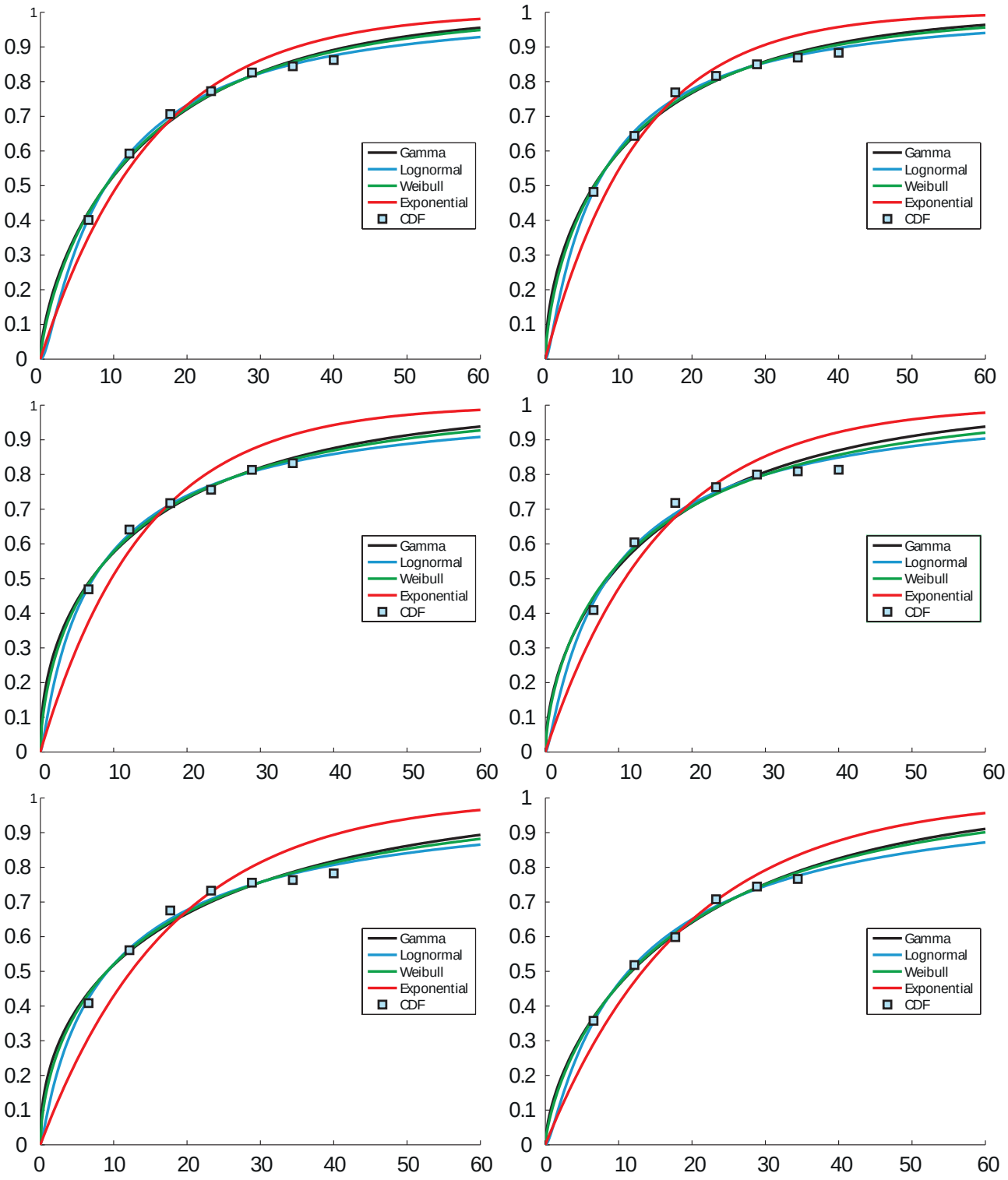

Figure 7.7: Non-dimensional step lengths (mm) CDF fits for all experiments: Case 'Shakes' excluded-7 Classes (TOP: 24^{th} Aug (left), 2^{nd} Sept (right); MID: 22^{nd} Sept (left), 23^{d} Sept (right); BOT: 29^{th} Sept (left), 1^{st} Oct (right);

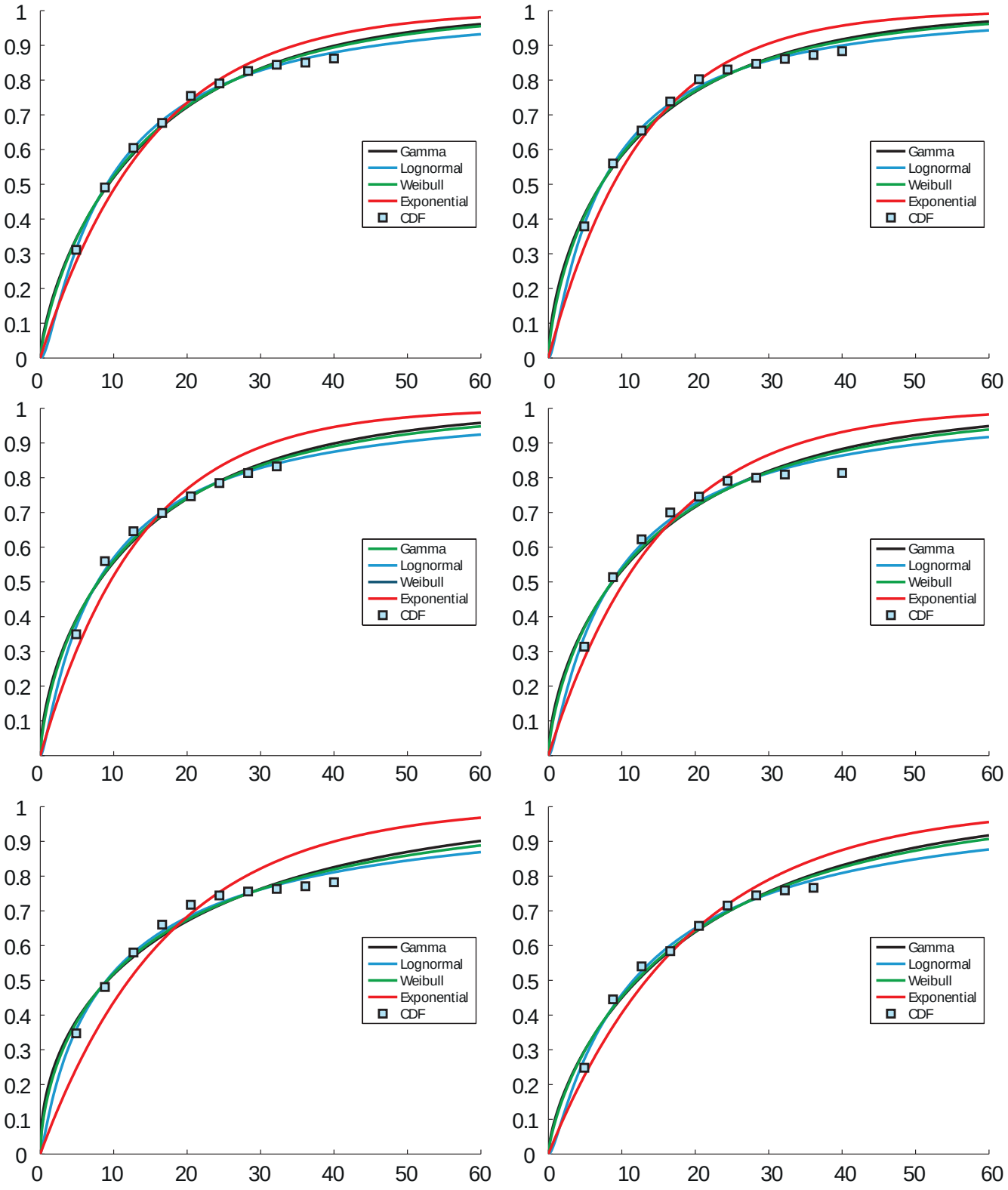

Figure 7.8: Non-dimensional step lengths (mm) CDF fits for all experiments: Case 'Shakes' excluded-10 Classes (TOP: 24^{th} Aug (left), 2^{nd} Sept (right); MID: 22^{nd} Sept (left), 23^{d} Sept (right); BOT: 29^{th} Sept (left), 1^{st} Oct (right);

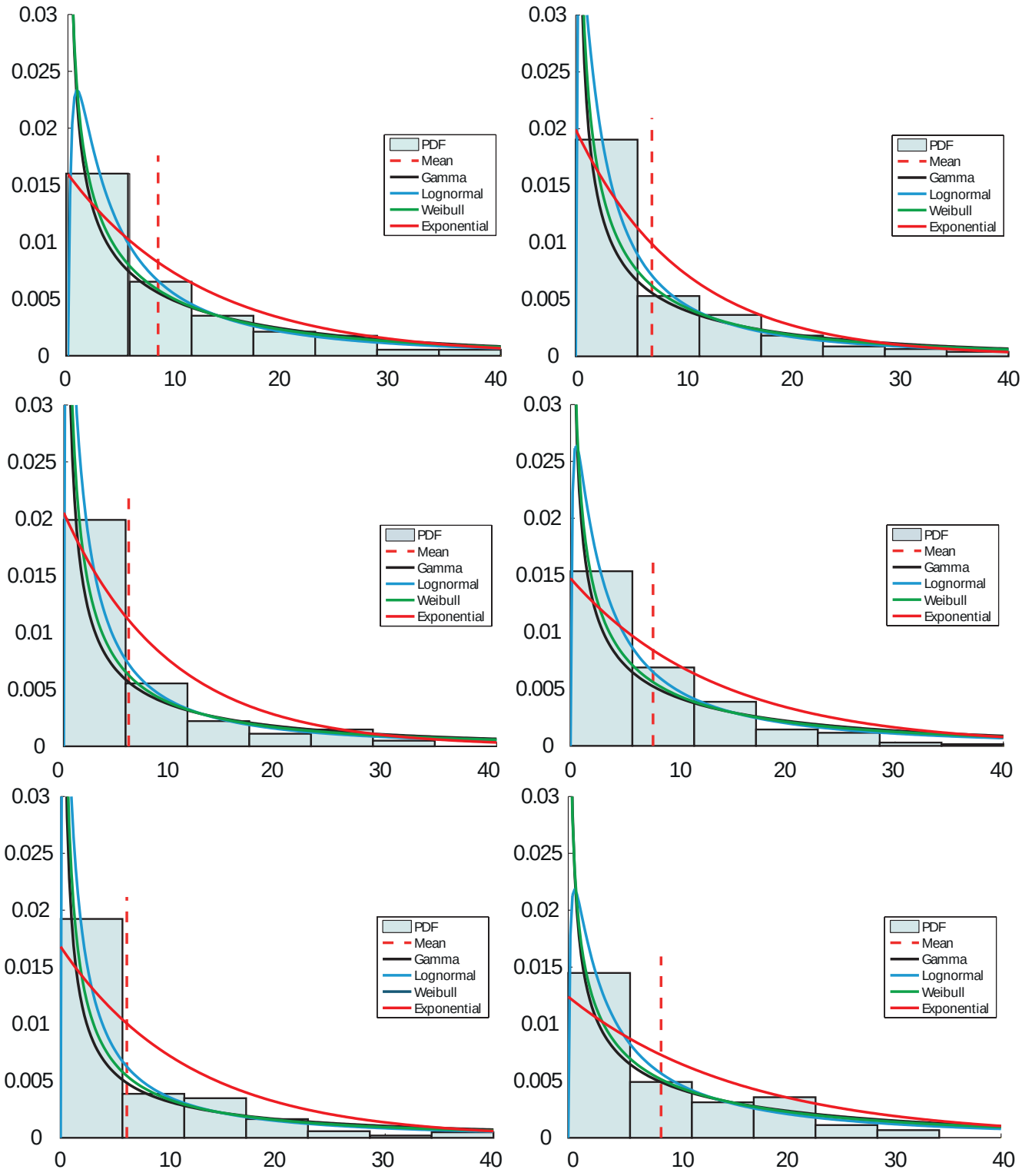

Figure 7.9: Non-dimensional step lengths (mm) PDF fits for all experiments: Case 'Shakes' included-7 Classes (TOP: 24^{th} Aug (left), 2^{nd} Sept (right); MID: 22^{nd} Sept (left), 23^{d} Sept (right); BOT: 29^{th} Sept (left), 1^{st} Oct (right);

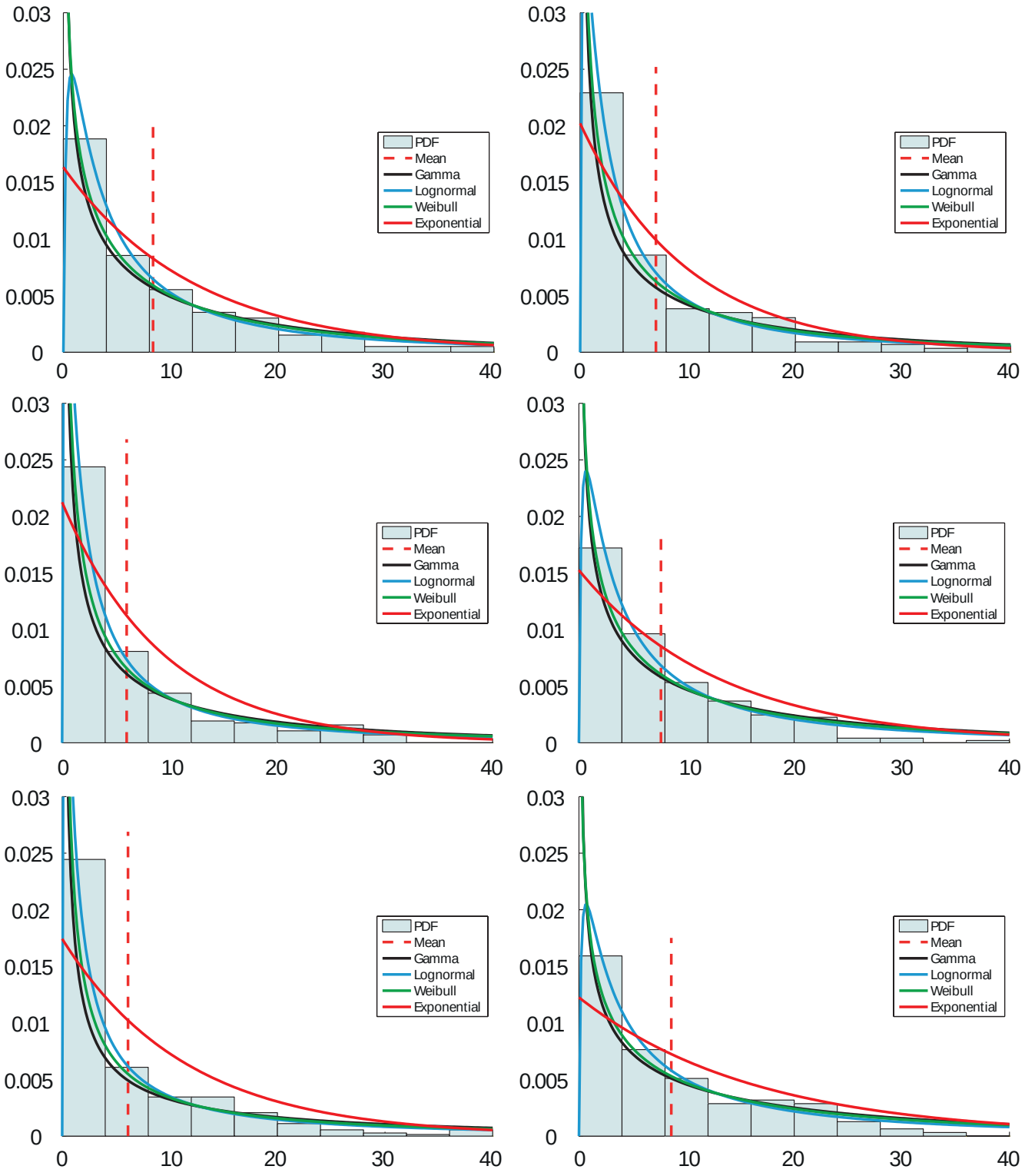

Figure 7.10: Non-dimensional step lengths (mm) PDF fits for all experiments: Case 'Shakes' included-10 Classes (TOP: 24^{th} Aug (left), 2^{nd} Sept (right); MID: 22^{nd} Sept (left), 23^{d} Sept (right); BOT: 29^{th} Sept (left), 1^{st} Oct (right);

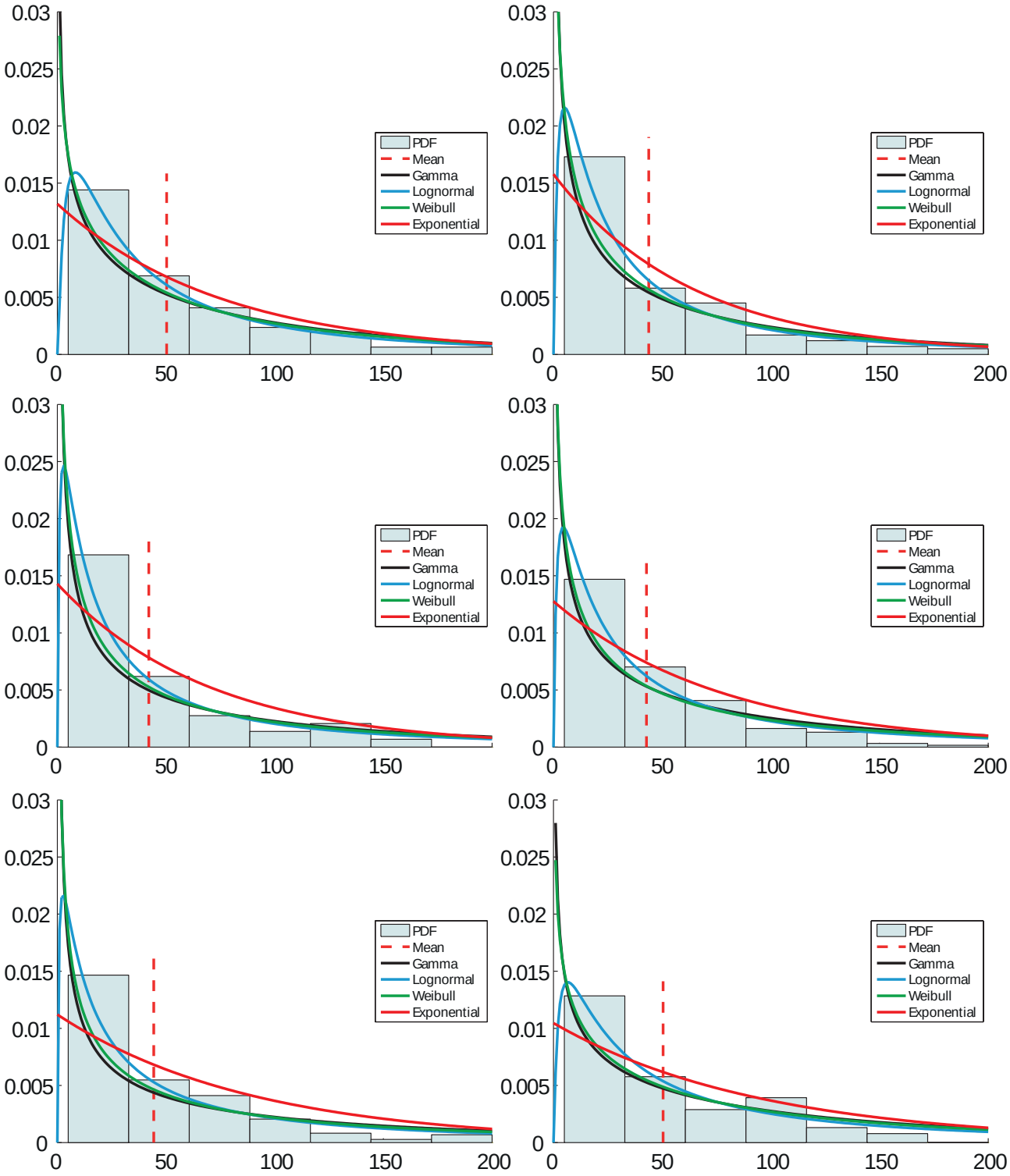

Figure 7.11: Non-dimensional step lengths (mm) PDF fits for all experiments: Case 'Shakes' excluded-7 Classes (TOP: 24^{th} Aug (left), 2^{nd} Sept (right); MID: 22^{nd} Sept (left), 23^{d} Sept (right); BOT: 29^{th} Sept (left), 1^{st} Oct (right);

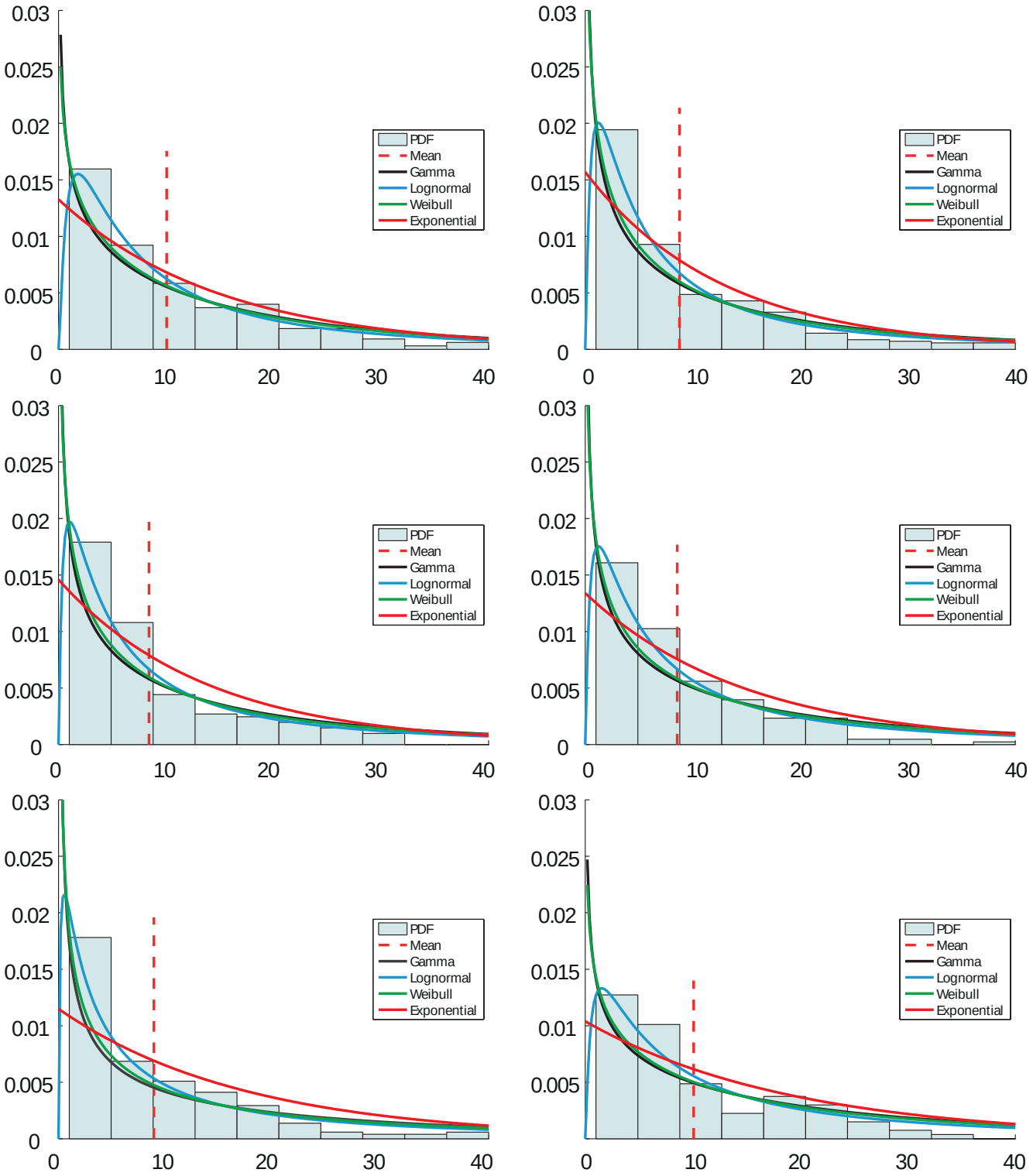

Figure 7.12: Non-dimensional step lengths (mm) PDF fits for all experiments: Case 'Shakes' excluded-10 Classes (TOP: 24^{th} Aug (left), 2^{nd} Sept (right); MID: 22^{nd} Sept (left), 23^{d} Sept (right); BOT: 29^{th} Sept (left), 1^{st} Oct (right);

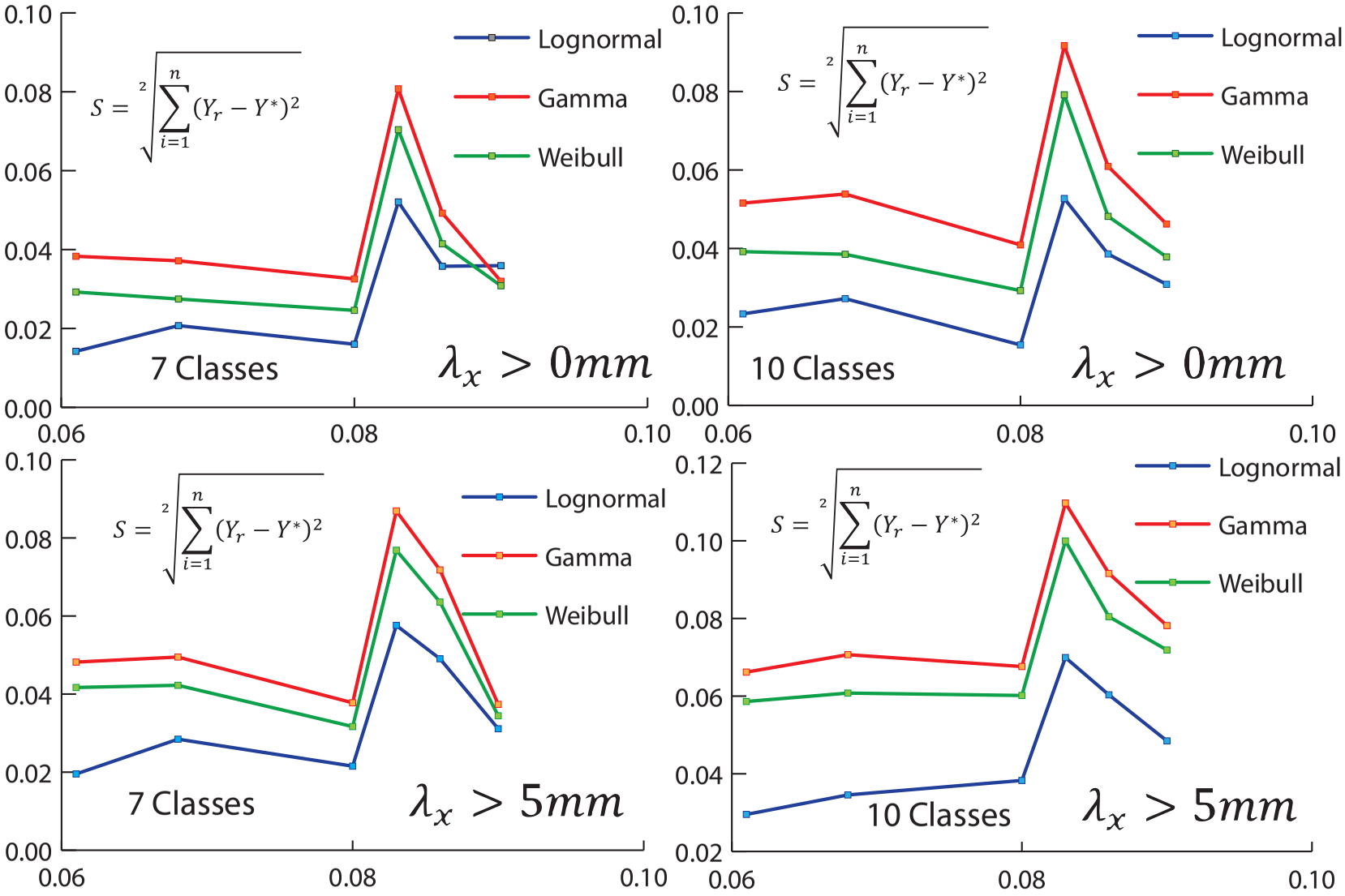

Figure 7.13: Sum of error vs. Shear stress parameter for each population and experiment: TOP: Shakes Included, 7 classes (left), 10 classes (right); BOTTOM: Shakes Included, 7 classes (left), 10 classes (right)

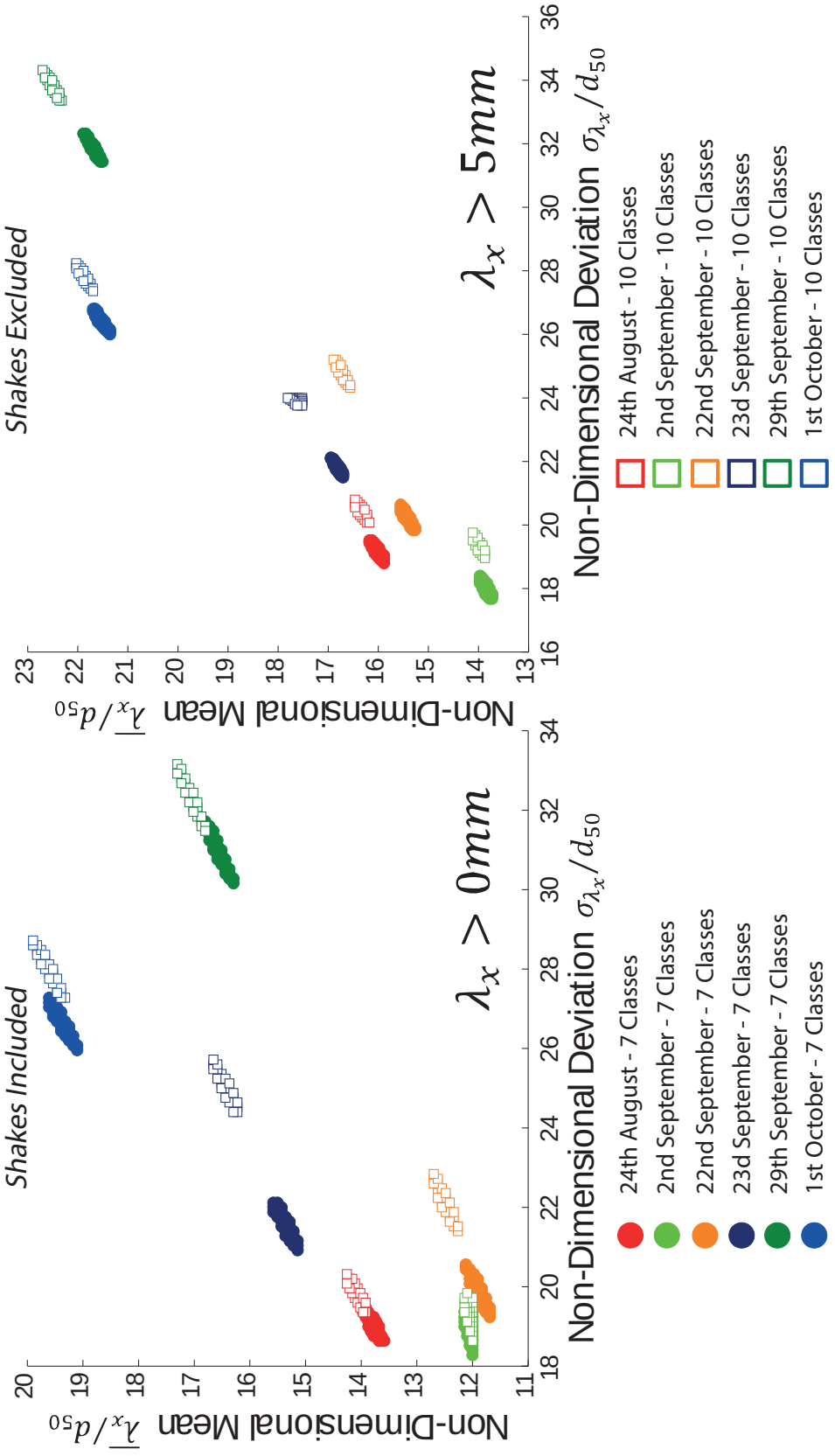

Figure 7.14: Position of the 30 points with lower sum of squared residuals for the case of gamma distribution in a mean/deviation chart. 'Shakes' included (left), 'Shakes' excluded (right)

Figure 7.15: Position of the 30 points with lower sum of squared residuals for the case of Weibull distribution in a mean/deviation chart. 'Shakes' included (left), 'Shakes' excluded (right)

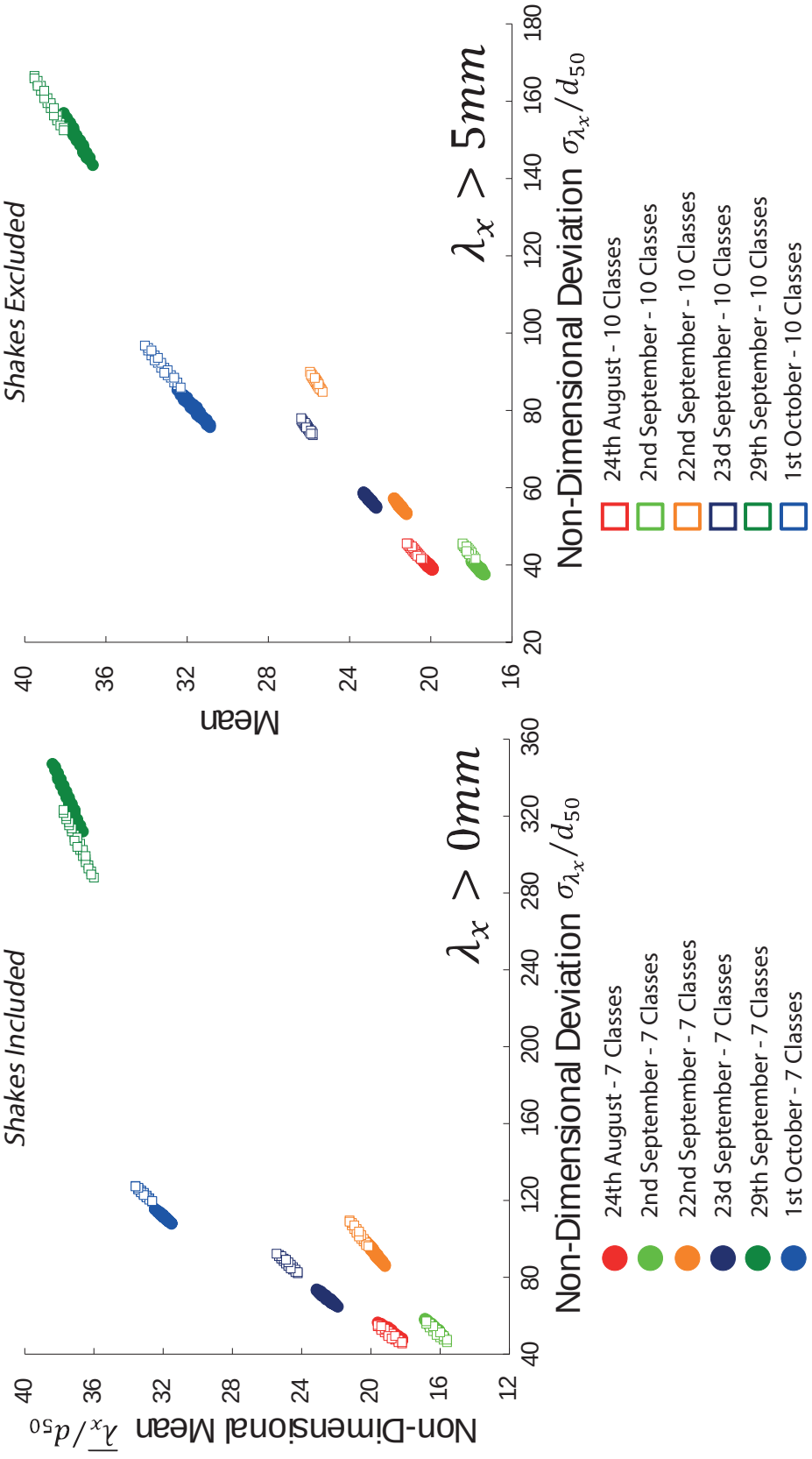

Figure 7.16: Position of the 30 points with lower sum of squared residuals for the case of lognormal distribution in a mean/deviation chart. 'Shakes' included (left), 'Shakes' excluded (right)

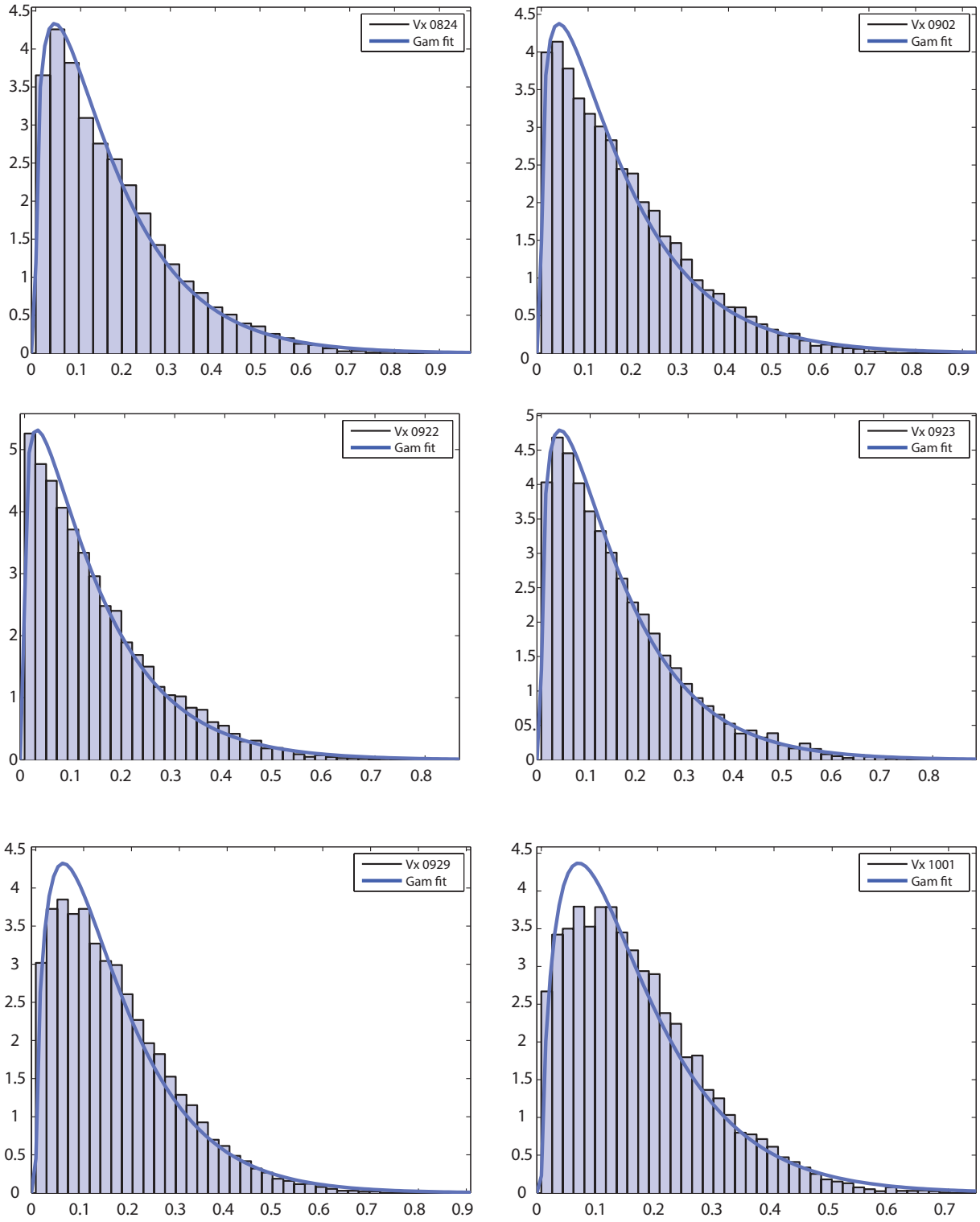

Figure 7.17: Non-dimensional stream-wise Grain Velocity fitting with Gamma distribution (TOP: 24^{th} Aug (left), 2^{nd} Sept (right); MID: 22^{nd} Sept (left), 23^{d} Sept (right); BOT: 29^{th} Sept (left), 1^{st} Oct (right);

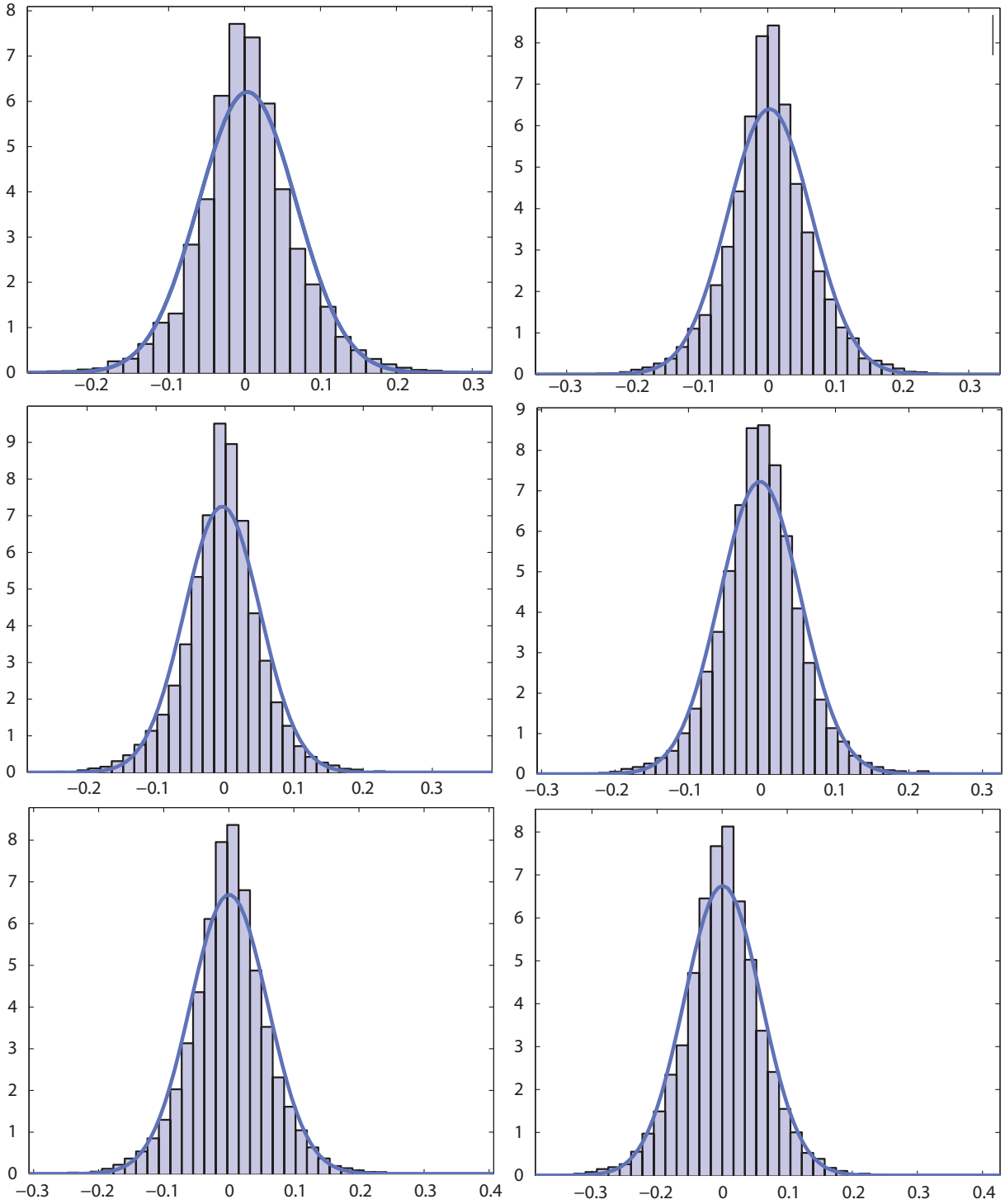

Figure 7.18: Non-dimensional Cross stream Grain Velocity fitting with Normal distribution (TOP: 24^{th} Aug (left), 2^{nd} Sept (right); MID: 22^{nd} Sept (left), 23^{d} Sept (right); BOT: 29^{th} Sept (left), 1^{st} Oct (right);

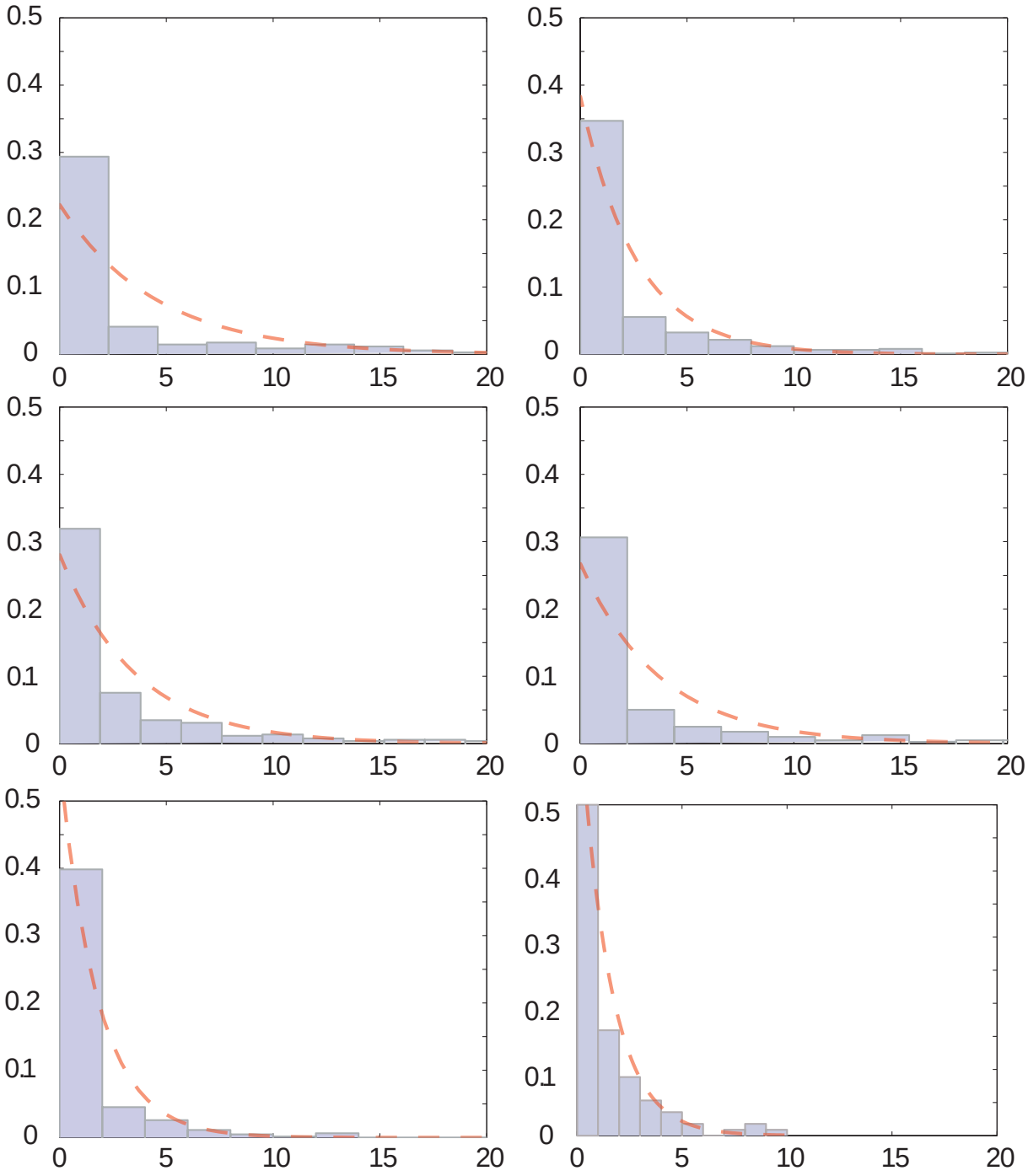

Figure 7.19: Grain Rest time probability density function (TOP: 24^{th} Aug (left), 2^{nd} Sept (right); MID: 22^{nd} Sept (left), 23^{d} Sept (right); BOT: 29^{th} Sept (left), 1^{st} Oct (right);

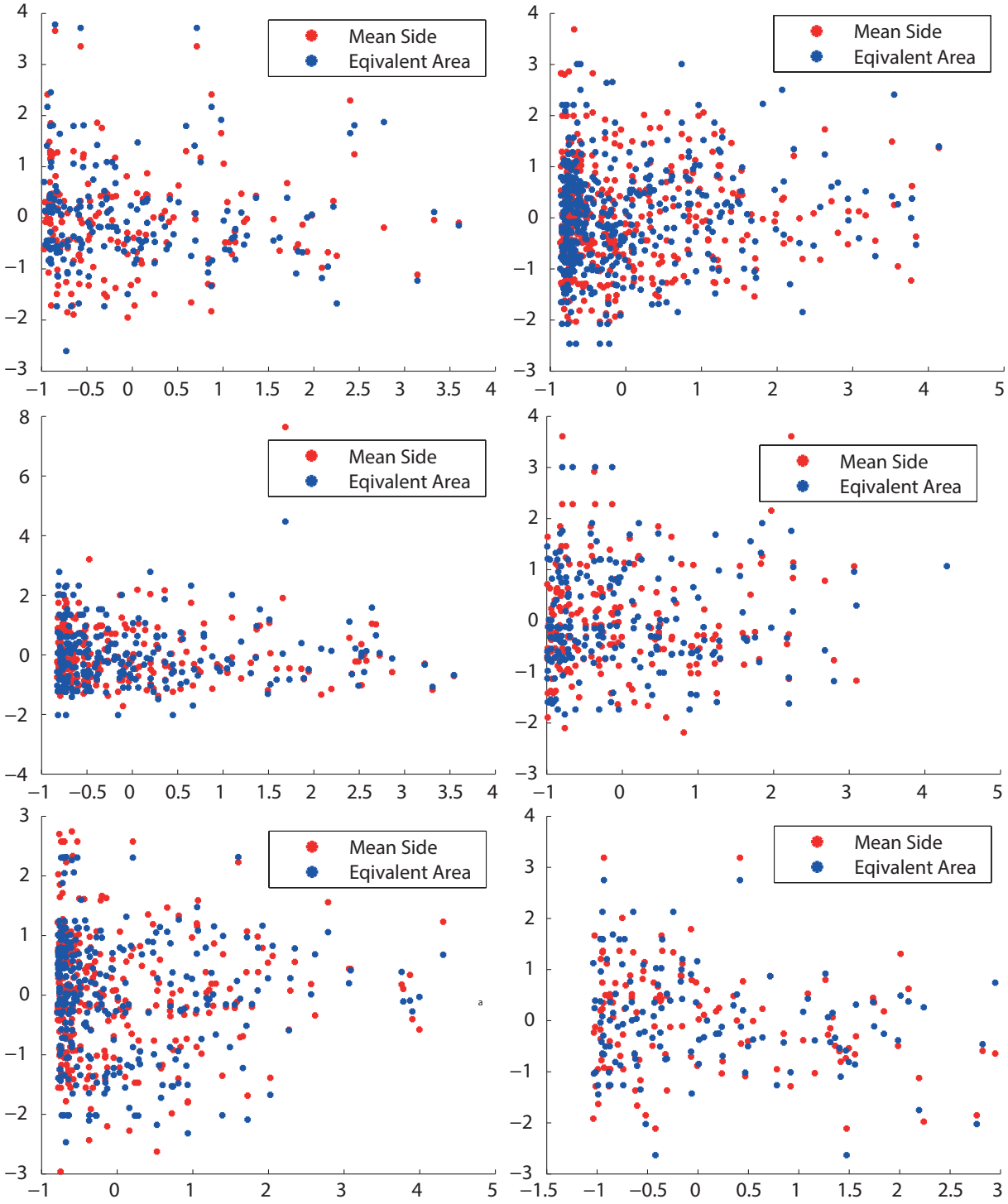

Figure 7.20: Normalized Step Length (x axis) versus Normalized Diameter (y axis) (TOP: 24^{th} Aug (left), 2^{nd} Sept (right); MID: 22^{nd} Sept (left), 23^{d} Sept (right); BOT: 29^{th} Sept (left), 1^{st} Oct (right);

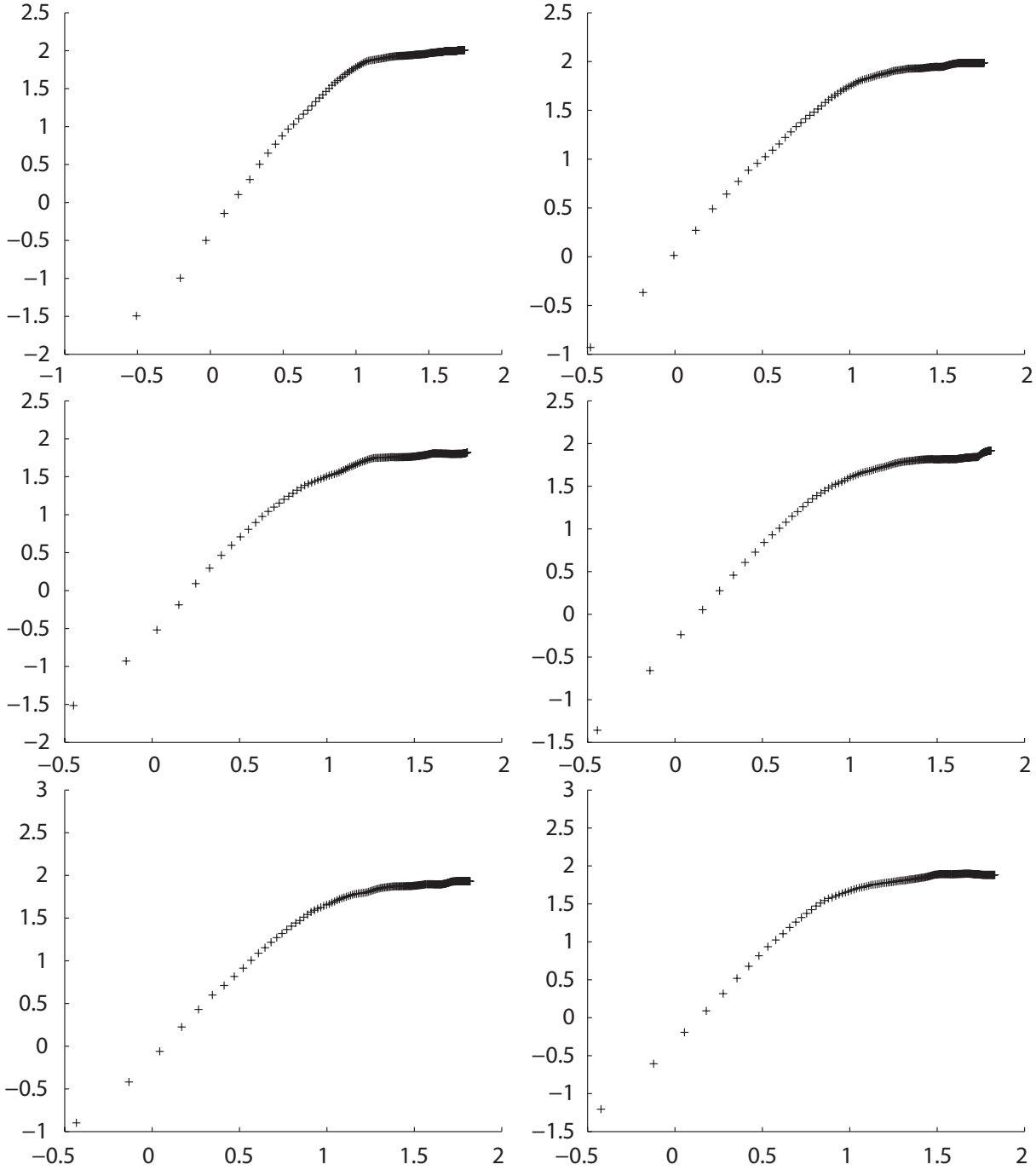

Figure 7.21: Diffusion curves in logarithmic scale (TOP: 24^{th} Aug (left), 2^{nd} Sept (right); MID: 22^{nd} Sept (left), 23^{d} Sept (right); BOT: 29^{th} Sept (left), 1^{st} Oct (right);

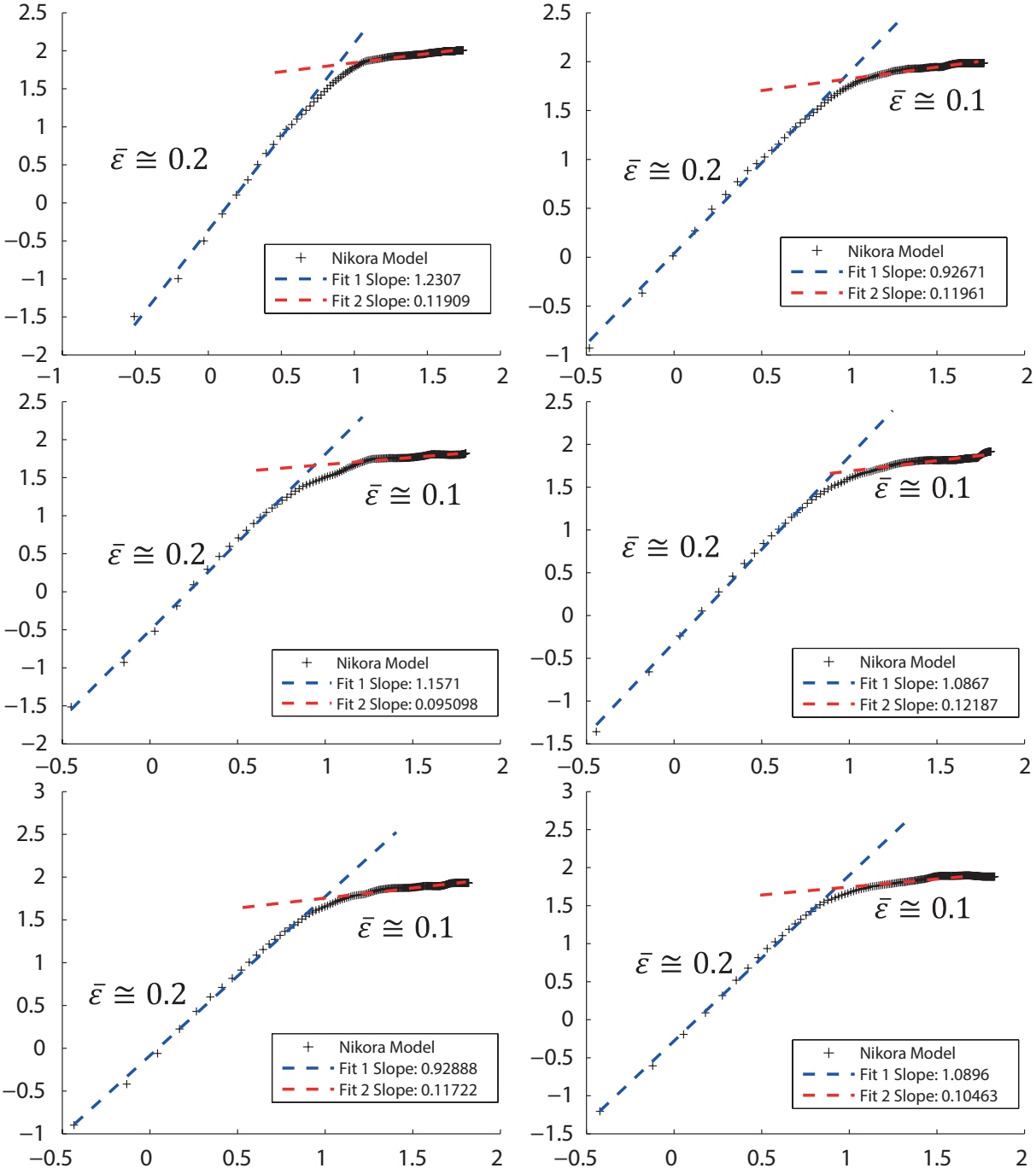

Figure 7.22: Fitted diffusion curves in logarithmic scale (TOP: 24^{th} Aug (left), 2^{nd} Sept (right); MID: 22^{nd} Sept (left), 23^{d} Sept (right); BOT: 29^{th} Sept (left), 1^{st} Oct (right);

Bibliography

Beheshti, A. & Ataie-Ashtiani, B. (2008), 'Analysis of threshold and incipient conditions for sediment movement', *Coastal Engineering* **55**(5), 423–430.

Bouchaud, J.-P. & Georges, A. (1990), 'Anomalous diffusion in disordered media: statistical mechanisms, models and physical applications', *Physics reports* **195**(4), 127–293.

Buffington, J. M. (1999), 'The legend of af shields', *Journal of Hydraulic Engineering* **125**(4), 376–387.

Buffington, J. M. & Montgomery, D. R. (1997), 'A systematic analysis of eight decades of incipient motion studies, with special reference to gravel-bedded rivers', *Water Resources Research* **33**(8), 1993–2029.

Cheng, N.-S. & Chiew, Y.-M. (1998), 'Pickup probability for sediment entrainment', *Journal of Hydraulic Engineering* **124**(2), 232–235.

Einstein, H. A. (1950), *The bed-load function for sediment transportation in open channel flows*, number 1026, US Department of Agriculture.

Gessler, J., Prych, E. A., Gessler, J. & Gessler, J. (1968), *The beginning of bedload movement of mixtures investigated as natural armoring in channels*, California Institute of Technology.

Graf, W. H. (1984), *Hydraulics of sediment transport*, Water Resources Publication.

Grass, A. J. (1970), 'Initial instability of fine bed sand', *Journal of the Hydraulics Division* **96**(3), 619–632.

Kreamer, D. K. (2012), 'The past, present, and future of water conflict and international security', *Journal of Contemporary Water Research & Education* **149**(1), 87–95.

Lajeunesse, E., Malverti, L. & Charru, F. (2010), 'Bed load transport in turbulent flow at the grain scale: Experiments and modeling', *Journal of Geophysical Research: Earth Surface (2003–2012)* **115**(F4).

Lee, H.-Y. & Hsu, I.-S. (1994), 'Investigation of saltating particle motions', *Journal of Hydraulic Engineering* **120**(7), 831–845.

McEwan, I., Sørensen, M., Heald, J., Tait, S., Cunningham, G., Goring, D. & Willetts, B. (2004), 'Probabilistic modeling of bed-load composition', *Journal of Hydraulic Engineering* **130**(2), 129–139.

Meyer-Peter, E. & Müller, R. (1948), Formulas for bed-load transport, IAHR.

Nelson, J. M., Shreve, R. L., McLean, S. R. & Drake, T. G. (1995), 'Role of near-bed turbulence structure in bed load transport and bed form mechanics', *Water Resources Research* **31**(8), 2071–2086.

Nikora, V., Habersack, H., Huber, T. & McEwan, I. (2002), 'On bed particle diffusion in gravel bed flows under weak bed load transport', *Water Resources Research* **38**(6), 17–1.

Nikora, V., Heald, J., Goring, D. & McEwan, I. (2001), 'Diffusion of saltating particles in unidirectional water flow over a rough granular bed', *Journal of Physics A: Mathematical and General* **34**(50), L743.

Niño, Y., García, M. & Ayala, L. (1994), 'Gravel saltation: 1. experiments', *Water resources research* **30**(6), 1907–1914.

Schlichting, H., Gersten, K. & Gersten, K. (2000), *Boundary-layer theory*, Springer Science & Business Media.

Shields, A. (1936), Application of similarity principles and turbulence research to bed-load movement, Technical report, Soil Conservation Service.

Tregnaghi, M., Bottacin-Busolin, A., Marion, A. & Tait, S. (2012), 'Stochastic determination of entrainment risk in uniformly sized sediment beds at low transport stages: 1. theory', *Journal of Geophysical Research: Earth Surface (2003–2012)* **117**(F4).

Tregnaghi, M., Bottacin-Busolin, A., Tait, S. & Marion, A. (2012), 'Stochastic determination of entrainment risk in uniformly sized sediment beds at low transport stages: 2. experiments', *Journal of Geophysical Research: Earth Surface (2003–2012)* **117**(F4).

Wu, F.-C. & Chou, Y.-J. (2003), 'Rolling and lifting probabilities for sediment entrainment', *Journal of Hydraulic Engineering* **129**(2), 110–119.

Wu, F.-C. & Lin, Y.-C. (2002), 'Pickup probability of sediment under log-normal velocity distribution', *Journal of Hydraulic Engineering* **128**(4), 438–442.

Yang, C. T. (1996), *Sediment transport: theory and practice*, McGraw-hill New York.

Yang, C. T. & Sayre, W. W. (1971), 'Stochastic model for sand dispersion', *Journal of the Hydraulics Division* **97**(2), 265–288.